

AD-A050 290

CONNECTICUT UNIV STORRS DEPT OF ELECTRICAL ENGINEERING--ETC F/6 19/5
EFFECTS OF TARGET MOTION AND IMAGE ON AAA TRACKING.(U)

NOV 77 D L KLEINMAN, A R EPHRATH, P K RAO

AFOSR-77-3126

UNCLASSIFIED

TR-77-7

AFOSR-TR-78-0138

NL

1 of 2

AD
A050290



AFOSR-TR- 78 - 0138

The University of Connecticut
SCHOOL OF ENGINEERING

Storrs, Connecticut 06268

2
B.S.

AD A050290



AD No. _____
DDC FILE COPY.

DDC
APR 22 1978
FEB 22 1978
F

Department of
Electrical Engineering and Computer Science

Approved for public release
distribution unlimited.

AIR FORCE OFFICE OF SCIENTIFIC RESEARCH (AFSC)
NOTICE OF TRANSMITTAL TO DDC
This technical report has been reviewed and is
approved for public release IAW AFR 190-12 (7b).
Distribution is unlimited.
A. D. BLOSE
Technical Information Officer

REPORT DOCUMENTATION PAGE		READ INSTRUCTIONS BEFORE COMPLETING FORM	
1. REPORT NUMBER AFOSR-TR-78-0138	2. GOVT ACCESSION NO.	3. RECIPIENT'S CATALOG NUMBER	
4. TITLE EFFECTS OF TARGET MOTION AND IMAGE ON AAA TRACKING	5. TYPE OF REPORT & PERIOD COVERED Scientific Interim Report Oct 76-Sep 77		6. PERFORMING ORG. REPORT NUMBER TR-77-71
7. AUTHOR(s) David L. Kleinman, Arye R. Ephrath P. Krishna Rao	8. CONTRACT OR GRANT NUMBER(s) AFOSR-77-3126		
9. PERFORMING ORGANIZATION NAME AND ADDRESS University of Connecticut Dept. of Electrical Engr. & Comp. Science Storrs, Conn. 06268		10. PROGRAM ELEMENT, PROJECT, TASK AREA & WORK UNIT NUMBERS 61102F, 2312/A6	
11. CONTROLLING OFFICE NAME AND ADDRESS Air Force Office of Scientific Research (NL) Bolling AFB, D.C. 20332		12. REPORT DATE 30 Nov 77	
14. MONITORING AGENCY NAME & ADDRESS (if different from Controlling Office)		13. NUMBER OF PAGES 192	
		15. SECURITY CLASS. (of this report) Unclassified	
		15a. DECLASSIFICATION/DOWNGRADING SCHEDULE n/a	
16. DISTRIBUTION STATEMENT (of this Report) Approved for public release; distribution unlimited.			
17. DISTRIBUTION STATEMENT (of the abstract entered in Block 20, if different from Report)			
18. SUPPLEMENTARY NOTES			
19. KEY WORDS (Continue on reverse side if necessary and identify by block number) Tracking Human Operator Modeling Target tracking Anti-Aircraft Artillery			
20. ABSTRACT (Continue on reverse side if necessary and identify by block number) The optimal control model of human response is applied to study target tracking performance of an AAA system. The effects on tracking error of different target motions, i.e. acceleration profiles, are studied via a covariance propagation modeling approach and via experiment. Different assumptions relative to the adaptive tracking behavior of the human are explored along with different schemes for inter-axis attention allocation. The effects of visual information inherent in a moving target image (e.g. size, aspect angle, etc.) are explored via comparison of results with a moving image vs image of fixed size and shape. Experimental tracking results are compared with those predicted by the model.			

410 576

UNIVERSITY OF CONNECTICUT
Department of Electrical Engineering & Computer Science

Scientific Interim Report
for period
Oct. 1, 1976-Sept. 30, 1977
Grant No. AFOSR 77-3126

EFFECTS OF TARGET MOTION AND
IMAGE ON AAA TRACKING

David L. Kleinman
Arye R. Ephrath
P. Krishna Rao

Technical Report TR 77-7
November 30, 1977

Prepared for:
Air Force Office of Scientific Research
Bolling AFB
Washington, D.C. 20332

ACCESSION for	
NTIS	Write Section <input checked="" type="checkbox"/>
DDC	Bull Section <input type="checkbox"/>
UNANNOUNCED	<input type="checkbox"/>
DISSEMINATION	
BY	
DISTRIBUTION/AVAILABILITY CODES	
SPECIAL	
A	

ABSTRACT

The optimal control model of human response is applied to study target tracking performance of an AAA system. The effects on tracking error of different target motions, i.e. acceleration profiles, are studied via a covariance propagation modeling approach and via experiment. Different assumptions relative to the adaptive tracking behavior of the human are explored along with different schemes for inter-axis attention allocation. The effects of visual information inherent in a moving target image (e.g. size, aspect angle, etc.) are explored via comparison of results with a moving image vs. image of fixed size and shape. Experimental tracking results are compared with those predicted by the model.

ACKNOWLEDGMENTS

This research project is being funded by the Air Force Office of Scientific Research under Grant No. 77-3126 to the University of Connecticut. Contract monitor for the Air Force was Lt. Col. Dominic Maio. Technical monitor for the Air Force was Dr. Carroll Day, AMRL/EMT. All of the support and assistance provided by Air Force personnel was invaluable throughout the project effort. We wish to acknowledge the assistance of Mr. Walt Summers (AMRL/EMT) in running the Monte-Carlo simulations, and of Mr. Maris Vickmanis (SRL) in the analysis of modeling modifications.

At the University of Connecticut, principal investigator was Dr. David L. Kleinman. Dr. Arye R. Ephrath had responsibility for the experimental program and presentation of results. He was given invaluable assistance by Ms. Barbara Chernoff and Mr. Jonathan Korn. Other graduate student research assistants were P. Krishna Rao and Roy Lancraft. Report preparation was done by Ms. Catherine Giard.

TABLE OF CONTENTS

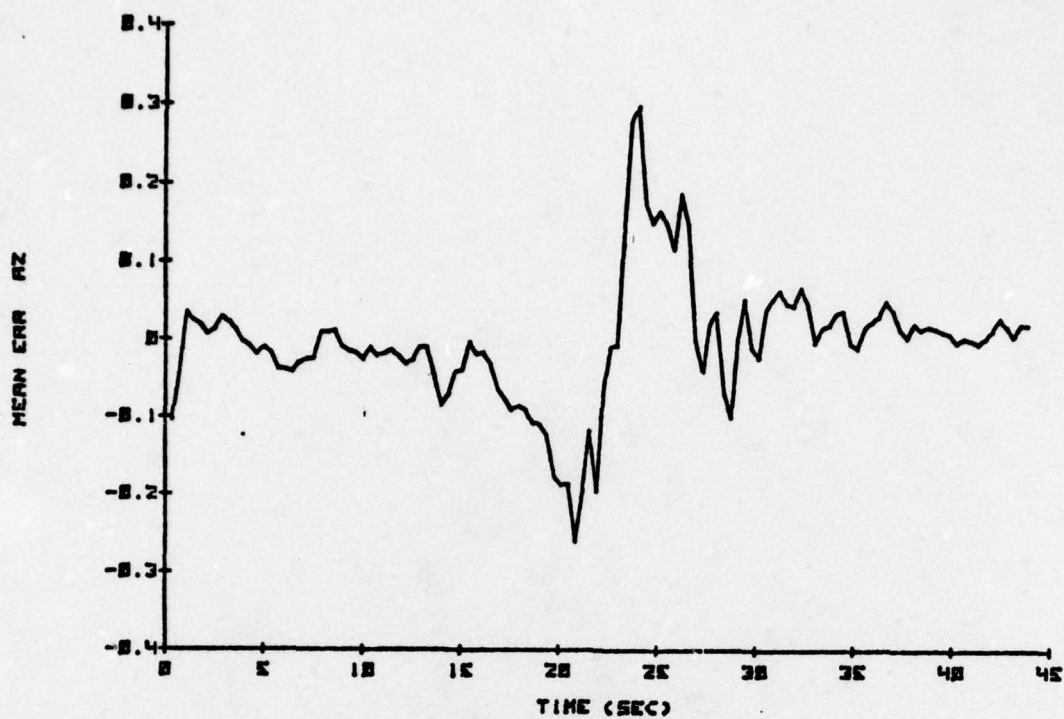
	<u>Page</u>
ABSTRACT	1
ACKNOWLEDGEMENTS	11
I. OVERVIEW	1
1.1 Project Background	1
1.2 Experimental Tracking Task	6
1.3 Modeling Approach	8
1.4 Overview of Model-Data Comparisons	13
1.5 Summary	24
II. EXPERIMENTAL PROGRAM	26
2.1 Hardware	26
2.2 Software	27
2.3 Pre-Experimental Detail	28
2.4 Experimental Design	32
2.5 Data Reduction and Analysis Methods	35
III. ANALYTIC MODELING	38
3.1 Adaptive Tracking Problem	38
3.2 Modeling Asymmetries in Tracking Errors	48
3.3 Attention Allocation Submodel	58
3.4 Modeling Target Visual Cues	71
IV. CONCLUSIONS	78
V. REFERENCES	79
APPENDIX A	80
APPENDIX B	86

I. OVERVIEW

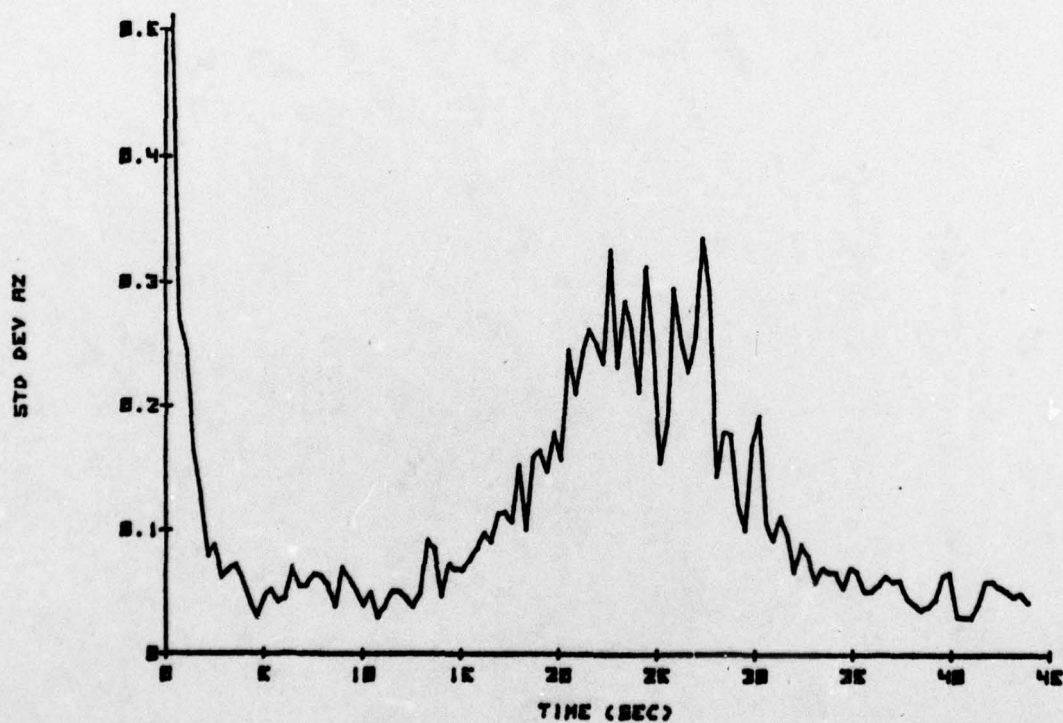
1.1 Project Background

The suggested use of control theoretic principles to model human operator response in AAA tracking tasks dates back to the 1946 work of Tustin [1]. However, it has only been of late that the tools of modern control and estimation theory have made the modeling process a reality [2-4]. In recent studies, model predictions -- generated via an optimal control approach -- were in excellent agreement with experimental ensemble statistics of target tracking error in both the Vulcan (VADS) [2] and S60 [3-4] weapons systems. Figures 1-4 show typical model-data comparisons for a straight-and-level target flyby against the S60 system [4]. Moreover, the quality of these results was uniformly consistent over a variety of (maneuvering) target profiles. Despite the success of these efforts, it was recognized that numerous assumptions made in the modeling process required further justification and analysis. Moreover, there were facets of human response in target tracking tasks not addressed by the earlier efforts. Accordingly, AFOSR-supported research at the University of Connecticut, and concomitant efforts at the Aerospace Medical Research Laboratory, WPAFB, has sought to enlarge our understanding of human information processing and control behavior in target tracking. Among the issues that have been studied via a combined experimental/analytic program during our first year's effort are the following:

1. Effect of target image and size. The experimental program reported in Refs. [3-4] used a target image of fixed size, shape and aspect ratio. The present work explores the added visual cues the human may derive from a realistic (moving) target image.
2. Sample-path simulation of human operator response. We have developed and documented the equations and necessary software with which to generate simulated time histories of pertinent variables in a target tracking

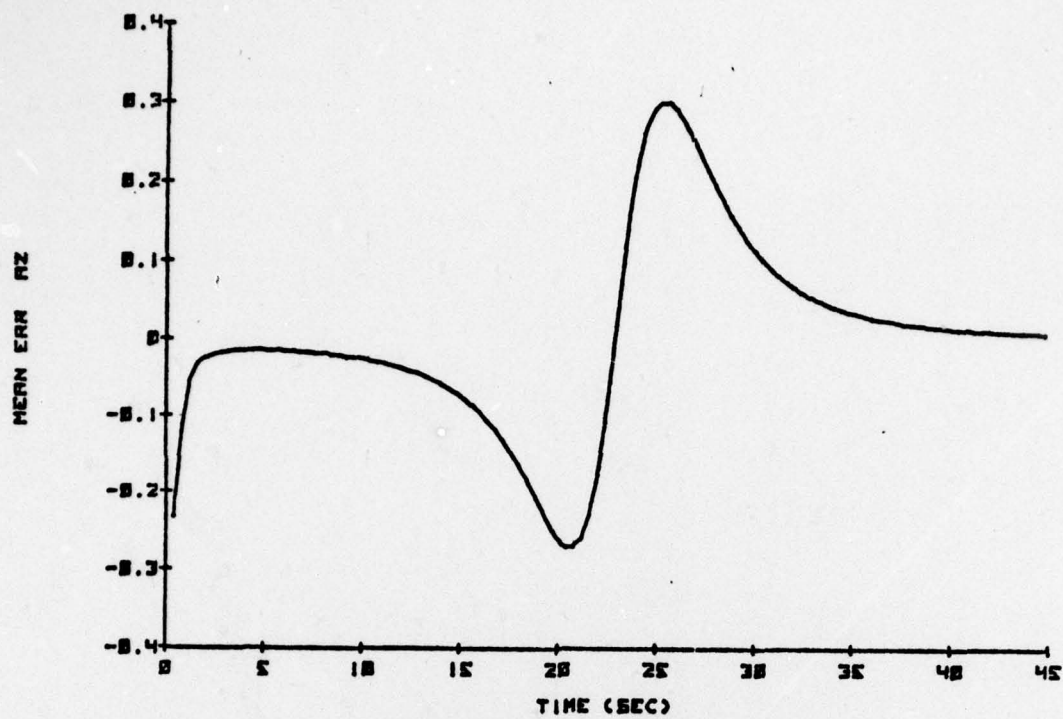


a) Ensemble Mean, N=15

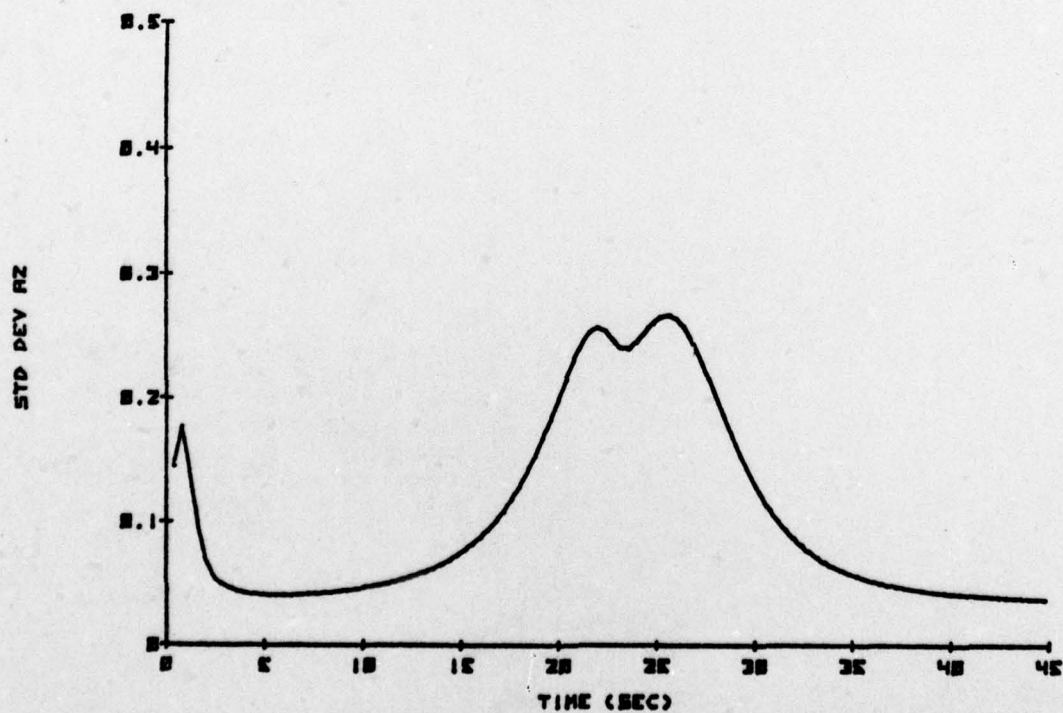


b) Ensemble Standard Deviation, N=15

Fig. 1: AZIMUTH TRACKING DATA, S60 SYSTEM WITH FLYBY

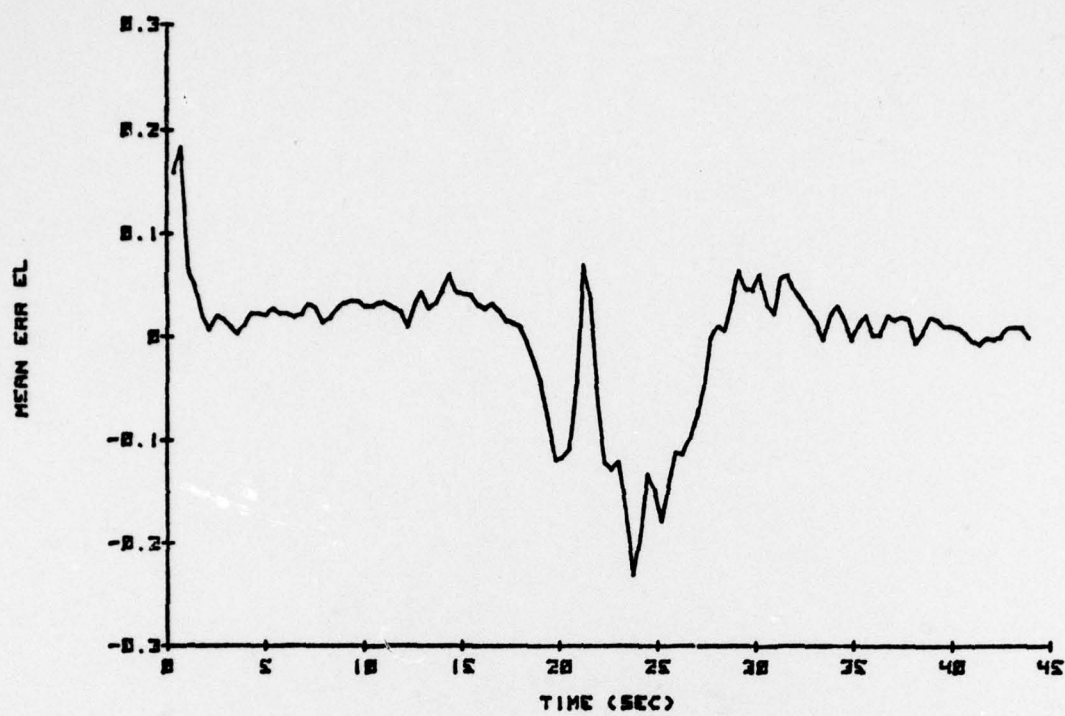


a) Ensemble Mean Predictions

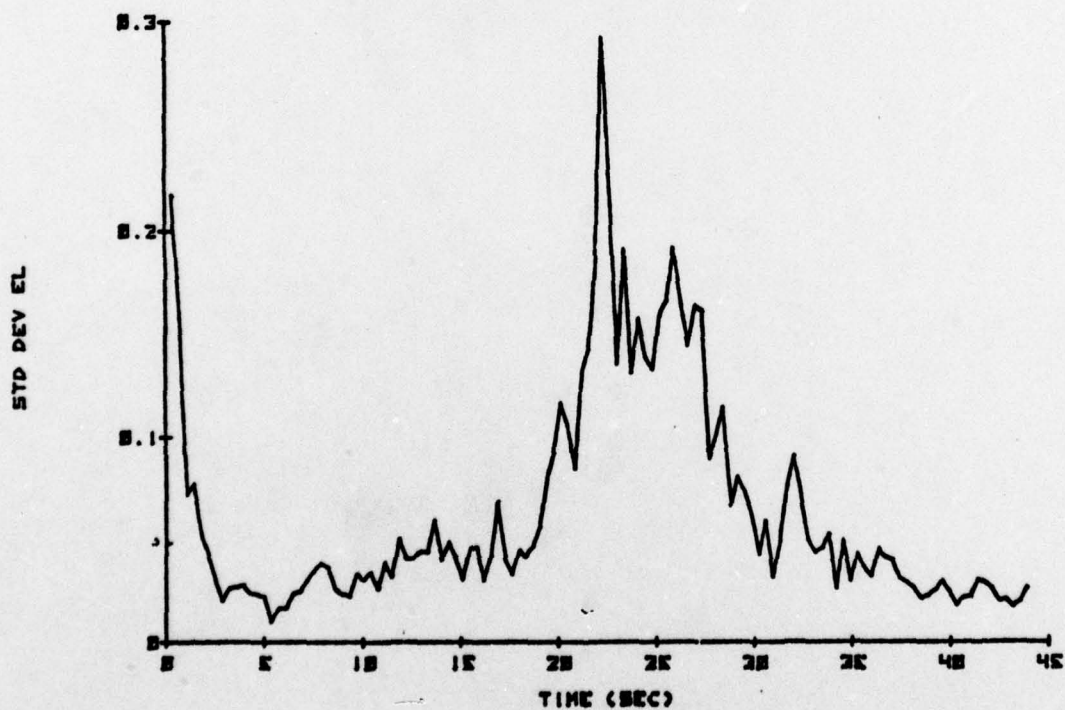


b) Ensemble Standard Deviation Predictions

Fig: 2: OCM AZIMUTH PREDICTIONS, S60 SYSTEM WITH FLYBY

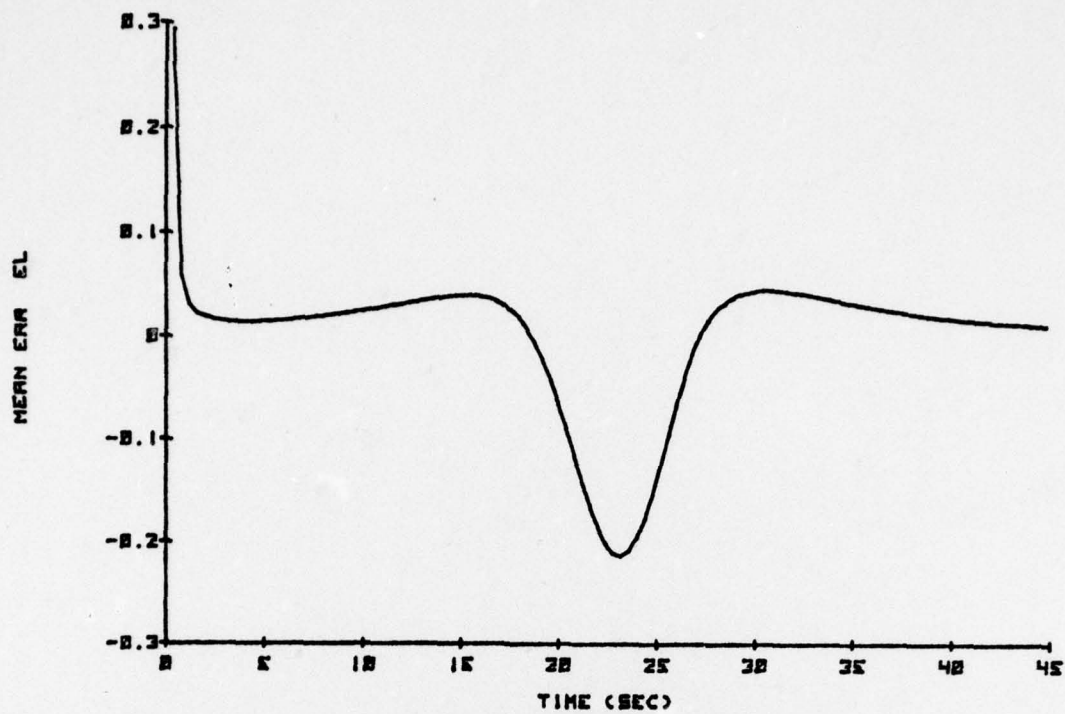


a) Ensemble Mean, N=15

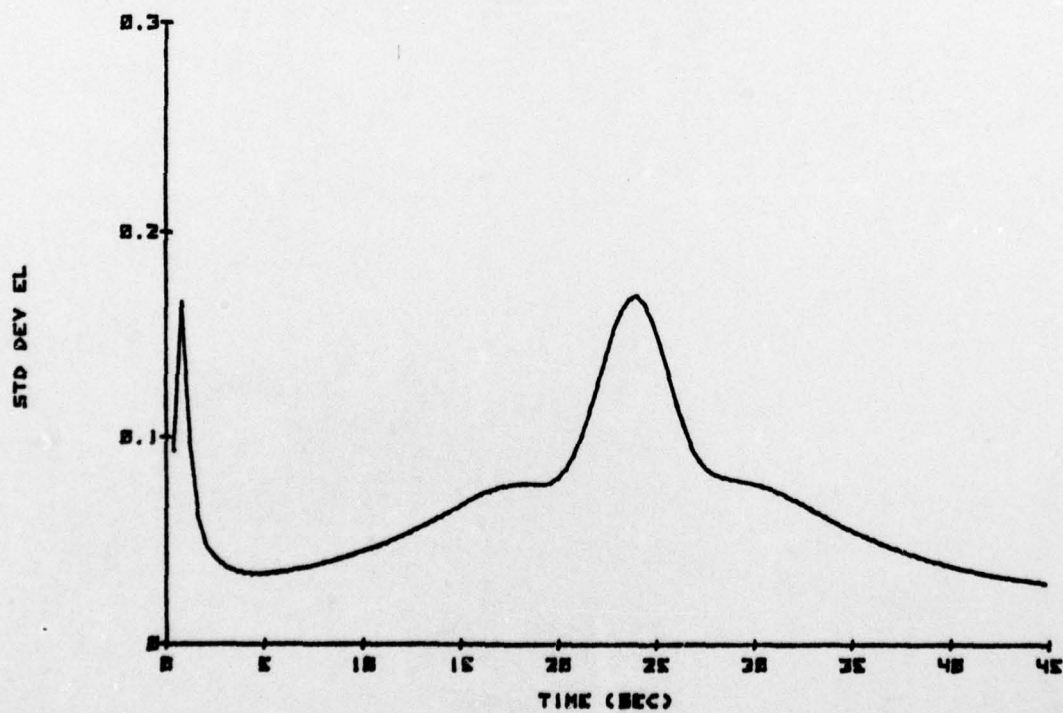


b) Ensemble Standard Deviation, N=15

Fig. 3: ELEVATION TRACKING DATA, S60 SYSTEM WITH FLYBY



a) Ensemble Mean Predictions



b) Ensemble Standard Deviation Predictions

Fig. 4: OCM ELEVATION PREDICTIONS, S60 SYSTEM WITH FLYBY

loop [8]. Sample paths have been compared with real AAA tracking data. The ensemble statistics of these model-generated paths are compared with averaged data and analytic covariance propagation results [9].

3. Effect of Attention Allocation. The tracking system of Refs. [3-4] had two operators for dual tasks of azimuth and elevation tracking. As such, inter-axis attention allocation was not of concern. VADS [2] was a single-operator system, and an ad-hoc attentional scheme was proposed. The issues of dynamic attention allocation are studied further in our work.
4. Use of High-order Derivatives. All of the past modeling efforts required use of either target acceleration, $\ddot{\theta}_T$, or jerk, $\dddot{\theta}_T$ by the state estimator/filter. This information was used to compute a pseudo-driving noise, to adaptively adjust filter bandwidth. We have now developed a technique for estimating the unknown (to the human) higher derivatives using the filter innovations process.
5. "Internal Model" Assumptions. The choice of target model in the Kalman filter had received little attention in previous efforts. The use of polynomial models (e.g. velocity vs. acceleration models), and first-order Markov models have now been explored in more detail within an analytic context.

1.2 Experimental Tracking Task

The intent is to focus our modeling efforts on the human's information processing and control behavior without the attendant complexities of high-order system dynamics. Accordingly, we shall consider a simplified k/s tracking loop with command input, θ_T =target angle, as shown in Fig. 5. Elevation and azimuth loops are assumed identical in structure. This is not a restrictive situation as most tracking systems employ essentially rate command dynamics, e.g. k/s modified by adding high frequency filtering.

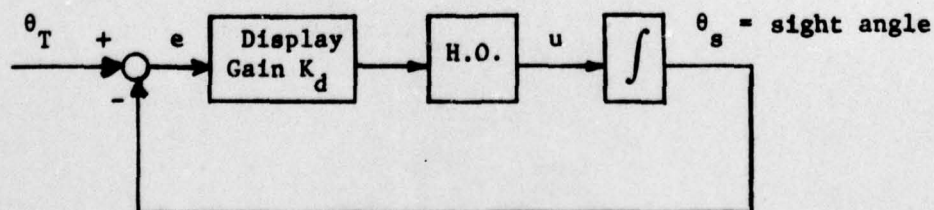


Fig. 5: BASIC TRACKING LOOP

The basic loop equations are, with $x_1 = \dot{\theta}_T$, $x_2 = e =$ tracking error,

$$\dot{\underline{x}}_0 = \begin{bmatrix} 0 & 0 \\ 1 & 0 \end{bmatrix} \underline{x}_0 + \begin{bmatrix} 0 \\ -1 \end{bmatrix} u + \begin{bmatrix} 1 \\ 0 \end{bmatrix} z(t) \quad (1.1)$$

where $z(t) = \ddot{\theta}_T$. Other forms for the target representation (here given by $\dot{x}_1 = z(t)$) will be considered in the sequel.

The experimental program that we conducted used two different trajectories $\theta_T(\cdot)$. A straight-and-level, constant velocity, aircraft flyby was used for baseline work and for comparisons with similar on-going efforts at AMRL. A target flyby with low-bandwidth random pitching was used to enhance the effects of any visual cues derived from the target image. For each target, two sets of experiments were conducted to study image effects. In one set, the target was represented on the CRT display as a triangle of fixed size and shape. In the second set, the target was assumed to be a Δ -shaped aircraft. The image presented on the CRT was the actual contour of the aircraft as would be seen by a human observer. Thus, the image appeared to rotate, change aspect angle and grow in size inversely with range.

Another set of experiments, using only the basic flyby trajectory, were done to isolate the effects of inter-axis attentional allocation. Azimuth and elevation axes were controlled separately, but with elevation and azimuth errors, respectively, held at zero. In this manner full attention is available for single-axis control. This set of single-axis tasks was repeated with and without explicit visual cues from the target image.

In all experiments the subjects tracked to minimize error, and were scored using an RMS criterion. The data collected were the time-histories of tracking error, $e(t)$, and human input, $u(t)$. For the same experimental condition, these time-histories were ensemble averaged to obtain mean tracking error, $\bar{e}(t)$, and standard deviation, $\sigma_e(t)$, vs. time. The averaging process first

was done for each subject, and then across subjects to obtain the "grand" averages. A complete description of the experimental setup and procedures is given in Chapter 2. The experimental results are plotted in Appendix B.

1.3 Modeling Approach

The application of the Optimal Control Model [5] of human response to obtain performance predictions is relatively straightforward [2]. The system dynamics are given in the requisite form

$$\dot{\underline{x}}_0(t) = \underline{A}_0 \underline{x}_0(t) + \underline{B}_0 u(t) + \underline{F} z(t) \quad (1.2)$$

via Eq. (1.1). The displayed information consists of tracking error $e(t)$, and hence also error rate $\dot{e}(t)$, in those cases where there are no target image cues. Thus,

$$\underline{y}(t) = \underline{C}_0 \underline{x}_0(t) + \underline{D}_0 u(t) = \begin{bmatrix} 0 & 1 \\ 1 & 0 \end{bmatrix} \underline{x}_0 + \begin{bmatrix} 0 \\ -1 \end{bmatrix} u \quad (1.3)$$

The visual assumption in the Optimal Control Model (OCM) is that the human perceives a delayed noisy replica of $\underline{y}(t)$,

$$\underline{y}_p(t) = \underline{y}(t-\tau) + \underline{v}_y(t-\tau) \quad (1.4)$$

where each white-gaussian noise $\underline{v}_{y1}(t)$ has covariance

$$\underline{v}_{y1}(t) = \frac{\pi \rho_{y1}}{f_1 N_1^2} \cdot E\{y_1^2(t)\} \quad (1.5)$$

The quantity $\rho_{y1} \approx .01$ is the noise/signal ratio, f_1 is the attention allocation to output pair $(y_1, \dot{y}_1)^\dagger$, and N_1 is the linearized describing function gain of the visual/indifference threshold of width $\pm a_1$. The gain N_1 is

[†]Since there is only one indicator per axis, $f_1 = f_A$ or f_E is the attention to either the azimuth or elevation axis tracking task, as the case may be. We require $f_A + f_E = 1$.

a function of the mean and standard deviation of $y_1(t)$ [6]. Figure 6 shows the structure of the Optimal Control Model. The human's feedback control strategy is represented by

$$\tau_n \dot{u} + u = -\underline{L} \hat{x}_0(t) + \tau_n v_u(t) \quad (1.6)$$

or

$$\dot{u} = -[\tau_n^{-1} \underline{L} \quad \tau_n^{-1}] \begin{bmatrix} \hat{x}_0 \\ u \end{bmatrix} + v_u(t) \quad (1.6a)$$

where the "neuro-motor" time-constant $\tau_n \approx .1$ and $v_u(t)$ is a white gaussian noise. In a slight departure from past modeling efforts, the covariance $v_u(t)$ is assumed to scale with commanded control rate as opposed to commanded control. This has been found to give results consistent with past steady-state modeling work, and is more appropriate to non-stationary tasks (as here) where large mean control inputs are usual. Thus,

$$V_u(t) = \pi \rho_u E\{\dot{u}_c\} \quad (1.7)$$

where $\rho_u \approx .01 - .003$.

The control gains $[L_1, L_2] = [\tau_n^{-1} \underline{L}, \tau_n^{-1}]$ are selected to minimize the quadratic cost functional

$$J(u) = \lim_{T \rightarrow \infty} \frac{1}{T} E \left\{ \int_0^T [y_1^2(t) + g \dot{u}^2(t)] dt \right\} \quad (1.8)$$

i.e., to minimize mean-squared tracking error. The control rate weighting, g is adjusted to give a value $\tau_n \approx .1$ sec. For this system, $g = .0004$.

The state estimate $\hat{x}(t) = [\hat{x}_0, \hat{u}]'$ is generated by the cascade combination of an (augmented) Kalman filter and a linear predictor. The filter equation is

$$\dot{\hat{x}}(t-\tau) = \underline{A} \hat{x}(t-\tau) + \underline{B} u_c(t-\tau) + \underline{G}(t-\tau) [y_p(t) - \underline{C} \hat{x}(t-\tau)] \quad (1.9)$$

where

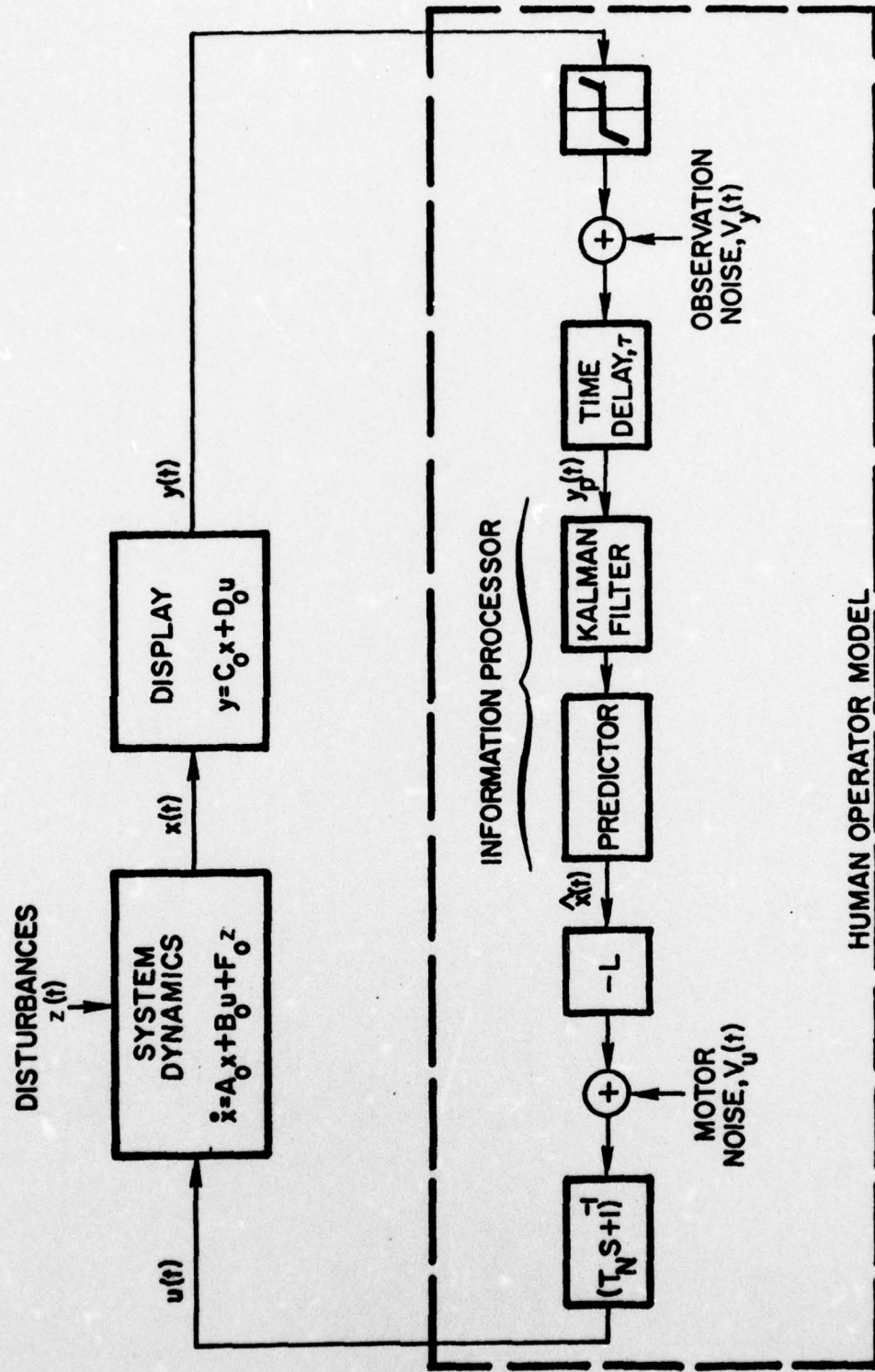


Fig. 6: OPTIMAL CONTROL MODEL OF HUMAN RESPONSE

$$\hat{\underline{x}}(t-\tau) = E \left\{ \underline{x}(t-\tau) \mid \underline{z}_p(\sigma), \sigma \leq t \right\}$$

$$\underline{A} = \begin{bmatrix} \underline{A}_0 & \underline{B}_0 \\ 0 & \tau_n^{-1} \end{bmatrix}; \underline{B} = \begin{bmatrix} 0 \\ 1 \end{bmatrix}; \underline{C} = [\underline{C}_0, \underline{D}_0]$$
(1.10)

and $u_c(t) = -\tau_n^{-1} \underline{L} \hat{\underline{x}}_0(t)$.

The filter gain $\underline{G}(t)$ is

$$\underline{G}(t) = \underline{\Sigma}(t) \underline{C}' \underline{V}_y^{-1}(t)$$
(1.11)

where $\underline{\Sigma}(t)$ is generated from the Riccati equation

$$\dot{\underline{\Sigma}} = \underline{A} \underline{\Sigma} + \underline{\Sigma} \underline{A}' - \underline{\Sigma} \underline{C}' \underline{V}_y^{-1}(t) \underline{C} \underline{\Sigma}(t) + \begin{bmatrix} \underline{W}_d & 0 \\ 0 & \underline{V}_u / \tau_n^2 \end{bmatrix}$$
(1.12)

The "pseudo-noise" \underline{W}_d is chosen such that the filter adapts to the changing characteristics of the input signal $z(t)$. In previous modeling efforts [2,4] it was found that choosing \underline{W}_d according to

$$\underline{W}_d(t) = \underline{F} z^2(t) \underline{F}'$$
(1.13)

gave model predictions that accurately matched human response data, viz Figs. 1-4. Although the agreements were excellent, it must be recognized that the signal $z(t)$ is not "observed" by the human, and so model modifications are warranted.

A method for estimating $z(t)$, or equivalently $\underline{F} z(t)$, was developed in the current effort. The signal $z(t)$ is what gives rise to the ensemble mean statistics via the mean filtering error equation,

$$\dot{\underline{e}}_f = (\underline{A} - \underline{G} \underline{C}) \underline{e}_f + \underline{F} \underline{z}(t-\tau)$$
(1.14)

where $\underline{e}_f(t) = E\{\underline{x}(t-\tau) - \hat{\underline{x}}(t-\tau)\}$. The mean error gives rise to a mean innovations in the Kalman Filter,

$$\bar{v}(t) = \underline{C} \bar{e}_f(t). \quad (1.15)$$

Rewriting Eq. (1.14) in the form

$$\dot{\bar{e}}_f = \underline{A} \bar{e}_f - \underline{C} \bar{v} + \underline{F} z(t-\tau), \quad (1.16)$$

a fading memory, recursive least-squares algorithm has been derived to estimate $z(t-\tau)$ from the non-zero mean residuals. The technique has been remarkably successful in generating an estimate $\hat{z}(t-\tau)$ that accurately "tracks" $z(t-\tau)$ for all target profiles considered to date. The details of the estimation scheme are presented in Section 3.1.

1.3.1 Model Application Process

Once the model parameters

$$\underline{\theta} = \{\tau, \rho_{y1}, \rho_{u1}, \tau_n, a_1\}$$

are specified, the OCM can be used to generate predictions of ensemble statistics for all pertinent variables in the tracking loop. The mean and covariance propagation equations that must be integrated to obtain these results are given in full detail in Ref. [7]. Also presented are the discretized equations for computer implementation.

The selection of model parameters can be a difficult subprocess in general. However, past research in human response theory has shown that typical parameter values are

$$\begin{array}{ll} \tau = .15 - .2 \text{ sec} & \rho_{y1} \sim -20 \text{ dB} \\ \tau_n = .08 - .1 \text{ sec} & \rho_{u1} = -20 \text{ to } -25 \text{ dB} \end{array}$$

and that these values are not dependent on the type of dynamics being controlled. Thus, when the OCM is applied to "match" target tracking data we have found it relatively easy to first make nominal predictions using a priori values, and then fine-tune using one or more parameters. Moreover, if one considers only tracking error statistics, changes in τ , ρ_{u1} and ρ_{y1} have been found

to produce very similar effects on model predictions: both $\bar{e}(t)$ and $\sigma_e(t)$ increase with larger parameter values. Thus one can fix any two of these parameters and adjust the third. In this effort we picked $\tau = .2$ sec, $\rho_u = -20$ dB (to reflect a medium quality hand-position controller), and adjusted ρ_y about its nominal value.

The identification of visual/indifference thresholds a_1 is a bit more subtle. Here one looks for periods of easy (and hence good) tracking, where $|z(t)|$ is small, and then adjusts a_1 to match the tracking error standard deviation. This is possible since sensitivity studies show that the value of a_1 has little or no effect on the ensemble mean error statistics. It is also possible to obtain estimates of a_1 from questionnaire, or more often by a simple analysis of display gain, format and/or scale markings. In our work we found it necessary to use a small visual display gain ($K_d \approx 1/8$), which resulted in a threshold value of about 1.5° on tracking error. In accordance with past work, error rate thresholds are selected as $1/2$ of this value.[†]

1.4 Overview of Model-Data Comparisons

Typical OCM predictions of (ensemble) mean tracking errors and standard deviations for a k/s-type system are shown in Figs. 2 and 4. These results are for a straight-and-level flyby. The mean errors are quite symmetric (or anti-symmetric) about crossover, with a structure that is very nearly proportional to $z(t) = \ddot{\theta}_T$. Changes in the basic model parameters $\{\tau, \tau_n, \rho_y, \rho_u\}$ produce a scaling effect on the magnitude of the mean error, but have little or no effect on the inherent symmetric structure. With these results as background, we give an overview of the modeling efforts conducted during the first year's research.

1.4.1 Internal Model Studies

Our experimentally obtained mean tracking error for a flyby (no visual

[†] A further analysis of the efficacy of this "rule-of-thumb" is being undertaken.

image cues, full attention to a single axis) is shown in Fig. 7. Notice that the mean errors have the same general form as the corresponding model predictions, but show an asymmetry. There is relatively more lag prior to crossover with less lead (overshoot) after crossover. Numerous attempts to reproduce this tracking characteristic by changing model parameters, cost functional weights, etc., have reached one conclusion: Since mean tracking error is similar in form to $z(t)$ in Eq. (1.2), it is necessary to change the internal target model so as to change $z(t)$. Accordingly, we model the target motion via a first-order Markov process

$$\dot{x}_1(t) = -\alpha x_1(t) + z(t) \quad (1.17)$$

where now

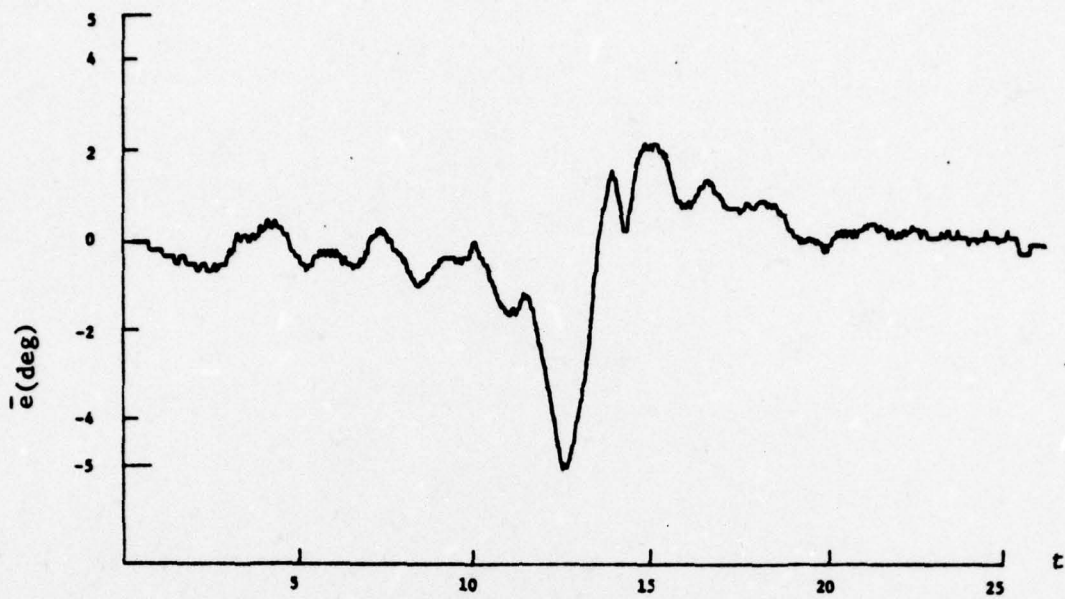
$$z(t) = \ddot{\theta}_T(t) + \alpha \dot{\theta}_T \quad (1.18)$$

The parameter $\alpha \geq 0$ represents, to some extent, the "bandwidth" of the signal $x_1(t)$. The form (1.17) is a natural extension of the earlier Weiner-process model, with $\alpha = 0$, and is examined in Section 3.2.

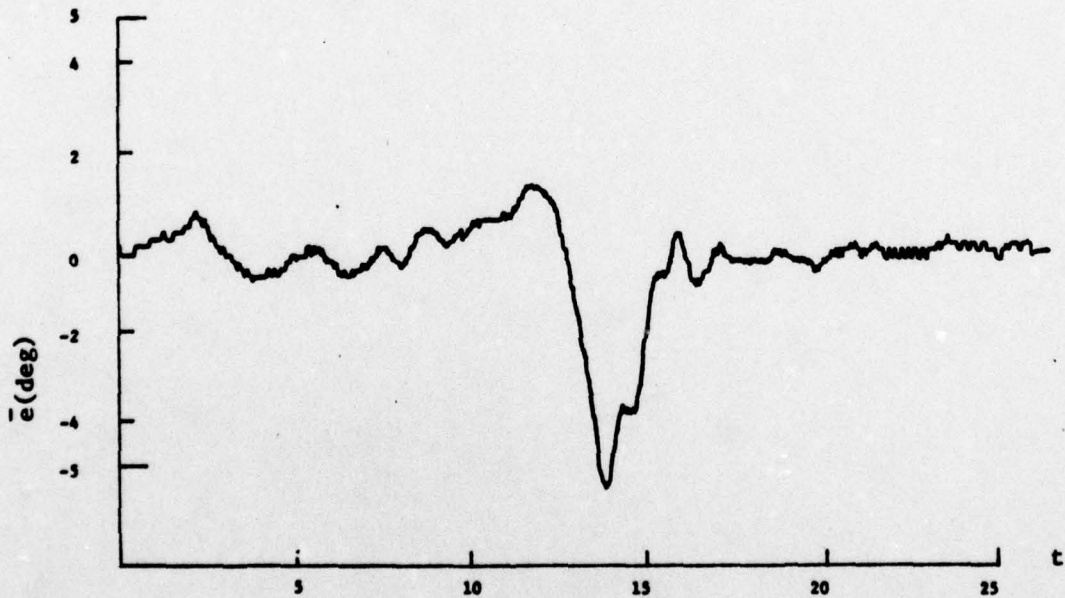
Model results have shown that this modification does indeed give the asymmetry required in $\bar{e}(t)$. However, α is not a constant. In order to match data, and provide consistent modeling hypotheses, α must be a function of (estimated) target acceleration and velocity, plus the human's uncertainty in the latter. This means that the correlation time $1/\alpha$ is directly dependent on target motion, but depends indirectly on target visual cues and/or attention allocation requirements. This also implies that changes in display quality can alter (indirectly) tracking error structure.

1.4.2 Velocity vs. Acceleration Models

The target representation $\dot{x}_1 = z(t)$ is called a "velocity" model. It is the simplest form of a general polynomial approximation to the target motion. The next model in the hierarchy would be an "acceleration" model. If we let



a) Azimuth Axis



b) Elevation Axis

Fig. 7: EXPERIMENTAL MEANS, S & L TARGET, FULL ATTENTION, NO VISUAL CUES

$x_1 = \dot{\theta}_T$, $x_2 = \ddot{\theta}_T$ then,

$$\dot{x}_1 = x_2 \quad (1.19a)$$

$$\dot{x}_2 = z(t) = \ddot{\theta}_T \quad (1.19b)$$

and with $x_3 = e(t) = \text{tracking error}$ we have the final state equation

$$\dot{x}_3 = x_1 - u \quad (1.19c)$$

This state-space representation is in the form of Eq. (1.2), where $\underline{F} = [0 \ 1 \ 0]^T$ and $z(t) = \ddot{\theta}(t)$. If the optimal control model is applied to this case, using $\underline{W}_d = \underline{F} z^2(t) \underline{F}^T$, then the mean tracking error is similar to $\ddot{\theta}(t)$. This does not match the data. Moreover there is no reason to stop the polynomial modeling process at $\ddot{\theta}$. A way out of this dilemma is provided by the scheme we have developed for estimation of $z(t)$. If Eq. (1.19a-b) is rewritten as

$$\dot{x}_1 = x_2 + z_1(t) \quad (1.20a)$$

$$\dot{x}_2 = z_2(t) \quad (1.20b)$$

we can then estimate, via the innovations technique, the vector process $\underline{z}(t) = [z_1, z_2]^T$. This gives the model the ability to ascribe uncertainty to both target velocity and acceleration. In actuality $z_1(t) = 0$. But when estimated we find

$$\hat{z}_1(t) \approx \ddot{\theta}_T(t) \quad \text{and} \quad \hat{z}_2(t) = 0 \quad (1.21)$$

Therefore, writing the target motion as a higher-order model has no effect on the OCM predictions, as should be the case. In retrospect this result is due to the fact that no information concerning $\ddot{\theta}(t)$ is contained in the observations $y_1 = e$, $y_2 = \dot{e}$. Hence, it is unreasonable to expect any estimation of $\ddot{\theta}$ in the Kalman filter. Of course this would not be the case if the human were presented or could derive, target acceleration cues.

1.4.3 Target Image Effects

Experimental results with and without the target image showed that
1) mean tracking errors were always reduced, but 2) error standard deviations had mixed changes when the human tracked a realistic image. It also appears that the structural form of $\bar{e}(t)$ tends to become slightly more symmetric when the visual cues are added.

Several different assumptions for modeling the added information are considered in Section 3.4. It is assumed that the visual cues can modify indifference thresholds and can provide information relative to target angular velocity $\dot{\theta}(t)$, and possibly angular acceleration, $\ddot{\theta}(t)$. These can be brought into the OCM structure by defining additional "observations".

$$y_3(t) = \dot{\theta}_T(t) ; y_4(t) = \ddot{\theta}_T(t) \quad (1.22)$$

Note that in order to write the observations y in the form of Eq. (1.3), when $y_4(t)$ is included, we must use an acceleration model for the target, Eq. (1.20a-b). Thus, $y_3(t) = x_1(t)$ and $y_4(t) = x_2(t)$.

We have addressed the problem of intra-axis attention allocation (using a steady-state model), and have found that $\dot{\theta}$ information has a small effect on performance, whereas $(\dot{\theta}, \ddot{\theta})$ information gives a large improvement in performance. With intra-axis attention allocation considered, a 50-50 split in attention between (e, \dot{e}) and $(\dot{\theta}, \ddot{\theta})$ was found to be best. Running the OCM for the tracking task with the expanded information base, and the acceleration model[†], gave predictions of mean tracking error that did not adequately match the data. The structural form of $\bar{e}(t)$ differed substantially from the data, and the error magnitudes were much too small. This leads us to conclude that little or no useful acceleration information is contained in the target image. Our

[†] Note that estimates of z_1 and z_2 are now generated, i.e. $z_2(t) \neq 0$.

present assumption is that the image does provide additional velocity information, $\dot{\theta}_T$. This does not alter the structural form of $\bar{e}(t)$, yet provides the potential for enhanced error rate information.

1.4.4 Inter-axis Attentional Allocation

As expected, the experimental results showed that single-axis tracking errors are less than their counterpart two-axis errors. The OCM includes attention allocation via a modification of the observation noise covariance. It further presupposes that the human chooses the attentions f_1 to minimize the cost functional $J(u^*, f)$. The problem of optimizing the measurement subsystem with respect to f_1 has been solved, but only for steady-state (stationary) manual control tasks [10]. If one is to model the results of the target tracking experiments, it is necessary to solve the dynamic attentional allocation problem. This is a very difficult requirement.

For a two-axis tracking task it can be shown that

$$J(u^*, f) \approx \frac{1}{T} \int_0^T [L_e \Sigma_A(t) L_e' + L_e \Sigma_E(t) L_e'] dt + \dots \quad (1.23)$$

where T is the time interval, L_e are "equivalent" gains and Σ_A (Σ_E) is the azimuth (elevation) axis filter Riccati solution. $\Sigma(t)$ is a function of $V_y(t)$, and thus of $f(t)$, via Eq. (1.5). An ad-hoc attention allocation scheme was proposed in Ref. [2], under the assumption that "optimal" attention was proportional to $L \Sigma L'$. The result was

$$f_A(t) = (1 + R)^{-1} \quad (1.24)$$

$$f_E(t) = 1 - f_A(t) ; \quad R = \frac{L_e \Sigma_E L_e'}{L_e \Sigma_A L_e'} \quad (1.25)$$

In Section 3.3 it is shown that this simple model gives reasonable results in reproducing the attention vs. no attention trends in the data. This brings up the question of whether development of a more complex dynamic attention

model is warranted. The question may be answered in part by comparing model predictions of tracking errors obtained with somewhat different, but plausible, ad-hoc attention allocation schemes. Accordingly, the ratio R in Eq. (1.24) was replaced with R^p where we consider $p=1$ (as before), $p=2$ and $p=\infty$. The latter case corresponds to 0-1, or time-shared behavior between the two axes. Each of these 3 schemes resulted in somewhat different time histories for $f_A(t)$ and $f_E(t)$. However, the various tracking error statistics showed little differences among the 3 schemes. Our conclusion is that almost any plausible inter-axis attention allocation scheme will give rise to very similar ensemble error statistics. Our preference is $p=2$ since Σ has a natural dependence on \sqrt{f} via the Riccati equation (1.12).

1.4.5 Monte-Carlo Modeling Results

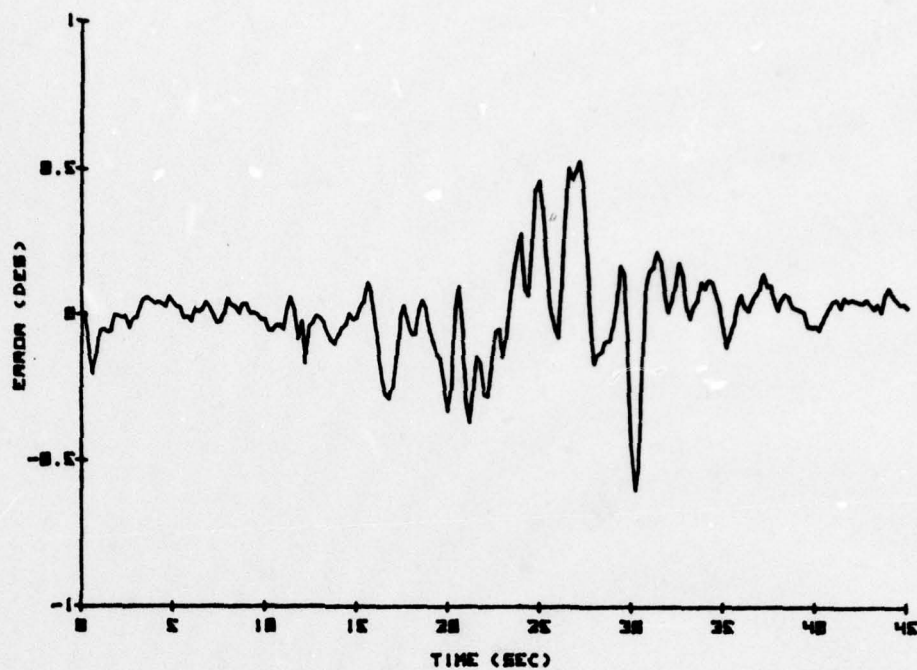
A major effort during the first year of the grant was the implementation of the OCM equations for Monte-Carlo, or sample path, simulation to generate time histories of tracking error, control input, etc., in response to any given target trajectory. Thus, the model mimics the input-output response of the human, complete with random noise generators to produce the operator's internal observation and motor noises. The three basic equations that are simulated are:

1) Kalman Filter

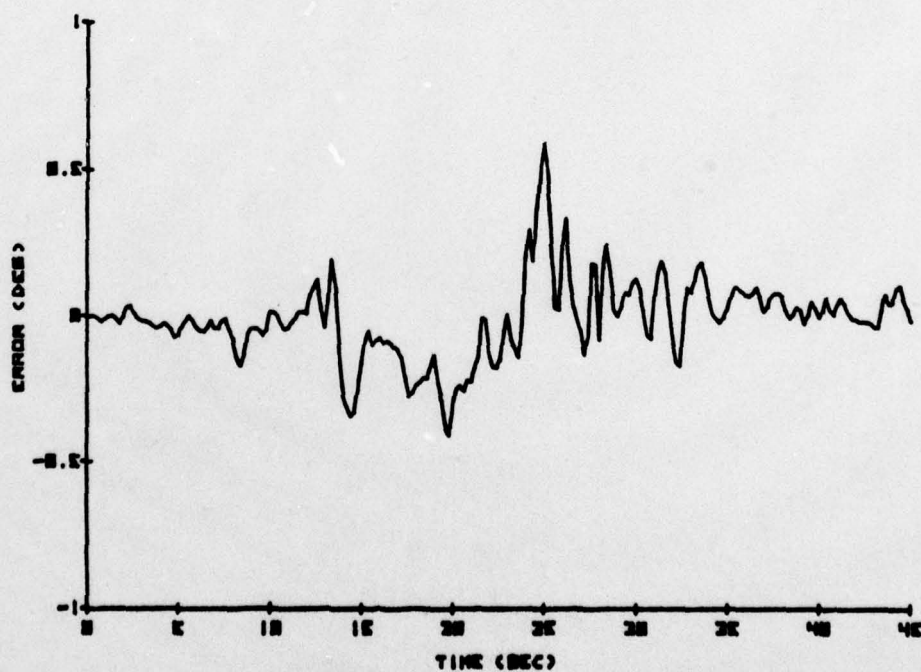
$$\frac{d\hat{x}}{dt}(t-\tau) = A \hat{x}(t-\tau) + B u_c(t-\tau) + G(t) \left[y_p(t) - C \hat{x}(t-\tau) \right] \quad (1.26)$$

2) Predictor

$$\hat{x}(t) = e^{A\tau} \hat{x}(t-\tau) + \int_{t-\tau}^t e^{A(t-\sigma)} B u_c(\sigma) d\sigma \quad (1.27)$$



a) Human Operator Data



b) Model Generated Data

Fig. 8: TYPICAL AZIMUTH ERROR SAMPLE PATHS, S60 SYSTEM

3) Controller

$$\tau_n \dot{u}(t) + u(t) = u_c(t) + v_u(t) \quad (1.28)$$

$$u_c(t) = -L \hat{x}(t)$$

In addition, the covariance equation for Σ must be integrated forward in time.

Using a Monte-Carlo model one can study performance measures not readily available from the averaged ensemble statistics, such as

1. Oscillation frequency content in the responses
2. Autocorrelation and cross-correlation functions
3. Spectral characteristics over time windows
4. Effects of transient phenomena
5. General time-domain oriented items.

Theoretically, the statistics of the ensemble of such model-generated waveforms will agree with the covariance propagation results obtained directly. Moreover, it is possible to study (numerically) the smoothing process in forming ensemble averages,

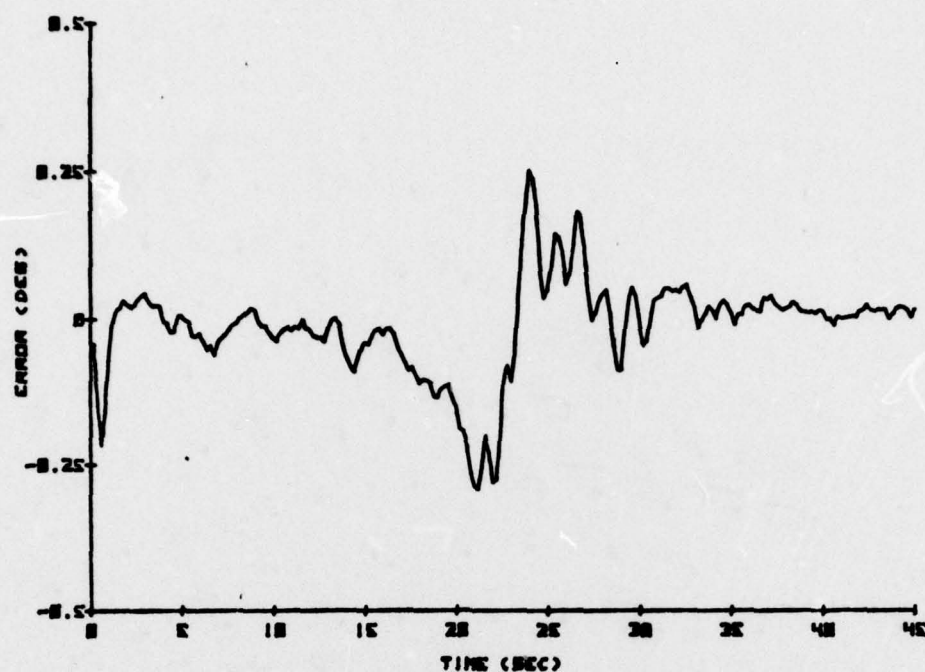
$$\bar{e}_N(t) = \frac{1}{N} \sum_{i=1}^N e_i(t) \quad (1.29)$$

to determine characteristics of $\bar{e}_N(t)$ vs N as $N \rightarrow \infty$.

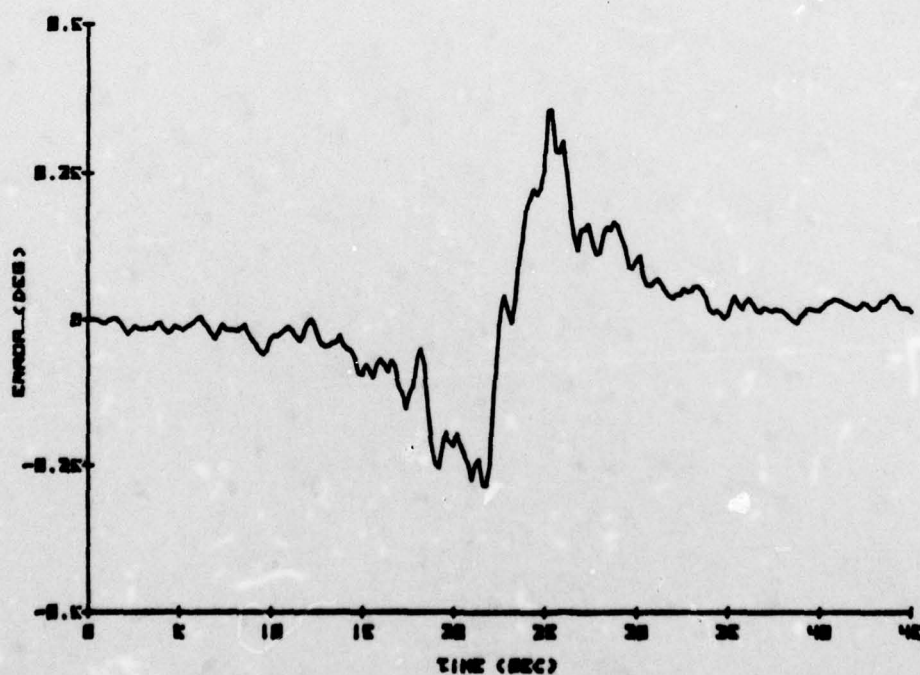
The model has been applied to a k/s azimuth axis tracking task with a straight-and-level aircraft flyby. The model results are compared with Air-Force (AMRL) experimental data gathered on the S60 System. Fig. 8 shows typical time histories of tracking error $e(t)$ generated by both a human and the model. They are quite similar in form, demonstrating oscillatory behavior that is not evident from the predicted ensemble statistics of Fig. 2 alone. As we build an ensemble, the oscillations tend to be smeared-out as the waveforms are averaged via Eq. (1.29). This process is seen in Fig. 9 where data and model ensemble means are presented for $N=15$ sample runs.

As $N \rightarrow \infty$ we expect $\bar{e}_N(t) \rightarrow \bar{e}(t)$ and the sample variance $\sigma_{e_N}(t) \rightarrow \sigma_e(t)$

where

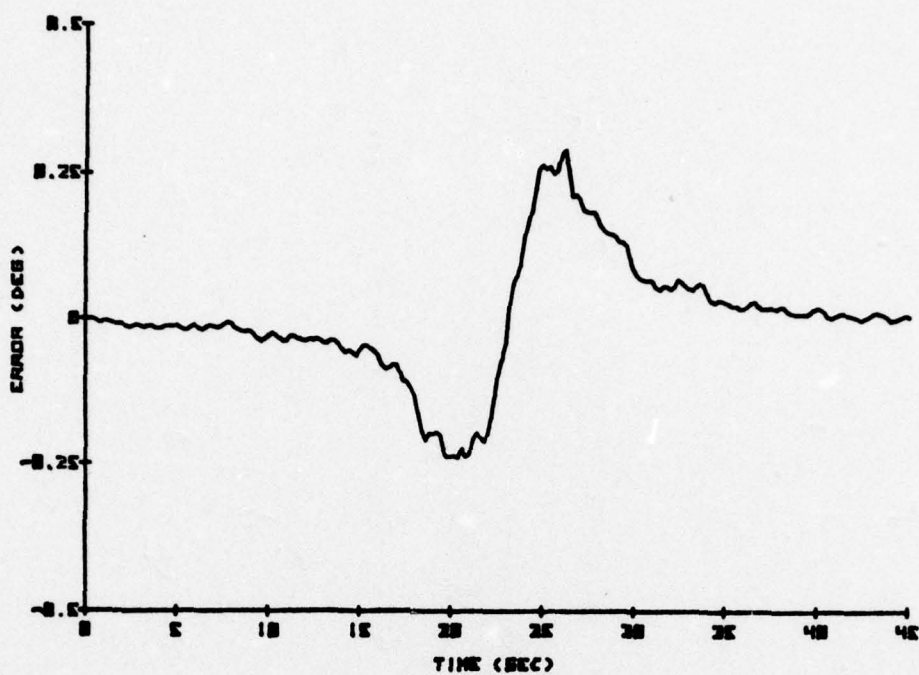


a) Human Operator Data

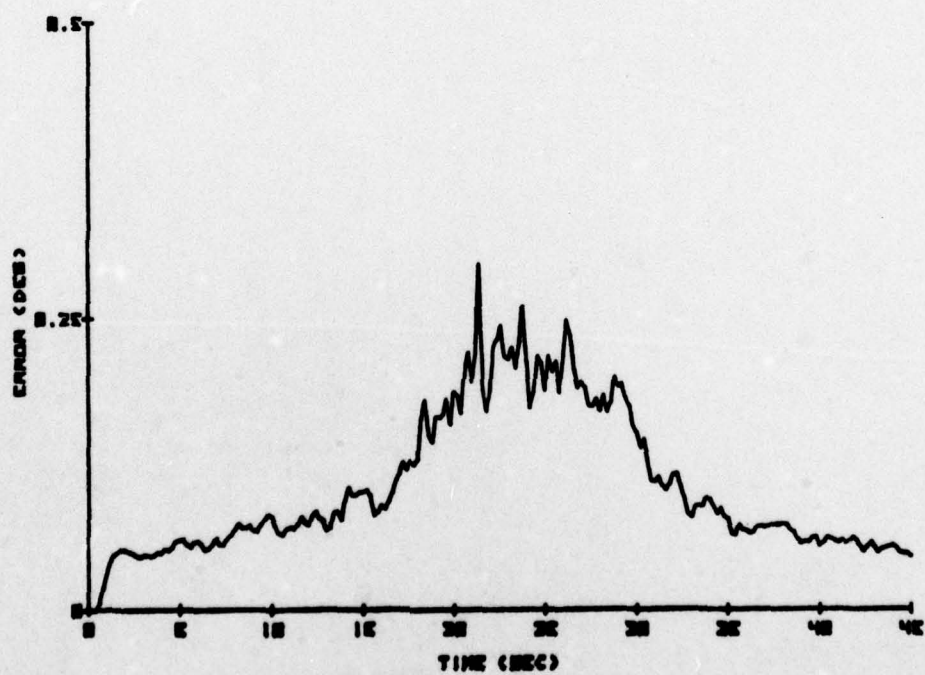


b) Model Generated Data

Fig. 9: CHARACTERISTICS OF ENSEMBLE MEAN AVERAGES, N=15



a) Ensemble Mean



b) Ensemble Standard Deviation

Fig. 10: MODEL-GENERATED AZIMUTH AVERAGES, N=100

$$\sigma_{e_N}(t) = \left\{ \frac{1}{N-1} \sum_{i=1}^N [e_i(t) - \bar{e}_N(t)]^2 \right\}^{\frac{1}{2}} \quad (1.30)$$

This is essentially true. Fig.10 shows the ensemble statistics of $\bar{e}_N(t)$ and $\sigma_{e_N}(t)$ for $N=100$. Compare these with $\bar{e}(t)$ and $\sigma_e(t)$ in Fig. 2. We see that $\bar{e}_N(t) \approx \bar{e}(t)^{\dagger}$, and that the standard deviations agree very well except for a small region near crossover. This "mismatch" is due in large part to temporal averaging of the observation noise covariance in the model implementation [8].

1.5 Summary

The first year's work has been directed towards analyzing the effects of human limitations on target tracking performance in a basic rate command system, by means of a combined analytic-experimental program. Our efforts to-date have focused primarily on the development of a human-centered model for target motion, and transient analysis/sample path simulation. An experimental facility for studying human operator tracking has been established in the Electrical Engineering and Computer Science department at UConn. With this facility, and concomitant OCM analytic efforts we have studied effects of visual cues and inter-axis attentional allocation. Data-model comparisons have been used to isolate plausible model assumptions and hypotheses. Further details on our results are given in Chapters 2 and 3, and in the Appendices.

Research is presently continuing at the University of Connecticut to examine further the various issues that have impact on human tracking performance. Target tracking experiments with interrupted (i.e. blanked) visual

[†] For Gaussian distributions we expect $|\bar{e}_N(t) - \bar{e}(t)| \leq \frac{2}{\sqrt{N}} \sigma_{e_N}(t)$ with 95% probability.

information have been completed, but the results have yet to be analyzed. We will continue sensitivity analyses of model results, and refine our parameter tuning methods. Further experimental/analytic work will focus on optimizing the man-machine interface via selected system/display modifications.

II. EXPERIMENTAL PROGRAM

In the first year of the program, efforts were directed towards establishing an experimental facility that would enable us to study human operator performance in simulated man-machine systems. Our goal was to generate the data needed to both refine and tune the optimal-control model, and to test that model's predictive accuracy. The effort concentrated on the simultaneous development of computer-controlled dynamic simulation and data-acquisition capabilities and involved five phases:

1. Hardware acquisition, configuration and interfacing,
2. Software development,
3. Experimental design and shakedown runs,
4. Final experiments, and
5. Data reduction and analysis.

These are detailed below.

2.1 Hardware

The heart of our experimental facility is a DEC PDP 11/20 computer with dual floppy disks; to this were added later a high-speed DEC-pack disk drive and a magnetic tape unit. An oscilloscope with an eight-inch CRT was connected to the computer's processor, via two digital-to-analog converters, to provide our display medium. The 10 bit D/A converters enable horizontal and vertical deflections of the oscilloscope's beam to any desired point on the screen with a 1024 x 1024 grid resolution.

Sampling the subjects' responses to the displayed stimulus required a spring-centered, two-axis joystick to be wired into the computer's processor via analog-to-digital converters. The A/D's map the joystick deflections in the two axes to digital quantities with a resolution of 10 bits (one part in 1024).

2.2 Software

The operating system of the PDP 11/20 was expanded to run FORTRAN programs, and handle the peripheral devices. Extensive software has been written to:

1. simulate arbitrary controlled-element dynamics of the tracking system,
2. generate simulated target trajectories with arbitrary attitude, altitude and cross-over range,
3. collect data in real time, storing it in memory buffers, and
4. shipping the data to files on mass-storage peripherals for off-line processing.

Our repertoire of target trajectories currently ranges from straight-and-level flybys to some quite complex profiles. For the more complex trajectories, the aircraft bank and/or pitch angles are computed as the sum of up to five sine waves of independent amplitudes, periods and phase angles.[†]

The output data files consist of the sampled time-histories of the tracking errors in azimuth and elevation, and of the joystick control inputs in these axes. The sampling time $T_s = .025$ sec. Additional subroutines were written to:

1. retrieve the output data files,
2. perform preliminary sequential analyses on the raw data, such as ensemble mean, variance, temporal RMS error scores,
3. compute ensemble t-tests to detect statistically significant differences among the experimental conditions (at any one of five levels of significance), and
4. to display the results in graphic form on the CRT screen and/or to produce hard copy on an X-Y plotter.

It was necessary to write special purpose software to display the simulated target on the screen and to sample the subject's control input signal. The standard DEC-supplied asynchronous interrupt-handling routines (LPSLIB)

[†]This is not a restriction -- any time history of $\phi(t)$ and/or $\gamma(t)$ may be used.

proved much too slow for real-time simulation of high-bandwidth dynamics. Even under the most favorable circumstances it could not effect sampling rates in excess of 10/second. Writing our own software enabled us, at the outset, to sample consistently at 20/second; further refinements and optimization increased the rate to 40/second for both sampling the input signal and refreshing the display. This rate of 40/second was used throughout the formal experimental runs.

2.3 Pre-Experimental Detail

A major goal of our first-year experimental program was to provide a data base for refining the Optimal Control Model of human response, with emphasis on the human information processing submodel. In order to avoid the attendant complexities of high-order system dynamics, a rate-command system was simulated with transfer function G_p (Figure 11) equal to K_p/s .

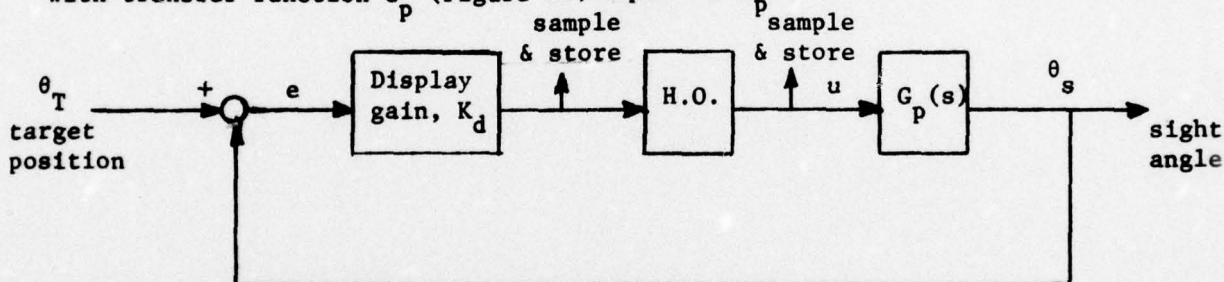


Fig. 11. STRUCTURE OF SIMULATION LOOP

The rate-command gain K_p was set at 1.70 as this value was judged "most comfortable" by subjects during the shakedown runs. The display gain K_d was set to 0.106. At this setting a straight-and-level pass (to be described shortly) fits exactly within one screen-width (8 inches).

2.3.1 Forcing Functions

The forcing function $\theta_T(t)$ was the position of a delta-shaped target image during a fly-by trajectory. We have the capability to specify the cross-

over range XOR, initial target altitude IA and its attitude (Figures 12 & 13). The target's velocity is computed from these to produce, in a straight-and-level flyby, a symmetric trajectory subtending a $2 \times 84.26^\circ$ angle (Figure 14), independent of the cross-over range. Therefore, all straight-and-level flybys effect identical profiles of angular velocity and angular acceleration ($\dot{\theta}_T$ and $\ddot{\theta}_T$, respectively) regardless of cross-over range. The only range cue is the size of the target image.

We used three trajectories (labeled "A", "B" and "C") which were defined as follows (see Figure 12):

Trajectory "A": IA = 50 ft., XOR = 50 ft., $\beta = \alpha$ (S & L fly by)

Trajectory "B": IA = 2000 ft., XOR = 2000 ft., $\beta = \alpha$ (S & L fly by)

Trajectory "C": IA = 50 ft., XOR = 100 ft., $\beta \neq \alpha$; the target follows a path in the vertical plane with its flight path angle γ defined by

$$\gamma(t) = \sin\left(\frac{2\pi}{T}t + 1\right) - 0.5 \sin\left(\frac{4\pi}{T}t - 0.5\right) + 0.5 \sin\left(\frac{6\pi}{T}t + 0.5\right) + 0.3 \sin\left(\frac{10\pi}{T}t + 0.375\right) \text{ radians}$$

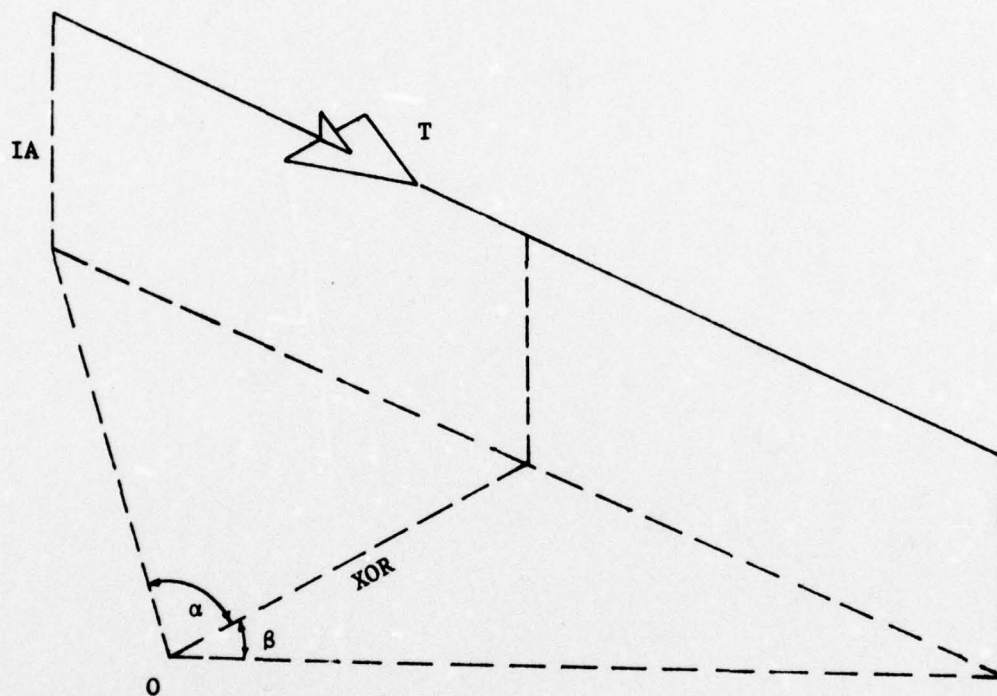
where T is the total time for a run.

Trajectories "A" and "B" looked identical -- that is, their forcing functions $\theta_T(t)$ were identical -- except that the target image was much smaller for trajectory "B" (due to its further range) and looked like a dot on our CRT screen.

2.3.2 Subjects and Training

Some thirty candidates were screened as potential subjects for our experiments. Of these, about half were then selected to participate in the experimental program, based on their ability, attitude and enthusiasm. These subjects were then trained on a variety of simulated trajectories, including the three flybys described above, until their performance met a preset criterion.

Fig. 12. GEOMETRY OF TARGET FLYBY



- T = Target
- O = Observer
- IA = Initial Altitude
- XOR = Cross-Over Range

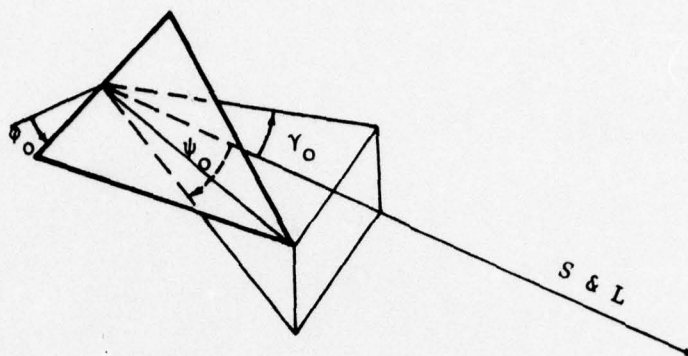


Fig. 13. ATTITUDE OF AIRCRAFT IMAGE

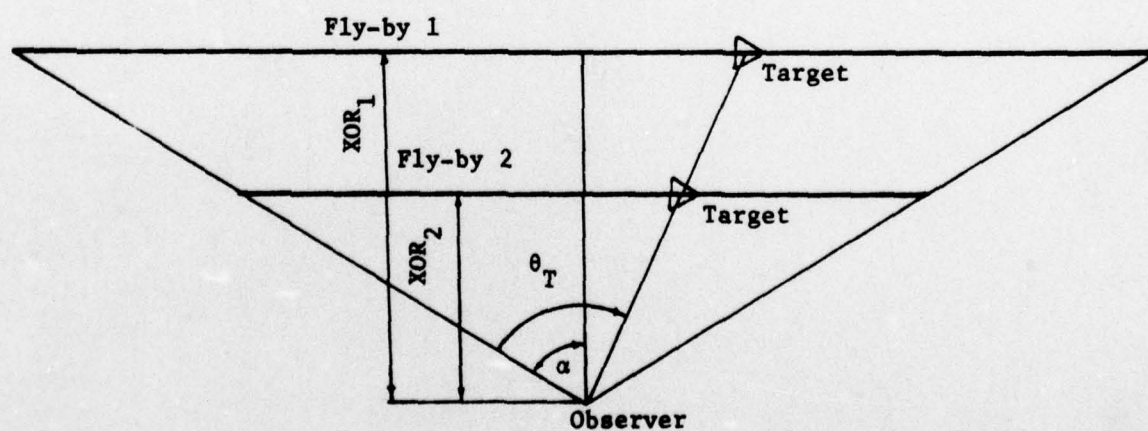


Fig. 14. EQUIVALENCES FOR STRAIGHT-AND-LEVEL PASSES

ion (RMS tracking error consistently below 5° in both azimuth and elevation). We chose our subjects from among the University's undergraduate students, graduate students and staff for the first two experiments (to be described in the next section) and from among Air Force ROTC candidates for subsequent experiments. All our subjects were male. Their ages ranged from 20 to 53 years for the seven subjects in the first group, with a mean of 31; the ages of the ROTC group ranged from 20 to 23 years with mean age of 21. There was one pilot, one subject with sharpshooting experience and one person with AAA experience in the first group. In the ROTC group there were three pilots, two sharpshooters and two subjects with some experience as radar operators. The training and familiarization runs were intended to ensure data homogeneity in spite of these diverse backgrounds by bringing all subjects to a common level of proficiency before the formal experimental runs. In addition, the data which were obtained from the individual subjects in the course of the formal experiments were tested for outliers, which were then eliminated from further analysis. This procedure will be discussed in more detail in the section on Data Reduction and Analysis.

2.4 Experimental Design

2.4.1 Visual vs. No Visual Cues

Our first experiment was designed to detect possible effects on tracking errors of direct observations of target visual cues such as target size and aspect ratio. A 3×2 factorial design was utilized, so that each of the seven subjects tracked three different trajectories ("A", "B" and "C"). Each trajectory was tracked both under conditions of "visual cues present" (i.e., a realistic target image) and of "no visual cues" (the target image retained a fixed size and shape). These six conditions were repeated by each subject from three to twelve times, depending on the subject's availability, in randomized blocks of 18 runs each.

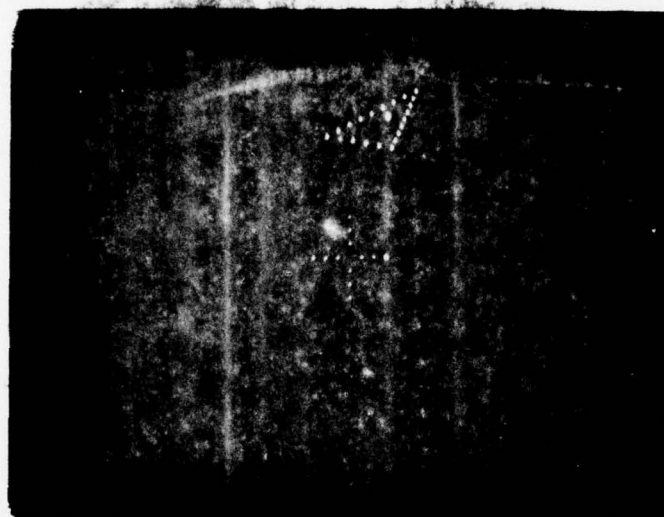


Fig. 15a: TARGET IMAGE WITH VISUAL CUES SIMULATED

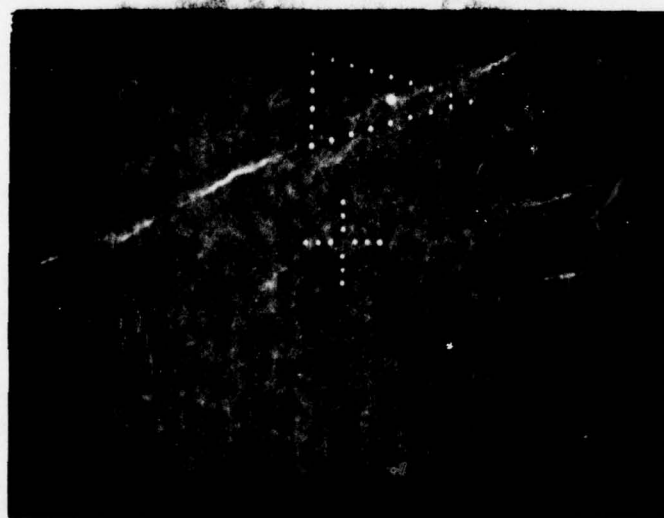


Fig. 15b: TARGET IMAGE WITH NO VISUAL CUES

The display presented a symbolic cross-hairs centered on the CRT screen (Fig. 15a) and a triangular target. Under the "visual cues present" condition the triangular image simulated a delta planform. It varied in size and shape as the simulated target's range, bearing and altitude varied (see Appendix A for details). Under the "no visual cues" condition, the triangular target followed identical trajectories but the triangle retained a fixed size and aspect ratio throughout the run (Fig. 15b).

Each experimental run lasted 25.575 seconds. At a sampling rate of 40/second we thus collected 1024 datum points per run for each variable of interest. The ensemble means and standard deviations of the tracking errors in azimuth and in elevation are grouped in Appendix B.

We have also been collaborating with Ms. Sandra Hart of the Biotechnology Division of NASA-Ames Research Center, who is studying possible correlation between subjective time estimation and mental workload associated with manual tracking. In the framework of this first experiment we recorded at the end of each run the subjects' estimate of the duration of that run. Even though all runs were of identical durations the subjects' estimates varied over a wide range. Subsequent analysis of the data, however, failed to reveal any correlation between the time estimates and the difficulty of the particular trajectory or the tracking performance. (Surprisingly, the means and variances of the time estimates under the different conditions come remarkably close to each other.)[†] We are continuing to collaborate with Ms. Hart and will include further results in next year's program plan.

2.4.2 Inter-axis Attentional Allocation

We attempted to control the unknown effects of inter-axis attention-

[†]It may be that intersubject variability masks any differences due to workload.

sharing in our second set of runs. This experiment was of a 2 x 2 factorial design, with each subject tracking two trajectories ("A" and "B") in azimuth alone (with the error in elevation clamped at zero) and in elevation alone (with zero azimuth error). Each of the three subjects repeated the experiment 6 times in a randomized order, for a total of 18 runs for each experimental condition.

As mentioned earlier, trajectories "A" and "B" were equivalent with respect to the forcing function θ_T and differed only by the range to the target and hence, by the size of the displayed target. Within the bounds imposed by the resolution of our equipment, the target image in trajectory "B" resembled a dot and hence trajectories "A" and "B" represented equivalent flybys, with visual cues and without visual cues, respectively. During the data-reduction phase that followed the first experiment, we had determined that, from the standpoint of visual cues, a target represented by a dimensionless dot and a target represented by a triangle of fixed size and shape were not different statistically.

The results of this set of runs are also grouped in Appendix B.

2.4.3 Interrupted Observations

A third experiment was begun during the last months of the first year. In this set of runs we attempted to investigate some transient and target-acquisition modes via interrupted observations. We are now in the data analysis phase of this study.

2.5 Data Reduction and Analysis Methods

Four variables were sampled and stored during each formal run: the instantaneous tracking errors in azimuth and elevation, and the control stick positions in these two axes. At a sampling rate of 40/second, each 25.575-second run produced 1024 datum points for each of these four variables. In

addition, some header information, such as forcing function, subject identification symbol, date and time of run, etc., was recorded.

The first step in analyzing this vast amount of data was to aggregate, i.e., to compute and store the point-by-point ensemble means and mean-squares. We utilized a sequential approach to the computation, by which the mean m_{k+1}^j of the j -th point ($0 < j \leq 1024$) of $k+1$ runs was computed from m_k^j by

$$m_{k+1}^j = \left(m_k^j \cdot k + z_{k+1}^j \right) / (k + 1) \quad (2.1)$$

where z_{k+1}^j is the value of the j -th point in the $(k+1)$ -th run, and $m_0^1 = 0$, $i = 1, 2 \dots 1024$.

The mean-square q_{k+1}^j was computed similarly from q_k^j by

$$q_{k+1}^j = \left(q_k^j \cdot k + (z_{k+1}^j)^2 \right) / (k+1) \quad (2.2)$$

and the unbiased estimate of the variance, v_k^j , was then found from

$$v_k^j = \left(q_k^j - (m_k^j)^2 \right) \cdot k / (k-1) \quad (2.3)$$

Utilizing the ensemble means and variances, two-sided t -tests could be performed (with the appropriate number of degrees of freedom) to test the null hypothesis of equality of the means. We first tested the assumption that our subjects came from a homogeneous population. If they did, then the mean tracking error of each subject should not be statistically different from the mean tracking error of all the subjects combined. For each subject we compared the mean tracking errors in azimuth and elevation to the corresponding mean tracking error of all the subjects combined for the same experimental conditions (trajectory, visual cues/no visual cues). We found that the mean tracking errors of one of the seven subjects were significantly different in the crossover region ($P_\alpha < 0.01$). This subject's data was removed from the combined mean,

and the averaging process was then repeated with the data of the remaining six subjects. The data obtained from the one outlying subject was not used in any of the subsequent analyses.

Plots of the summarized data are grouped in Appendix B. As expected, the availability of visual cues (target image's size and shape) effected smaller tracking errors ($P_\alpha < 0.05$) and error variances. Unexpected, however, were some characteristics of the data, such as

1. the asymmetry in the tracking error profile before and after crossover, with a tendency to lag prior to crossover,
2. the slight lagging tendency during the first 5 seconds of the run,
3. the smaller variance associated with the tracking error in elevation without visual cues (trajectory C) than with visual cues (Figures B6 vs. B12).
4. the large ($\sim 1^\circ$) standard deviations in the tracking errors during periods of good mean tracking.

The last point has been attributed to the choice of small display gain, $K_d \sim 1/9$, which in turn, resulted in large visual/indifference thresholds for the subjects. Thresholds vary inversely with display gain.[†] In previous studies, visual thresholds used in the OCM were in the order of $.15-.2^\circ$. Thus, we might expect values for $a_1 \approx 1.5-2.0^\circ$. An analysis of the display image/resolution gives comparable numbers: For example, the angle between the center of the "crosshairs" and the first dot is $\beta \sim 4.5^\circ$. When we lack an explicit zero reference point, the OCM adds an observation noise $V = .01\pi\beta^2$. It can be shown that this effect is almost equivalent to a threshold of value $\beta/3$ (This corresponds to a "middle-third" indifference region). Finally, the minimal quanta of display resolution is $168/1024 = .16^\circ$. With a spot of light smearing over 10-15 quanta, a $1.5-2.0^\circ$ threshold value is to be expected. Indeed, OCM-data matching gave position threshold values $a_1 \approx 1.5^\circ$.

[†]See also Section 1.3.1.

III. ANALYTIC MODELING

This chapter describes the various modifications and extensions that were made to the OCM during the analytic phase of the project. These include adaptive tracking of target acceleration, methods for modeling visual cues and attentional allocation, and use of generalized first-order aircraft motion models. Model predictions of tracking error statistics are given for comparison with the experimental results of Appendix B.

3.1 Adaptive Tracking Problem

A weighted-least-square technique is proposed for estimating higher derivative target information from the OCM Kalman filter residuals process. The results have application in areas beyond human operator modeling in systems with non-random inputs. Some of these areas are:

- Compensation of modeling errors caused by linearization of non-linear systems
- Design of adaptive filters to determine the path of a maneuvering target
- Estimation of unknown, time-varying mean and variance of a random input disturbance
- Detection of sudden changes in the state of a system with application to failure detection

3.1.1 Problem Background

The relevant discretized equations that describe the OCM in non-stationary systems are given in Ref. [7]. For notational simplicity in the subsequent development it is assumed that $N = \tau/\delta = 0$. This is not a theoretical restriction as the Kalman filter/estimator does not involve state prediction. The (augmented) state equation of the system is given by[†]

[†]We follow the notation and definitions of Ref. [7].

$$x_{k+1} = \phi_k x_k + B_k u_{c,k} + E_k w_k + F_k z_k \quad (3.1)$$

where z_k is a deterministic input that represents the target motion. It is assumed that z_k is unknown to the human.

The Kalman filter generates p_k , the (a priori) estimate of x_k , from the observations

$$y_{pk} = C_k x_k + v_k \quad (3.2)$$

The estimation error $e_k = x_k - p_k$ is given by

$$e_{k+1} = \tilde{\phi}_k e_k - \phi_k G_k v_k + E_k w_k + F_k z_k \quad (3.3a)$$

or, equivalently by

$$e_{k+1} = \phi_k e_k + E_k w_k + F_k z_k - \phi_k G_k v_k \quad (3.3b)$$

where G_k is the filter gain and $\tilde{\phi} = \phi(I - GC)$ is the closed-loop filter matrix.

The innovations process is

$$v_k = y_{pk} - C_k p_k = C_k e_k + v_k \quad (3.4)$$

When the Kalman filter is optimal, v_k is a zero-mean white noise sequence.

However an input z_k renders v_k non-white. This fact will be exploited to generate \hat{z}_k , an estimate of z_k .

In the OCM a pseudo-noise matrix $F_k W_{d,k} F_k'$ is added to the filter Riccati equation to account for the human's uncertainty in the signal z_k . It has been shown that choosing

$$W_{d,k} = \text{diag} \left[\frac{\tau_{c1}}{\delta} z_{k,1}^2 \right]; \quad \tau_{c1} \approx 1 \quad (3.5)$$

approximately minimizes the mean-square filtering error, and results in model predictions that match data quite well (see Figs. 1-4). Eq. (3.5) has physical appeal, as the uncertainty in target estimation, (and hence the Kalman filter bandwidth), increase as target motion z_k increases. However, there is an

inconsistency in this model: z_k was assumed to be unknown to the human!

A way out of this dilemma is the obvious modification of Eq. (3.5) to replace z_k with an on-line computed estimate \hat{z}_k .

3.1.2 Adaptive Estimation Algorithm

Eqs. (3.3-3.4) are the basic set of equations for generating \hat{z}_k . Taking expectations, noting that $\bar{w}_k = 0$, $\bar{v}_k = 0$ and $\bar{z}_k = z_k$, yields

$$\bar{e}_{k+1} = \bar{\phi}_k \bar{e}_k + F_k z_k \quad (3.6a)$$

$$\bar{v}_k = C_k \bar{e}_k \quad (3.7)$$

From "measurements" of \bar{v}_k (the signal v_k is readily available in the Kalman filter), we will obtain an estimate of z_k . Note that this problem is tantamount to designing the inverse system to Eq. (3.6-3.7).

In actual implementation an estimate of \bar{v}_k would be obtained by on-line filtering (i.e., averaging) of v_k . We would thus obtain an estimate of $C_k \bar{e}_k$, where \bar{e} now denotes the temporal mean, from

$$\bar{v}_k = C_k \bar{e}_k + \bar{v}_k \quad (3.8)$$

where \bar{v}_k is filtered white observation noise.

Solving Eqs. (3.6a-3.7) for \bar{v}_k , assuming $\bar{e}_0 = 0$, yields

$$\bar{v}_k = C_k \sum_{i=0}^{k-1} \tilde{\Psi}(k-1, i) F_1 z_i \quad (3.9)$$

where

$$\tilde{\Psi}(k-1, i) = \tilde{\phi}_{k-1} \tilde{\phi}_{k-2} \dots \tilde{\phi}_{i+1} ; \tilde{\Psi}(j, j) = I \quad (3.10)$$

If $\hat{z}_{1/k}$ $i \leq k$ denotes the estimate of z_i given all the measurements $\{\bar{v}_0, \dots, \bar{v}_k\}$ then our best estimate of \bar{v}_k is

$$\hat{\bar{v}}_k = C_k \sum_{i=0}^{k-1} \tilde{\Psi}(k-1, i) F_1 \hat{z}_{1/k} \quad (3.11)$$

The estimates $\hat{z}_{1/k}$ can be obtained via a weighted-least-squares method to minimize the criterion (at step k),

$$J_k = \sum_{j=0}^k \beta^{k-j} \left\| \bar{v}_j - \hat{v}_j \right\|_{R_j}^2 \quad (3.12)$$

where R_j is an NY by NY diagonal matrix used to give relative weighting to the importance of each measurement $\bar{v}_{j,i}$; $i=1, \dots, NY^+$. The constant $0 < \beta < 1$ is a fading memory factor used to place greater emphasis on the more recent data. This is particularly helpful when z varies rapidly.

The minimization of J_k , Eq. (3.12), is a formidable problem as it requires the recomputation (i.e. smoothing) of past estimates \hat{z}_i . Thus storage and CPU time increase with k . Since there is no evidence of such behavior in human operator tracking, we simplify the WLS problem by replacing the smoothed estimate $\hat{z}_{1/k}$ in Eq. (3.11) with the filtered estimate $\hat{z}_{1/i+1}$. The minimization of J_k with respect to the on-line computable quantity $\hat{z}_{1/i+1} \triangleq \hat{z}_1$ follows least-squares theory. Define the "effective" measurement \tilde{y}_k as

$$\tilde{y}_k = \bar{v}_k - C_k \Phi_{k-1} \sum_{i=0}^{k-2} \tilde{\Psi}(k-2, i) F_i \hat{z}_i \quad (3.13)$$

Thus, by construction,

$$\begin{aligned} \tilde{y}_k &= C_k F_{k-1} \hat{z}_{k-1} + \epsilon_k \\ &= H_k \hat{z}_{k-1} + \epsilon_k \end{aligned} \quad (3.14)$$

where ϵ_k is the residual $\bar{v}_k - \hat{v}_k$, and H_k is NZ by NY.

The estimate \hat{z}_{k-1} (obtained at step k) is generated recursively according to

[†]If $R_j = \text{cov} [\bar{v}_j - \hat{v}_j]$ we obtain a minimum variance estimator, assuming white residual sequence. Plausible choices are $R_j = V_j$ or $R_j = I$.

$$\hat{z}_{k-1} = \hat{z}_{k-2} + \Gamma_k (\tilde{y}_k - H_k' \hat{z}_{k-2}) \quad (3.15)$$

where

$$\Gamma_k = S_k^- H_k' (H_k' S_k^- H_k + R_k)^{-1} \quad (3.16)$$

$$S_k^+ = S_k^- - S_k^- H_k' (H_k' S_k^- H_k + R_k)^{-1} H_k' S_k^- \quad (3.17)$$

$$S_{k+1}^- = \frac{1}{\beta} S_k^+ \quad (\text{time propagation})$$

and $S_0^- = 10^5 I$ is the initial condition. The update Eq. (3.17) can also be written in the more computationally stable Joseph's form,

$$S_k^+ = (I - \Gamma_k H_k') S_k^- (I - \Gamma_k H_k')' + \Gamma_k R_k \Gamma_k' \quad (3.17a)$$

The least squares algorithm operates most efficiently when the NY "measurements" $\tilde{y}_{k,1}, \dots, \tilde{y}_{k,NY}$ are processed through the update sequence Eqs. (3.15)-(3.17) one at a time. Dropping the time index, for simplicity, the pertinent recursive replacements are, for $i = 1, \dots, NY$

$$\begin{aligned} \gamma &= S h_i' (h_i' S h_i' + r_i)^{-1} \\ S &\leftarrow (I - \gamma h_i') S \quad (\text{or use Joseph's form}) \\ \hat{z} &\leftarrow \hat{z} + \gamma (\tilde{y}_{k,i} - h_i' \hat{z}) \end{aligned}$$

If we start with $\hat{z} = \hat{z}_{k-2}$, $S = S_k^-$ we end up with $\hat{z} = \hat{z}_{k-1}$ and $S = S_k^+$. It is worth noting that if we define $\Sigma = \beta S$, the Equations (3.16-3.17) remain the same but with Σ replacing S and βR_k replacing R_k .

The above algorithm for \hat{z} is very simple to implement and requires minimal extra storage. In computing \tilde{y}_k via Eq. (3.13) note that the summation term is \hat{e}_{k-1} , i.e. the result of passing \hat{z}_1 , $1 \leq k-2$ through the "system" Eq. (3.6a) with initial condition $\hat{e}_0 = 0$. Thus, \tilde{y}_k is easily obtained recursively by using

$$\hat{e}_{k-1} = \tilde{\phi}_{k-2} \hat{e}_{k-2} + F_{k-2} \hat{z}_{k-2} \quad (3.18a)$$

and

$$\tilde{y}_k = \bar{v}_k - C_k \tilde{\phi}_{k-1} \hat{e}_{k-1} \quad (3.19a)$$

3.1.3 Modifications and Extensions

The WLS algorithm, as derived, was based upon Eq. (3.3a) which involves the closed-loop matrix $\tilde{\phi}_k$. An alternate formulation is based on using Eq. (3.3b), involving the open-loop system matrix ϕ_k . Taking expectations of Eq. (3.3b) yields

$$\bar{e}_{k+1} = \phi_k \bar{e}_k + F_k z_k - \phi_k G_k \bar{v}_k \quad (3.6b)$$

where the "measurements" \bar{v}_k are known. If we use Eq. (3.6b) in lieu of Eq. (3.6a) in estimating \hat{z}_{k-1} , we find that all of the previous equations remain exactly as before, except that the estimated mean and "measurement" Eqs. (3.18a)-(3.19a) become, respectively

$$\hat{e}_{k-1} = \phi_{k-2} \hat{e}_{k-2} + F_{k-2} z_{k-2} - \phi_{k-2} G_{k-2} \bar{v}_{k-2} \quad (3.18b)$$

$$\tilde{y}_k = \bar{v}_k + C_k \phi_{k-1} G_{k-1} \bar{v}_{k-1} - C_k \phi_{k-1} \hat{e}_{k-1} \quad (3.19b)$$

We have found that these equations produce somewhat better estimates of \hat{z}_k than do their closed-loop counterparts. Fig. (16) shows open-vs-closed loop results for the k/s tracking system with a straight-and-level flyby. The estimation of $z_k = \ddot{\theta}_k$ is excellent; model predictions of \bar{e} and σ_e (not shown) are virtually identical for these cases.

Another modification to the basic algorithm gathers more information before estimating. Of course this introduces a lag into the process. We assume that z_k is constant over the last $l \geq 1$ time steps, i.e.

$$z_{k-1} = z_{k-2} = \dots = z_{k-l}$$

and we estimate \hat{z}_{k-1} . This modifies Eqs. (3.13-3.14) to

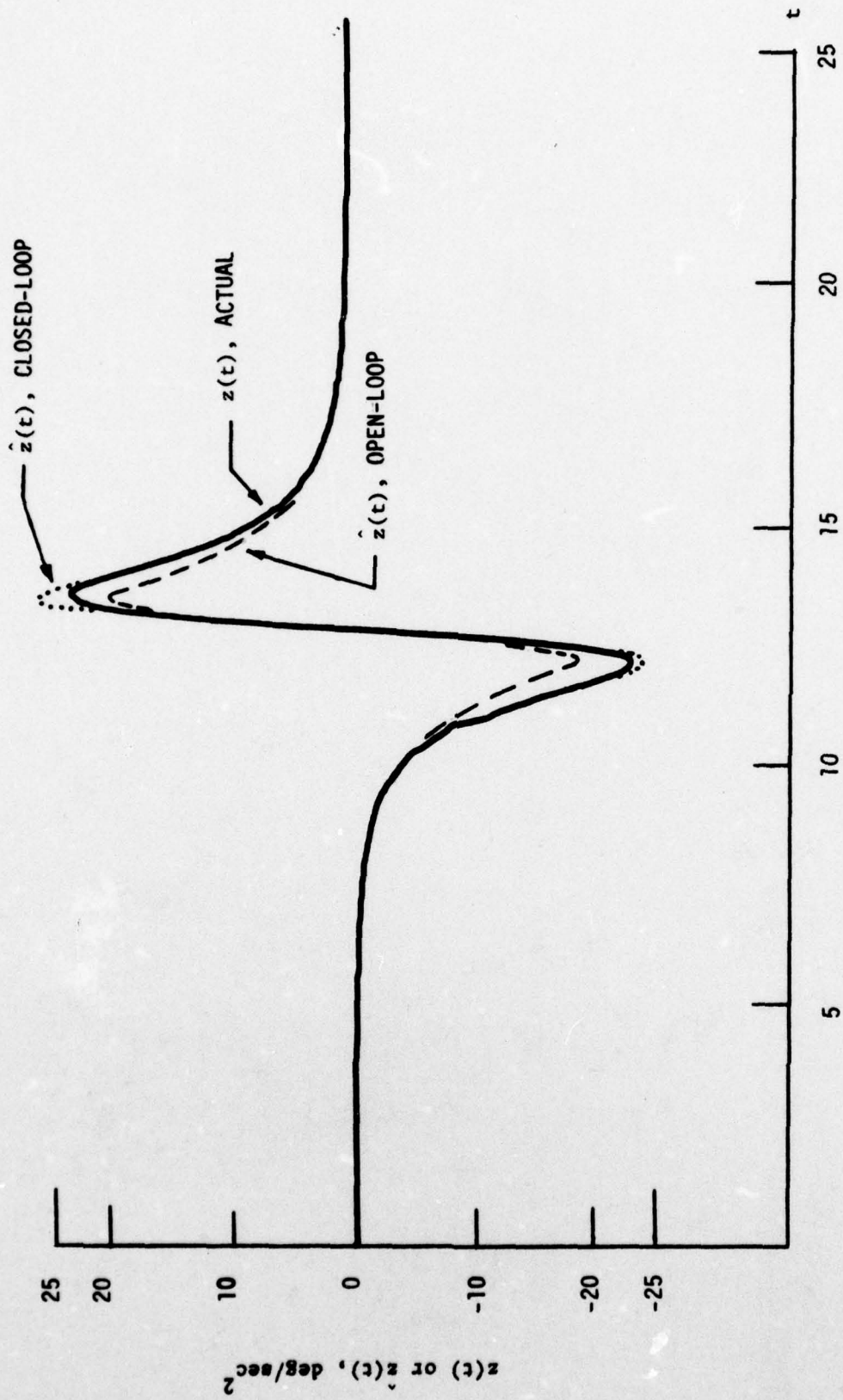


Fig. 16: COMPARISON OF BIAS ESTIMATION SCHEMES

$$\begin{aligned}
\tilde{y}_k &= \tilde{v}_k - C_k \sum_{i=0}^{k-1-\ell} \tilde{\Psi}(k-\ell, i) F_i \hat{z}_i \\
&= \tilde{v}_k - C_k \tilde{\phi}_{k-1} \tilde{\phi}_{k-2} \cdots \tilde{\phi}_{k-\ell} \hat{e}_{k-\ell}
\end{aligned} \tag{3.20}$$

where

$$\hat{e}_{k-\ell} = \tilde{\phi}_{k-1-\ell} \hat{e}_{k-\ell-1} + F_{k-1-\ell} \hat{z}_{k-1-\ell} \tag{3.21}$$

and Eq. (3.14) becomes

$$\begin{aligned}
\tilde{y}_k &= \left[\sum_{i=k-\ell}^{k-1} C_k \tilde{\Psi}(k-1, i) F_i \right] \hat{z}_{k-1} + \epsilon_k \\
&= H_k' \hat{z}_{k-1} + \epsilon_k
\end{aligned} \tag{3.22}$$

In this latter case the matrix H_k will become better conditioned as ℓ is increased.

In many situations, such as in an aircraft subject to turbulence, the human does not know a priori which states of the system are affected by z_k . Therefore, it is necessary to extend the estimation scheme to allow for z to affect any state (or a subset of states such as those associated with the target motion). This is possible by setting $F = I$, and $H_k = C_k'$ in the algorithm. We now will estimate a full NX -dimensional vector \hat{z} , and construct the Kalman pseudo-noise matrix via

$$W_{d,k} = \text{diag} \left[\frac{\tau_{c1}}{\delta} \hat{z}_{k,1}^2 \right]$$

The modifications to this scheme when z_k is assumed to affect a subset of states is trivial. Application of this method has been made to study the utility of higher-order target models in k/s tracking. Use of an "acceleration"

submodel for the target motion gives a system model

$$\dot{\underline{x}} = \begin{bmatrix} 0 & 1 & 0 \\ 0 & 0 & 0 \\ 1 & 0 & 0 \end{bmatrix} \underline{x} + \begin{bmatrix} 0 \\ 0 \\ -1 \end{bmatrix} u + \begin{bmatrix} 1 & 0 \\ 0 & 1 \\ 0 & 0 \end{bmatrix} \begin{bmatrix} z_1 \\ z_2 \end{bmatrix}$$

$$\underline{y} = \begin{bmatrix} 0 & 0 & 1 \\ 1 & 0 & 0 \end{bmatrix} \underline{x} + \begin{bmatrix} 0 \\ -1 \end{bmatrix} u$$

$$z_1(t) = 0 ; \quad z_2(t) = \ddot{\theta}(t)$$

Application of the estimation scheme gave

$$\hat{z}_1(t) \approx \ddot{\theta}(t) ; \quad \hat{z}_2(t) = 0$$

so that we get the same results as with the basic "velocity" model! This is because

$$C_k F_k = \begin{bmatrix} 0 & 0 \\ 1 & 0 \end{bmatrix}$$

i.e., z_2 does not enter into \tilde{y} . However, these same results would not be true if an $\ell > 1$ step delayed estimation is used as in Eqs. (3.20)-(3.22). In this case the WLS formulation is quite poorly conditioned, and the scheme diverges, $\hat{z}_1 \rightarrow \infty$. The problem is that the continuous CF is not of full rank. If we set $F=I$, allowing uncertainty on all states, the model predictions of $\bar{e}(t)$ and $\sigma_e(t)$ agree with the basic "velocity" model. We conclude that to expect meaningful results from an "acceleration" model, $x_2 = \ddot{\theta}$ must be included within the human's observation set $\{\underline{y}\}$. This is discussed further in Section 3.4.

When $NZ < NY$ the matrix H_k is usually of rank NZ . In this case the estimates of z_k are relatively insensitive to the fading memory factor β over a wide range. For our k/s tracking system with $NZ=1$ this range was .1-.99. However, when $NZ = NX \gg NY$ there is a lower limit to β below which the decrease in S^+ is offset by the increase $1/\beta$, resulting in instability. For our k/s system, this limit $\beta_{\min} \sim .85$. Instability of z_k can sometimes be avoided by

using Eqs. (3.20-3.22), which assume constancy of z_i over an interval, to obtain augmented measurements.

When the innovations sequence $\{v_i\}$ is filtered temporally, in an on-line manner to obtain \bar{v}_k ,

$$\bar{v}_k = b \bar{v}_{k-1} + (1-b) v_k ; \quad b = e^{-\delta/\tau_m} \quad (3.23)$$

it is recommended that a test be performed to determine whether the computed \bar{v}_k is statistically different from zero. If v_k is white, \bar{v}_k is a Gaussian process with

$$\text{Cov}[\bar{v}_k] = \frac{1}{2\tau_m} (v_k + \delta C_k \Sigma_k C_k') = \bar{v}_k \quad (3.24)$$

Thus, a t-test can be performed on each component of \bar{v}_k (using this a priori covariance), thereby effecting a probabalistic editing of \bar{v}_k . Preliminary work, using a covariance propagation model to study the ensemble characteristics of Eqs. (3.23)-(3.24), has shown the following:

1. Model predictions are not very sensitive to the time constant τ_m over the range 0.1-1.0. This is due in part to the use of overall ensemble statistics in Eq. (3.23).
2. Probabalistic editing gives results that are similar to those obtained using Eqs. (3.16)-(3.17) with $R_k = V_k$, i.e. uncertain measurements are discounted.
3. With no probabalistic editing, filtering v_k gives (on the ensemble average) model predictions that are similar to filtering the estimate \hat{z}_k obtained via Eq. (3.15).

On the basis of our limited experience to date, it appears that editing is advantageous and will give improved model-data comparisons. We expect to study this process in more detail, using both covariance propagation and Monte-Carlo models, investigating several different (but related) schemes for applying the editing feature.

Alternate methods for estimating z_k and/or W_d have been investigated in

the course of our work. Two methods estimate z_k from the non-zero-mean property of the suboptimal Kalman filter innovations. A third method represents z_k by an "equivalent" white noise, and then estimates W_d by using innovation correlations with a WLS algorithm. The last method requires excessive computations, whereas the first two methods are quite ad-hoc in nature. None of these other schemes have been implemented, due in part, to the excellent performance of the method we are now using. A description of these alternate methods, along with a brief review of relevant adaptive estimation literature, is given in Ref. [13].

3.2 Modeling Asymmetries in Tracking Errors

The predictions of ensemble error statistics using the OCM are shown in Figs. 17-18, for azimuth and elevation axes, respectively. As discussed previously, the a priori model parameters are

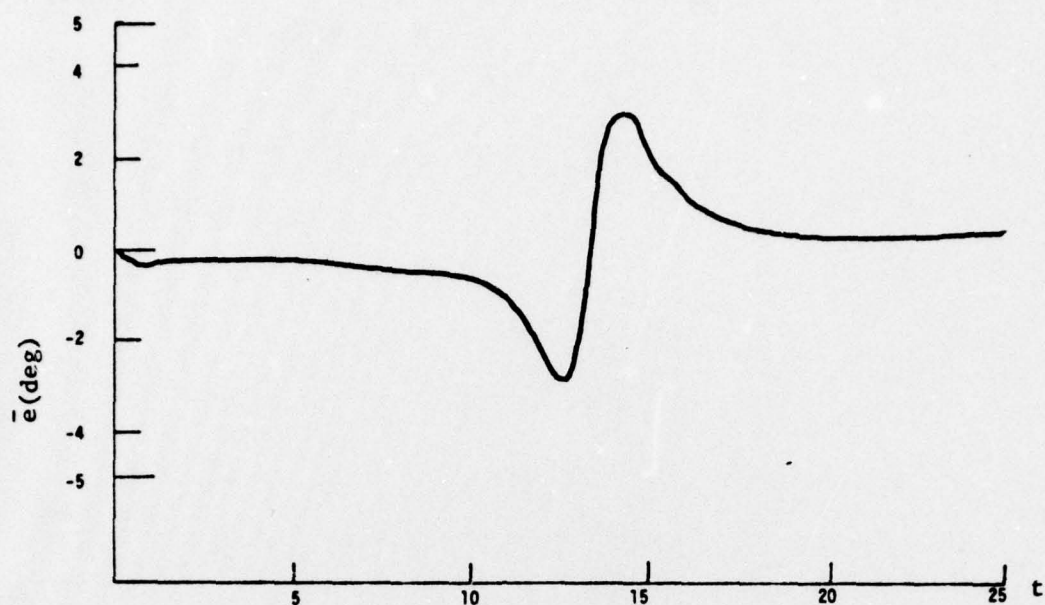
$$\begin{array}{ll} \tau = .2 & \rho_y = -20 \text{ db on all observations} \\ \tau_n = .1 & \rho_u = -20 \text{ db} \end{array}$$

The indifference thresholds were $a_1 = 1.5^\circ$ for position errors and $1.5/2$ for their rates. These results correspond to the case of full attentional allocation, i.e.,

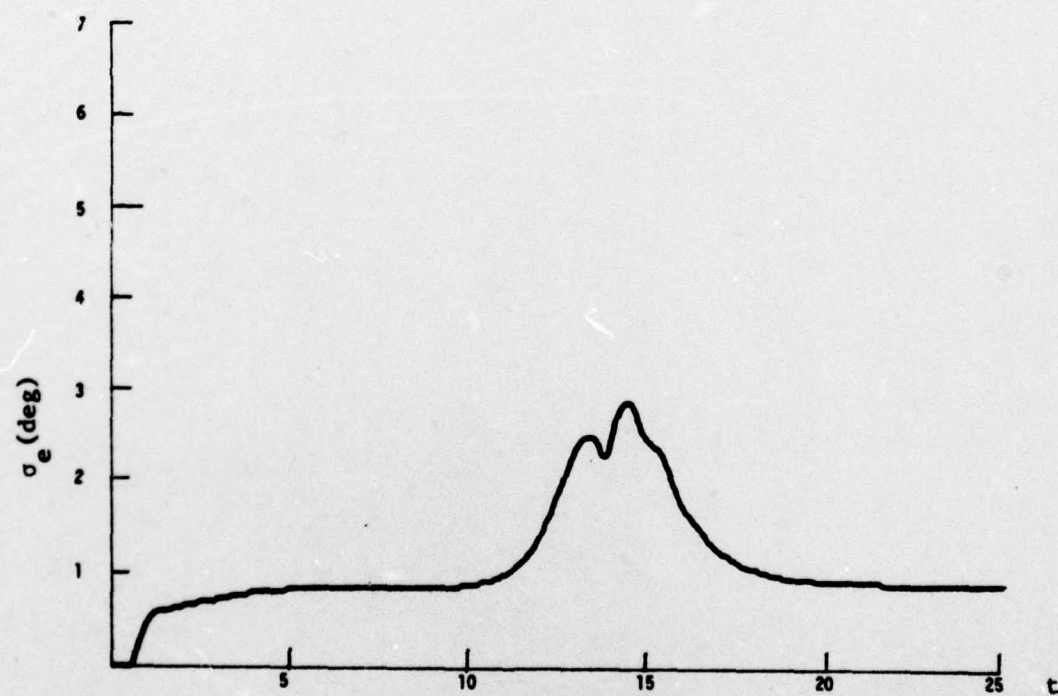
$$f_A = f_E = 1.0$$

and where no model modifications have been introduced for target image effects. Thus, the predictions of Figs. 17 and 18 should be compared with the no visual cues, full attention experimental results of Figs. B1 and B2, respectively.

The model-data agreements are reasonably good -- being generally within 1 experimental standard deviation. However, our concerns in this study are to understand the reasons behind the mismatches, and to modify the OCM accordingly. Major points we note from the comparisons are the following:

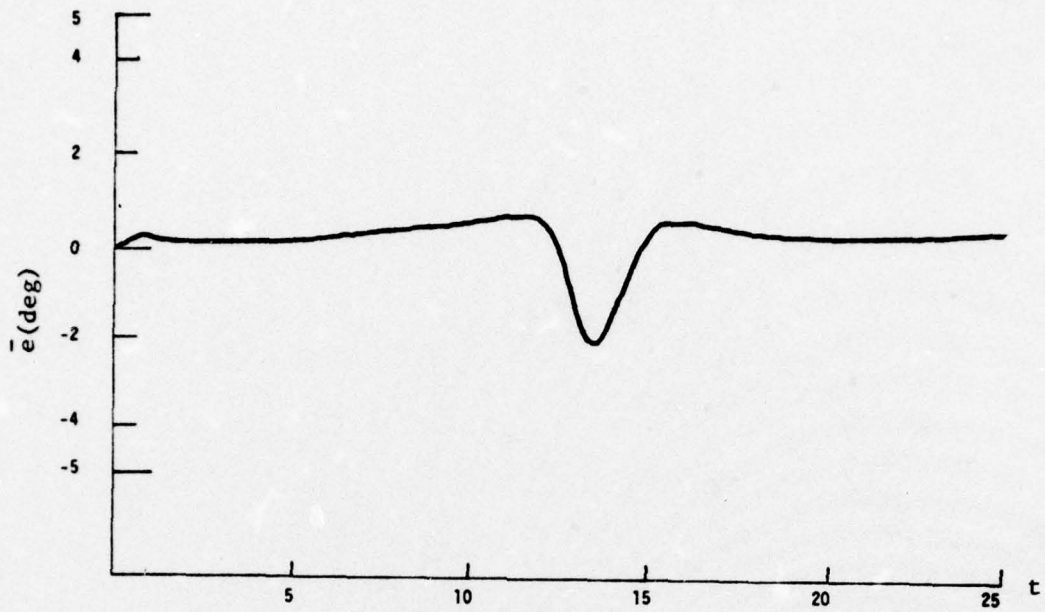


a) Mean Tracking Error

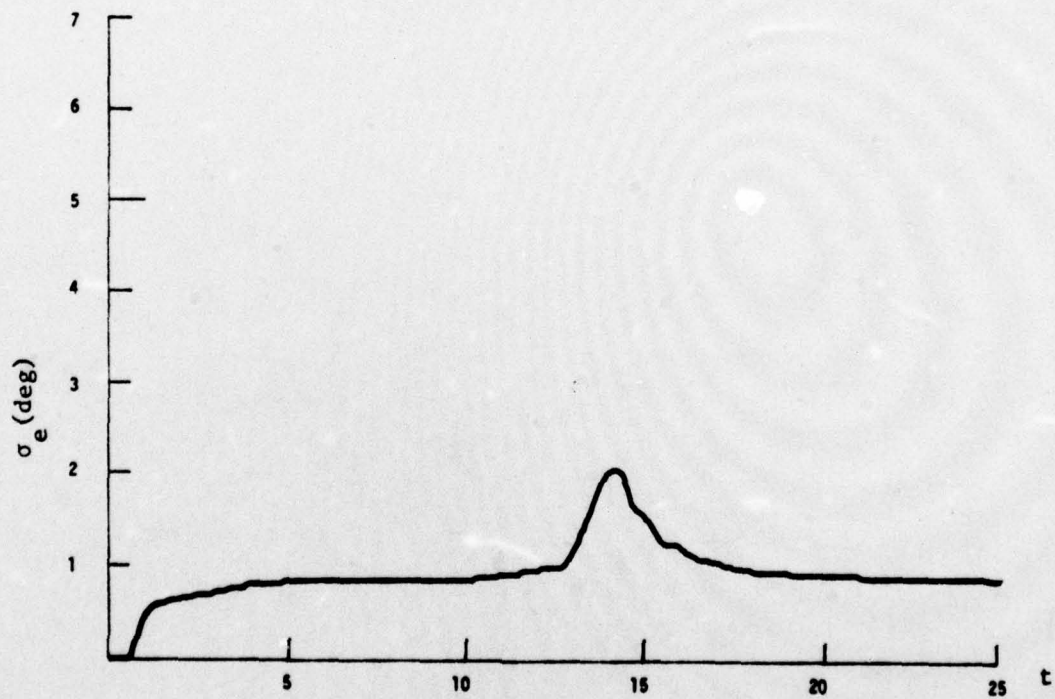


b) Standard Deviation

Fig. 17: AZIMUTH MODEL PREDICTIONS, S & L TARGET, FULL ATTENTION, NO VISUAL CUES



a) Mean Tracking Error



b) Standard Deviation

Fig. 18: ELEVATION MODEL PREDICTIONS, S & L TARGET, FULL ATTENTION, NO VISUAL CUES

1. The predicted $\bar{e}(t)$ are essentially symmetric, much as previous results using the OCM have shown. But the data show an asymmetry towards more lag prior to crossover.
2. Predicted mean errors are somewhat smaller than the experimental results, especially for elevation axis. The max-to-min spread for azimuth is $\sim 6^\circ$ vs. $7\text{--}8^\circ$ for data. For elevation it is $\sim 3^\circ$ vs. $5\text{--}6^\circ$ for data.
3. Predicted standard deviations agree quite closely with experimental results in general form. σ_e for azimuth has a broader peak than that for elevation in both model and data.

We do not find any major concern in items 2 and 3, which deal primarily with the relative magnitude of the model vs. data results. Sensitivity analyses have shown that such data-model mismatches can be adjusted via tuning of one or more key parameters. For example, an increase in ρ_y (dB)[†] will impart a scaling increase to both $\bar{e}(t)$ and $\sigma_e(t)$, with a greater effect being seen in $\sigma_e(t)$. On the other hand, the correlation time τ_c in Eq. (3.5) has little effect on $\bar{e}(t)$; but a \pm factor of 2 in τ_c has about the same effect on $\sigma_e(t)$ as a ± 1 dB change in ρ_y . Thus, to "match" data one could adjust ρ_y to match $\bar{e}(t)$, and then adjust τ_c to match $\sigma_e(t)$. As it was not our objective to continually fine-tune the results (once the possibility was established), we merely fixed $\rho_y = -20$ dB and $\tau_c = 1$ sec to explore the more challenging first point of model structure. Follow-on efforts will deal more with parameter identification schemes.

The asymmetry in mean tracking errors is noticable in most all of our data runs. Similar trends also occurred in some recent 2-axis Q-23 system experiments at AMRL. However, these trends were not readily apparent in earlier S60 data (different system, display, etc.), as shown in Figs. 1 and 3.

[†]Changes in ρ_y , ρ_u and τ have similar effects on error statistics. We thus keep τ and ρ_u fixed and vary only ρ_y .

We feel that this asymmetry phenomenon is statistically significant, and have spent considerable effort to find a suitable explanation.

It is not believed that use of a priori knowledge of the target plays a role. If it did, the relative spread $|e_{\max} - e_{\min}|$ would have been much smaller than the OCM [11] -- not merely shifted. In cooperation with colleagues at AMRL, various modifications to the OCM were tested in order to induce an asymmetry in OCM results, e.g.

1. changing basic parameters, e.g. τ_n , ρ_y , etc.,
2. adding cost functional weights to $\dot{e}(t)$ and control magnitude, $u^2(t)$,
3. filtering the estimated signal $\hat{z}(t)$ before using it to form W_d ,
4. filtering the residual process v_k as in Eq. (3.23),
5. using an "acceleration" model for target motion.

As noted earlier, the last item circles back to a velocity model when we require estimation of $z(t) = [z_1, z_2]^T$. If we impose $\hat{z}(t) = z(t) = [\ddot{\theta}, 0]^T$ without estimation, mean tracking errors (which resemble z or \hat{z}) have a different form structurally than the data. The other items were found to give little structural change to the model results; errors generally increased or decreased uniformly. Any asymmetries that developed were generally in the wrong direction -- i.e. towards higher post-crossover overshoot. It was believed that items 3 or 4 would introduce the sought-for lagging tendency. They had little effect on $\bar{e}(t)$, but did reduce $|\sigma_e(t)|$ slightly.

The only model modification that was found to have a structural impact on $\bar{e}(t)$ was a generalized Markov model for the target motion, viz.

$$\dot{x}_1 = -\alpha x_1 + z(t) \quad (3.25)$$

with $x_1 = \dot{\theta}_T$, $z = \ddot{\theta}_T + \alpha \dot{\theta}_T$. When included with the system dynamics we have

$$\dot{\underline{x}}(t) = \begin{bmatrix} -\alpha & 0 \\ 1 & 0 \end{bmatrix} \underline{x}(t) + \begin{bmatrix} 0 \\ -1 \end{bmatrix} u(t) + \begin{bmatrix} 1 \\ 0 \end{bmatrix} z(t) \quad (3.26)$$

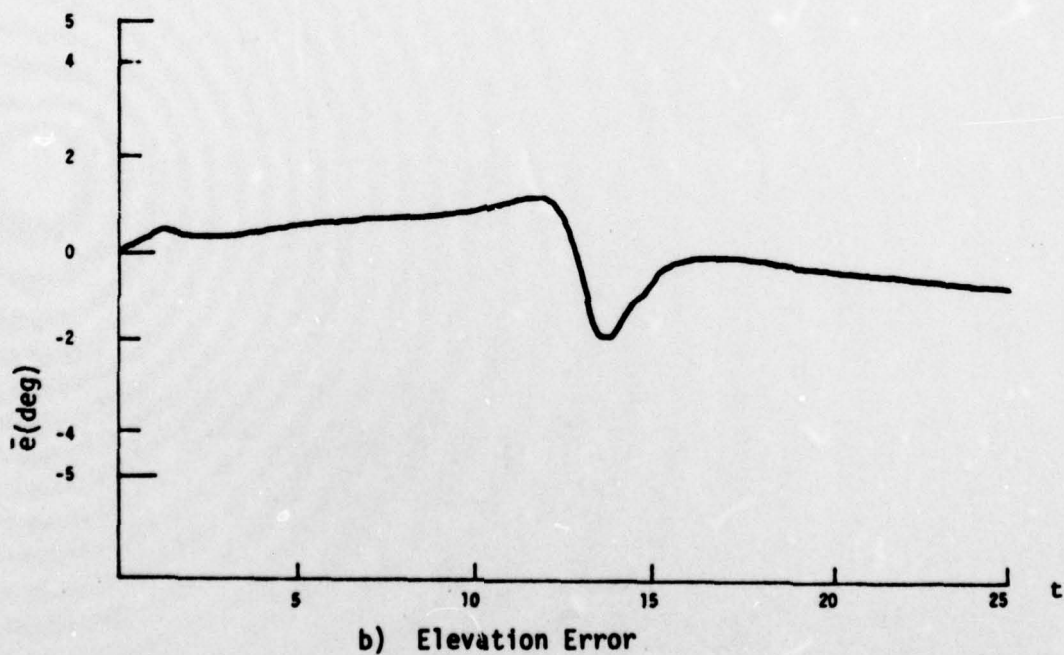
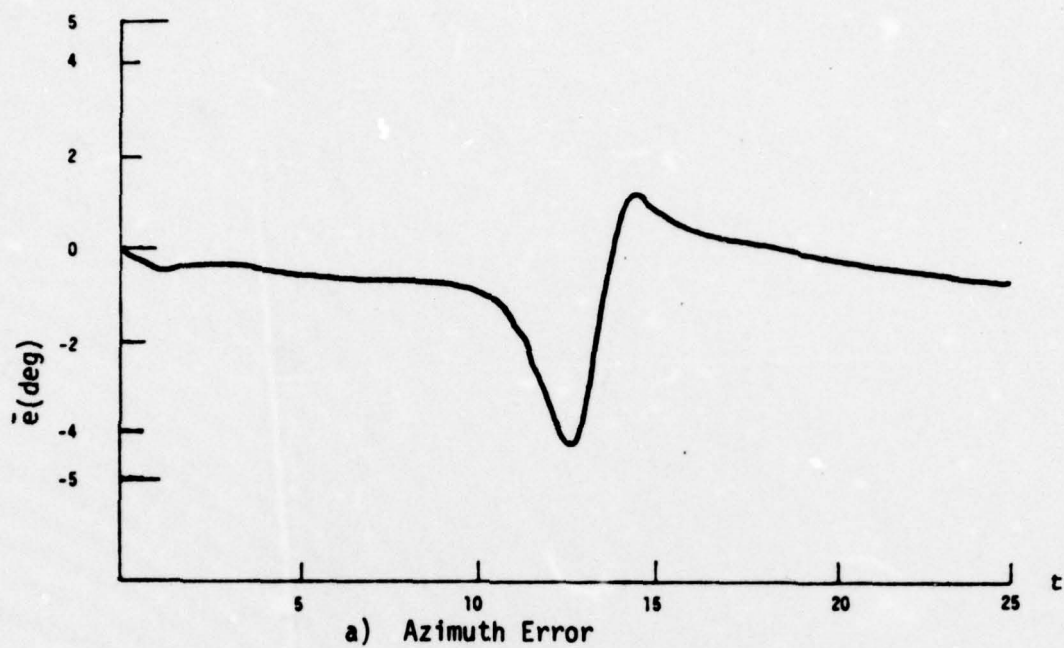


Fig. 19: MEAN TRACKING ERROR PREDICTIONS, $\alpha=.5$, FULL ATTENTION

$$y(t) = \begin{bmatrix} 0 & 1 \\ 1 & 0 \end{bmatrix} x(t) + \begin{bmatrix} 0 \\ -1 \end{bmatrix} u(t) \quad (3.27)$$

The "lag" $1/\alpha$ introduces the asymmetric lagging tendency observed in the data. However α cannot simply be a constant. Figure 19 shows that the lagging tendency would persist well past crossover -- a trend not seen in the data. We conclude that α must be a function of $\dot{\theta}_T, \ddot{\theta}_T, \hat{z}$, etc., in order to match data. Indeed, $\alpha(t)$ can be interpreted as a "local" bandwidth, so that an $\alpha(t)$ of the form

$$\alpha(t) \sim \left[\frac{E\{\dot{x}_1^2\}}{E\{x_1^2\}} \right]^{1/2} = c_1 \frac{|\ddot{\theta}_T|}{|\dot{\theta}_T|} \sec^{-1} \quad (3.28)$$

could be expected. We assume that $\alpha \geq 0$.

Several different ad-hoc combinations of target-related variables were simulated for $\alpha(t)$, with varying degrees of success. The question of whether an "optimal" value of α exists was studied using Eq. (3.25). The Kalman filter implementation for this equation assumes

$$\dot{x}_1(t) = -\alpha x_1(t) + \xi(t) \quad (3.29)$$

where $\xi(t)$ is a white-noise with covariance $W_d \sim \tau_c (\alpha \dot{\theta}_T + \ddot{\theta}_T)^2$. Neglecting the other states, and assuming an "observation" of $x_1(t)$ with measurement noise $V_1 = c^2 E\{x_1^2(t)\}$, a Kalman filter would estimate x_1 with covariance error

$$\dot{\Sigma}_1 = -2\alpha \Sigma_1 + W_d - \Sigma_1^2/V_1 \quad (3.30)$$

Assuming

$$W_d \sim \tau_c \alpha^2 E\{\dot{\theta}^2\} + \tau_c E\{\ddot{\theta}^2\}$$

we see that there exists a value of α that minimizes Σ_1 -- the local rate of

increase of the estimation uncertainty. Setting $\partial \Sigma_1 / \partial \alpha = 0$ gives

$$\alpha^* = \Sigma_1 / \tau_c E\{\dot{\theta}^2\} \quad (3.31)$$

For small α , $\Sigma_1 \approx \sqrt{V_1 W_d}$ and we see that Eq. (3.31) is quite similar to Eq. (3.28). An alternate approach "solves" Eq. (3.30) for its steady-state (frozen-point) value. Finding the α that minimizes Σ_{ss} gives results that are quite similar to Eq. (3.31).

Motivated by the above approximate analysis, we have selected $\alpha(t)$ over the interval $[k, k+1]$ according to the uncertainty in \hat{x}_1 ,

$$\alpha_k = \frac{3\sqrt{\Sigma_{k,11}}}{57.3} \text{ sec}^{-1} \quad (3.32)$$

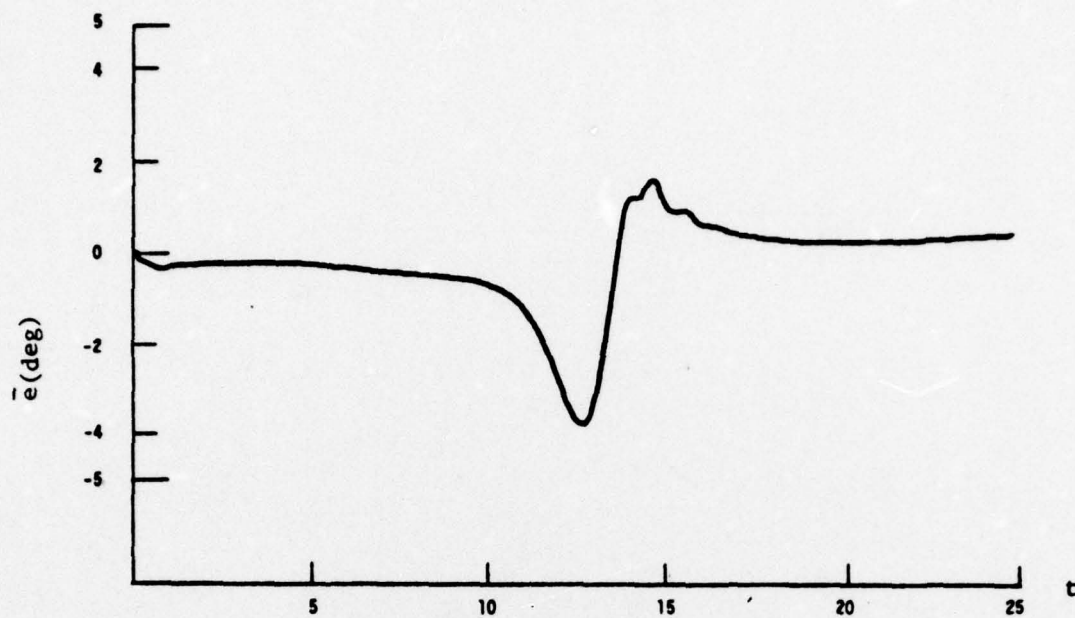
The scaling of α_k with $\Sigma_k^{1/2}$ is particularly appealing. It implies that there should be more lag (asymmetry) with higher uncertainties, as for example when observation noises increase or target motions become more rapid. It also corroborates subject's comments that they "felt more comfortable when lagging". The quantity $\xi = 3\sqrt{\Sigma}$ is the model's anticipated spread in the x_1 estimate, i.e., $x_1(t) \in [\hat{x}_1 - \xi, \hat{x}_1 + \xi]$ with 99% probability.

Note that with $\alpha(t)$ now time-varying, the system matrix $A = A(t)$. This means that $\Phi = \exp(A\delta)$ and the feedback gain l_1 on $x_1(t)$ must be recomputed each time α changes. Fortunately, the only α -dependent terms in Φ_k are

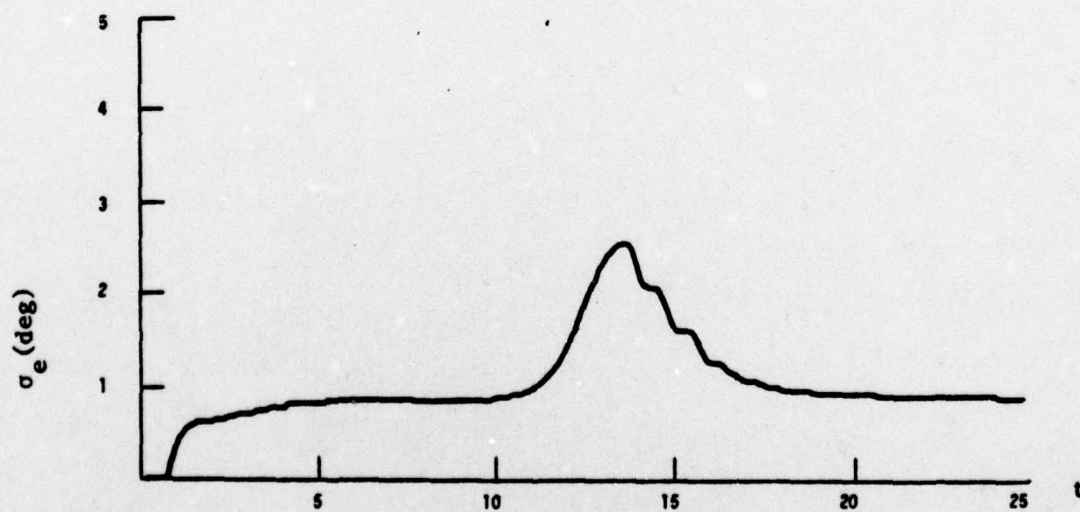
$$\Phi_{11} = e^{-\alpha\delta} ; \quad \Phi_{21} = (1 - e^{-\alpha\delta}) / \alpha$$

so that Φ_k is easy to change. Also, it can be shown that the continuous gains $L = (l_1 \ l_2 \ l_3)$ on the augmented state are

$$l_1 = -\frac{1}{r} \left[\frac{\sqrt{2/r} - \alpha}{\alpha^2 - 10\alpha + 50} \right] \quad (3.33a)$$



a) Mean Tracking Error



b) Standard Deviation

Fig. 20: AZIMUTH PREDICTIONS WITH TIME-VARYING α , FULL ATTENTION

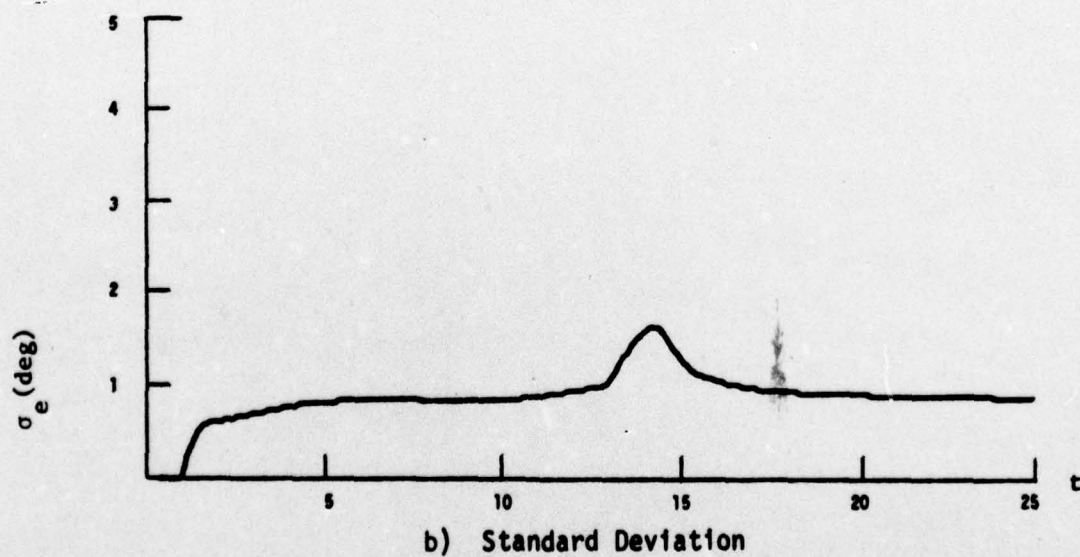
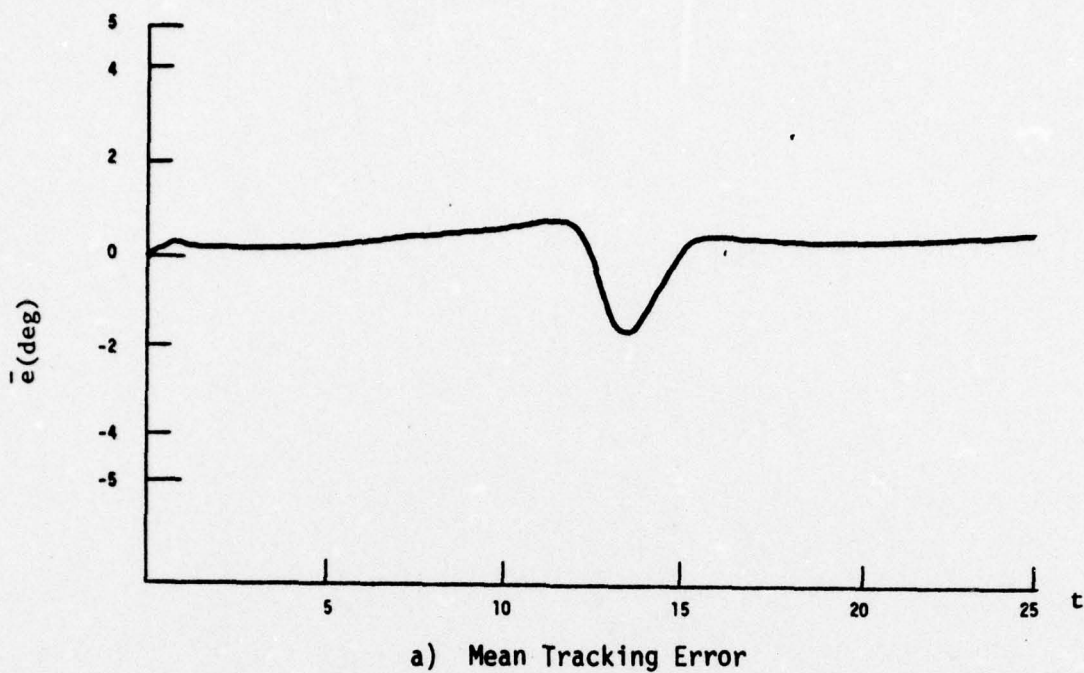


Fig. 21: ELEVATION PREDICTIONS WITH TIME-VARYING α , FULL ATTENTION

$$k_2 = -\frac{1}{r} \quad (3.33b)$$

$$k_3 = \sqrt{2/r} \quad (3.33c)$$

where $r = g^{\frac{1}{2}}$ (g = control-rate weighting). For $r=.02$ (corresponding to $\tau_n=.1$), a simple approximation to the discrete gain equivalent to Eq. (3.33a) is

$$k_1 \approx -8.765 + .75\alpha \quad ; \quad \alpha \leq 2$$

so that k_1 does not depend strongly on α .

The model predictions with α generated according to Eq. (3.32) are shown in Figs. 20 and 21. Clearly this gives a closer facimile to data than did the previous model plots.

3.3 Attention Allocation Submodel

When a human is required to track azimuth and elevation axes simultaneously, there must be a mechanism by which attention is allocated between the two parallel tasks. This issue of interaxis attentional allocation is not of concern in a dual operator system (such S60) where each operator controls but one axis. In a single operator system tracking performance degrades, as workload increases. If we define f_A (f_E) as the fractional attention allocation to azimuth (elevation) tracking with

$$f_A + f_E = 1.0,$$

our objective is to model the allocation process via prediction of f_A vs. time.

As indicated in Section 1.4.4, a model for obtaining optimal attention allocation has been derived for stationary single-axis tracking tasks. In such cases, the total cost functional is given by

$$J(u^*, f) = L_e \int L_e' + \text{terms independent of } \Sigma \quad (3.34)$$

where L_e are "equivalent" gains

$$L_e = g^{\frac{1}{2}} L_e^{At} \quad (3.35)$$

and Σ is the steady-state error covariance matrix which satisfies the Riccati equation. The matrix Σ depends on the observation noise covariance V_y , and thus in turn on the attentional allocations f_i to each position-velocity observation pair via Eq. (1.5). For two-axis tracking in a non-stationary context, $J(u^*, \underline{f})$ is given approximately by Eq. (1.23). In this case the optimal choice of $f_A(t)$ and $f_E(t)$ is not straightforward, involving the solution of a complex non-linear dynamic programming problem.

A simpler, suboptimal, approach has been followed in our work. Borrowing from the techniques of Ref. [2], we attempt to find $f_A(t)$ and $f_E(t)$ so as to minimize at every time instant the integrand of Eq. (1.23),

$$L_e \Sigma_A(t) L_e' + L_e \Sigma_E(t) L_e' \quad (3.36)$$

The matrix $\Sigma_A(t)$ decreases with increases in $f_A(t)$. If we assume $\Sigma \propto 1/f$, then the "optimal" attention allocation should be proportional to $L_e \Sigma L_e'$.

Under the constraint $f_A + f_E = 1$, we then have

$$f_A(t) = (1 + R)^{-1} \quad (3.37)$$

$$f_E(t) = 1 - f_A(t) ; \quad R = \frac{L_e \Sigma_E L_e'}{L_e \Sigma_A L_e'} \quad (3.38)$$

This was the model suggested in Ref. [2].

Depending on the assumed relationship between $\Sigma(t)$ and $f(t)$, other models are possible. For example, the choice $\Sigma \propto 1/\sqrt{f}$ is motivated by the $\Sigma C' V_y^{-1} C \Sigma$ term in the Riccati equation. When V_y is small (i.e. good observations), this term becomes dominant. Under this assumption, the "optimal" attention allocation is proportional to $(L_e \Sigma L_e')^2$. A third, plausible approach to model the attentional subprocess is to assume that the human is a single channel processor, internally switching full attention between the axes in

turn.[†] Thus f_A and f_E will be either 0 or 1, depending on the relation

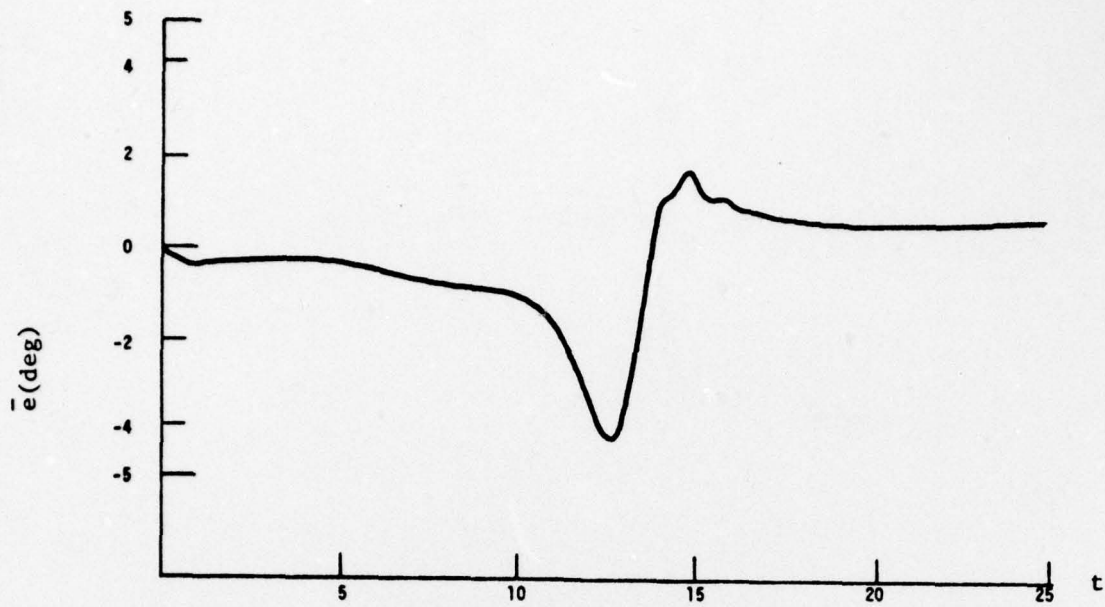
$$L_e \Sigma_A L_e' \leq L_e \Sigma_E L_e'.$$

All three of these models may be combined in the same mathematical framework by replacing the ratio R in Eq. (3.28) with R^p where $p=1, 2$, or ∞ . The model predictions of ensemble error statistics are given in Figs. 22-23 ($p=1$) and Figs. 24-25 ($p=2$). The corresponding time histories of $f_A(t)$ are shown in Figs. 26a and b, respectively. As can be seen, the ensemble error results and the attentional time histories are virtually identical, with an elevation vs. azimuth attention split approximately 50-50 during the "good tracking" phases.

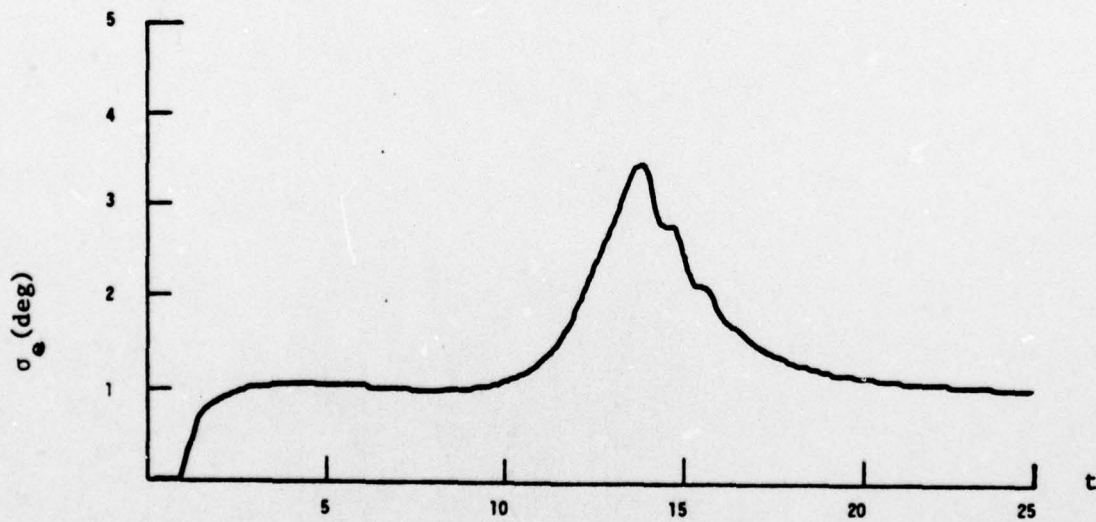
The results for $p=\infty$ are shown in Figs. 27-28; the time history of $f_A(t)$ is not shown. $f_A(t)$ was found to switch rapidly between 0 and 1 with a period of .1 to .3 sec. During the "good-tracking" phases approximately equal time was spent on elevation and azimuth, further corroborating the results of Fig. 26b. In the immediate pre-crossover interval most time was spent on azimuth; the reverse was found in the immediate post-crossover region. The error statistics $\bar{e}(t)$, $\sigma_e(t)$ are quite similar to those of $p=1$ or 2, especially for azimuth tracking. Some differences are noted in elevation mean tracking immediately before crossover, and in standard deviations during crossover, with slightly more oscillatory behavior noted.

The basic trend exhibited by all three schemes, over the full attentional results, is that both error mean and especially standard deviations increase. Relatively little change is seen in $\bar{e}(t)$ with max-to-min excursions increasing from 5° to 6° for azimuth and from $2\frac{1}{2}^\circ$ to $3\frac{1}{2}^\circ$ for elevation. The corresponding

[†]In steady-state cases it has been shown that, under rapid switching, single channel and parallel processing models are equivalent [12].



a) Mean Tracking Error



b) Standard Deviation

Fig. 22: AZIMUTH PREDICTIONS, SHARED ATTENTION $p=1$

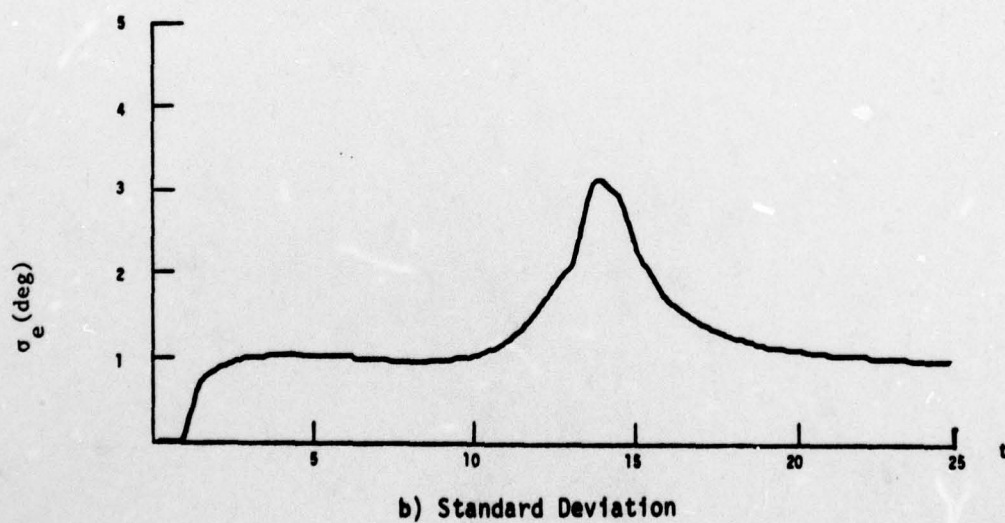
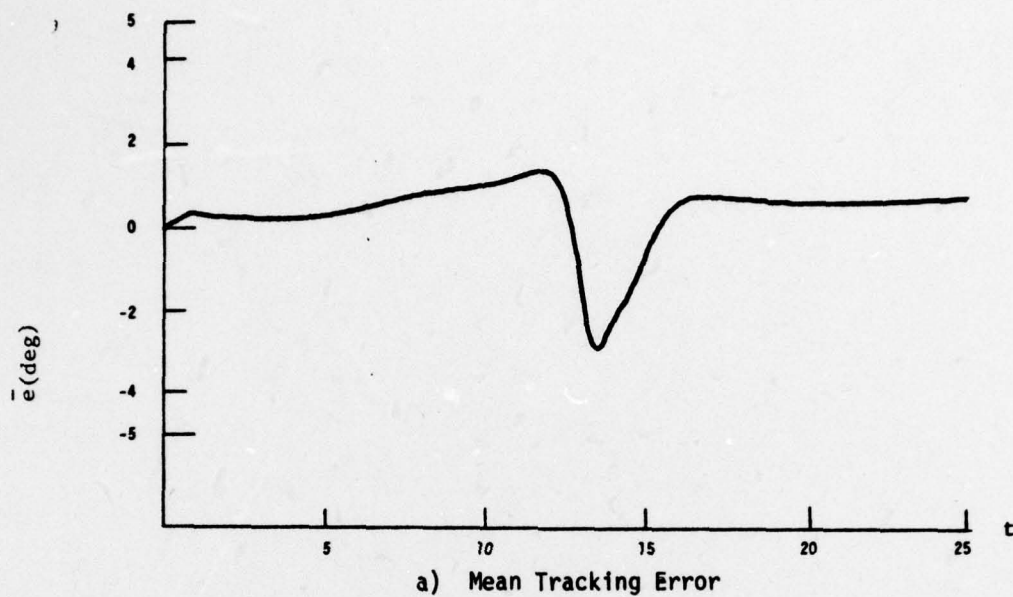


Fig. 23: ELEVATION PREDICTIONS, SHARED ATTENTION $p=1$

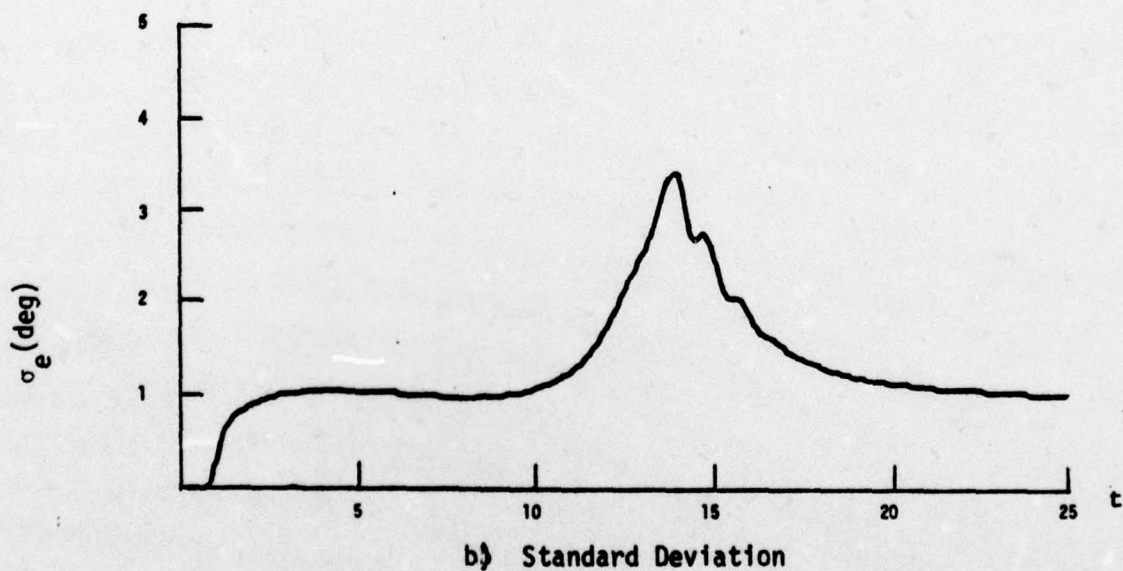
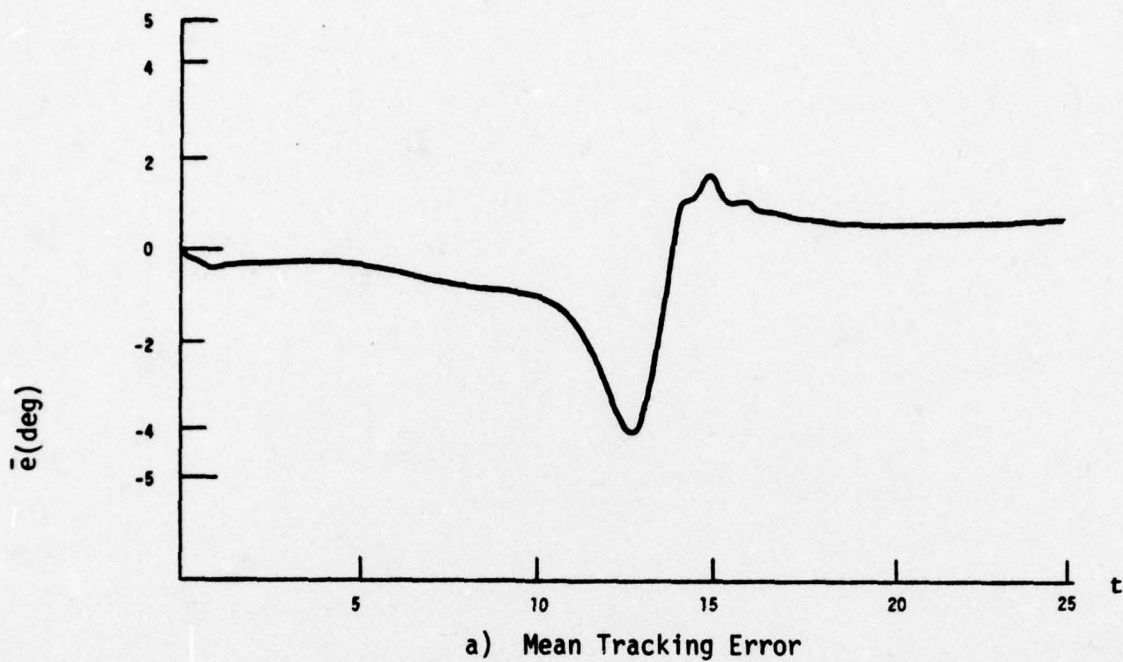
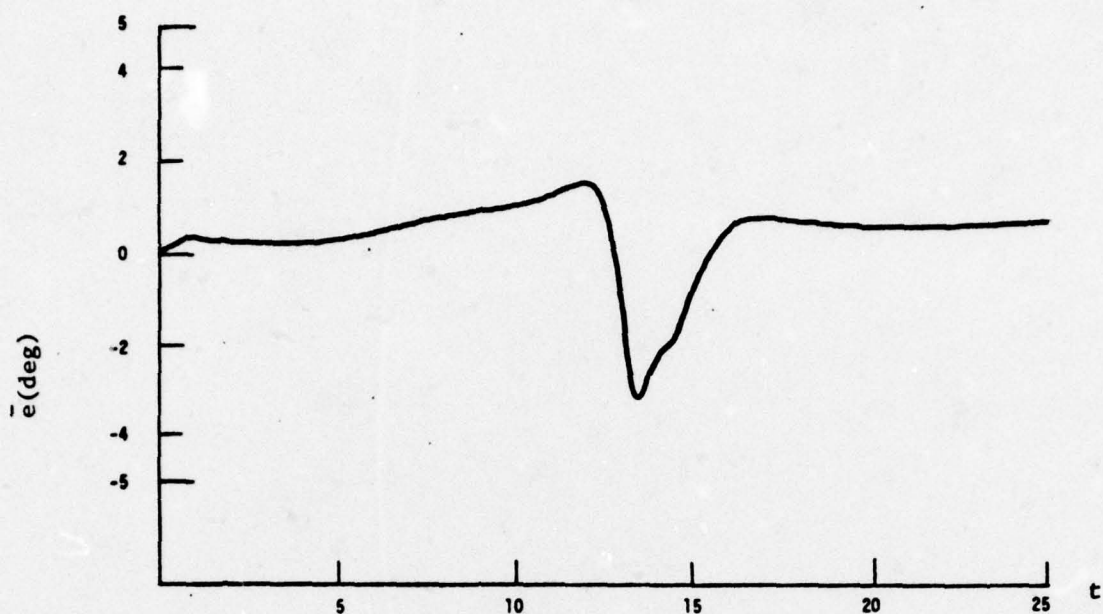
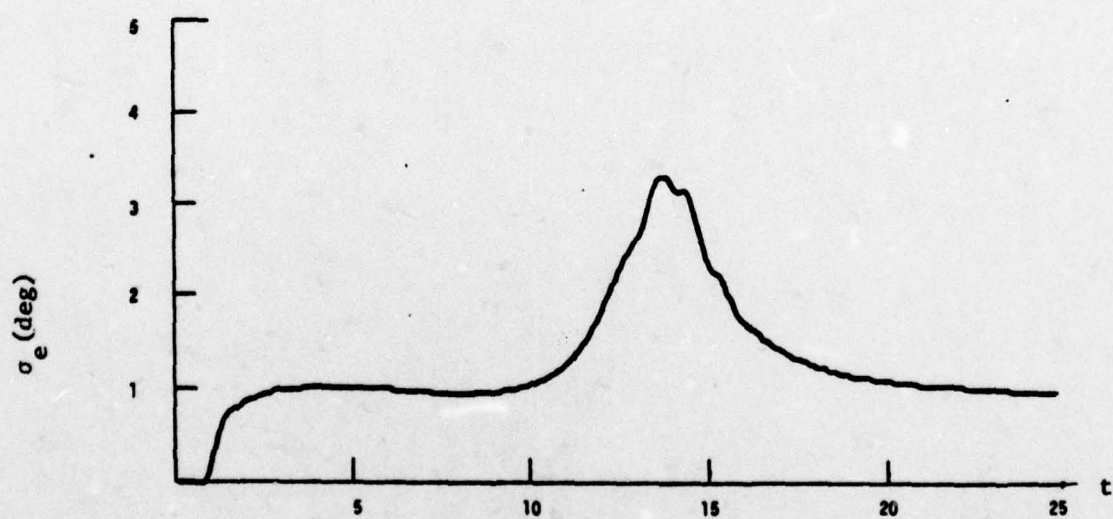


Fig. 24: AZIMUTH PREDICTIONS, SHARED ATTENTION $p=2$



a) Mean Tracking Error



b) Standard Deviation

Fig. 25: ELEVATION PREDICTIONS, SHARED ATTENTION $p=2$

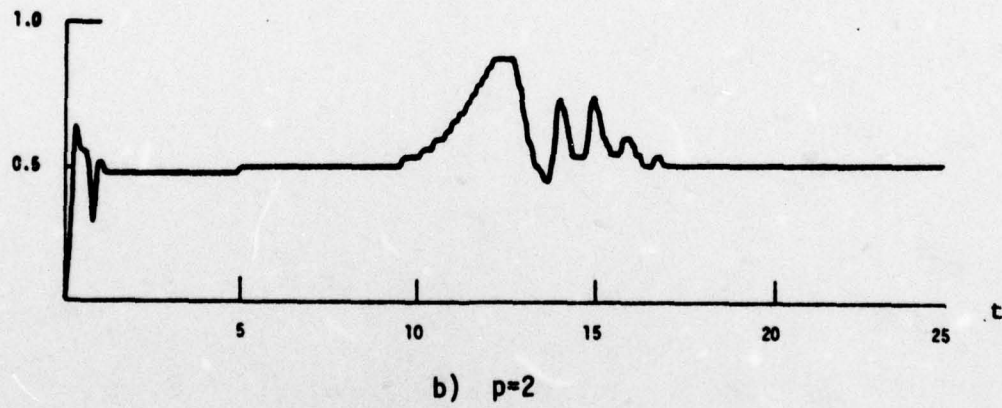
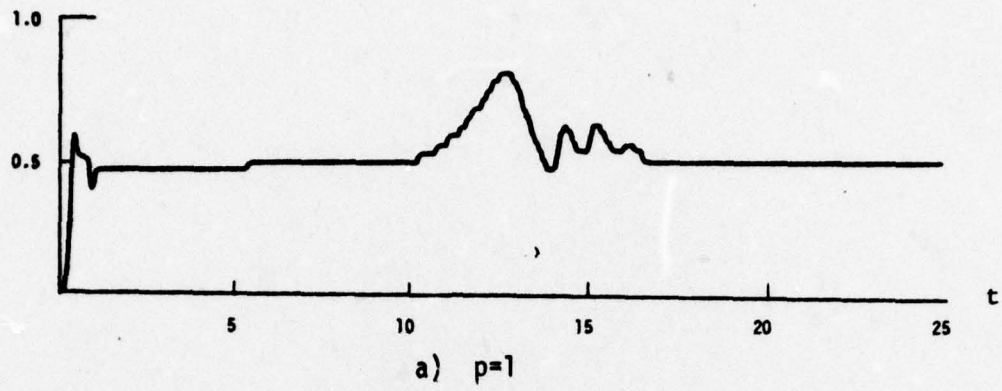


Fig. 26: PREDICTED ATTENTIONAL ALLOCATION TO AZIMUTH AXIS, f_A

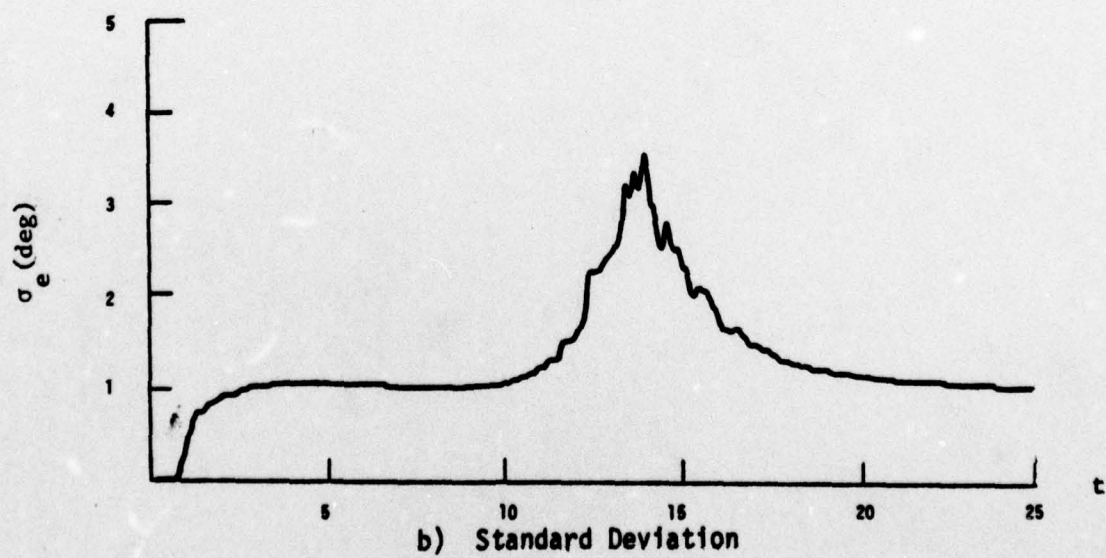
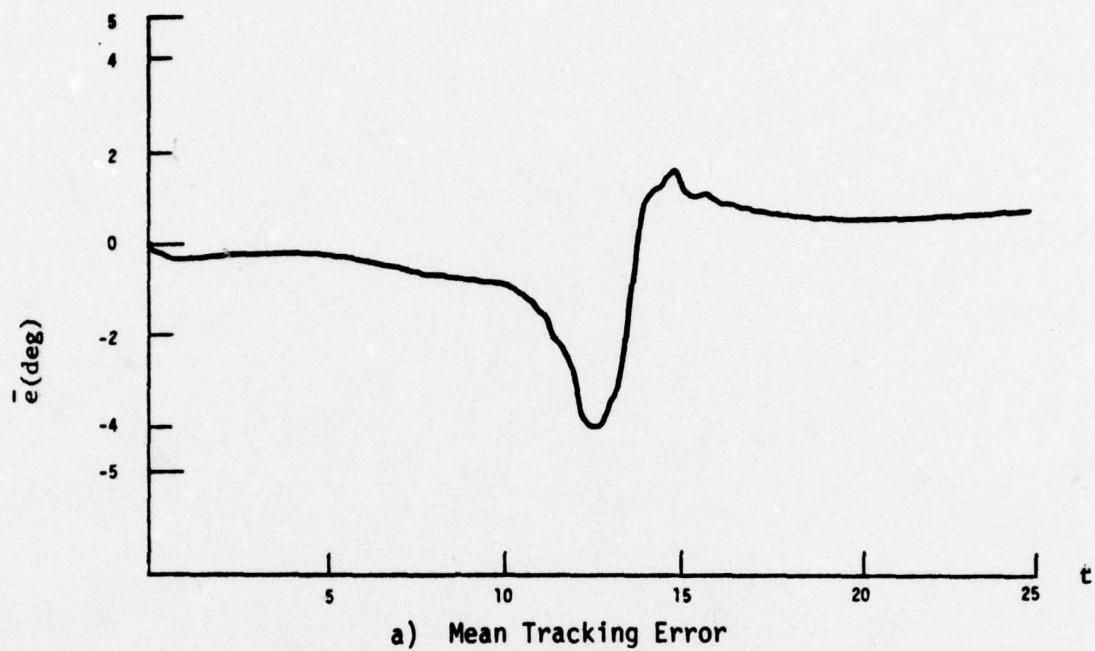


Fig. 27: AZIMUTH PREDICTIONS, SHARED ATTENTION $p = \infty$

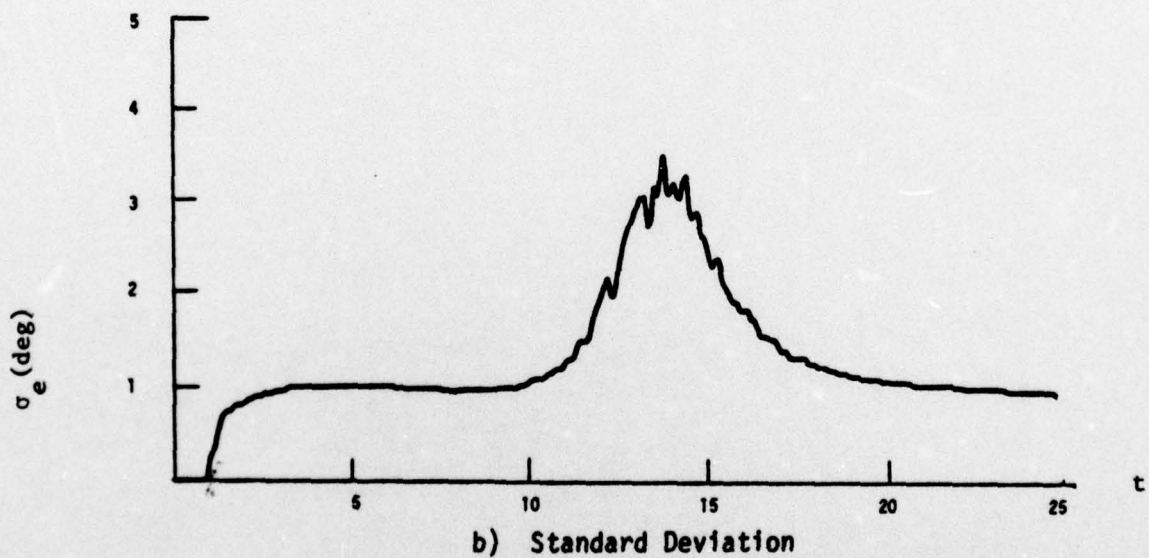
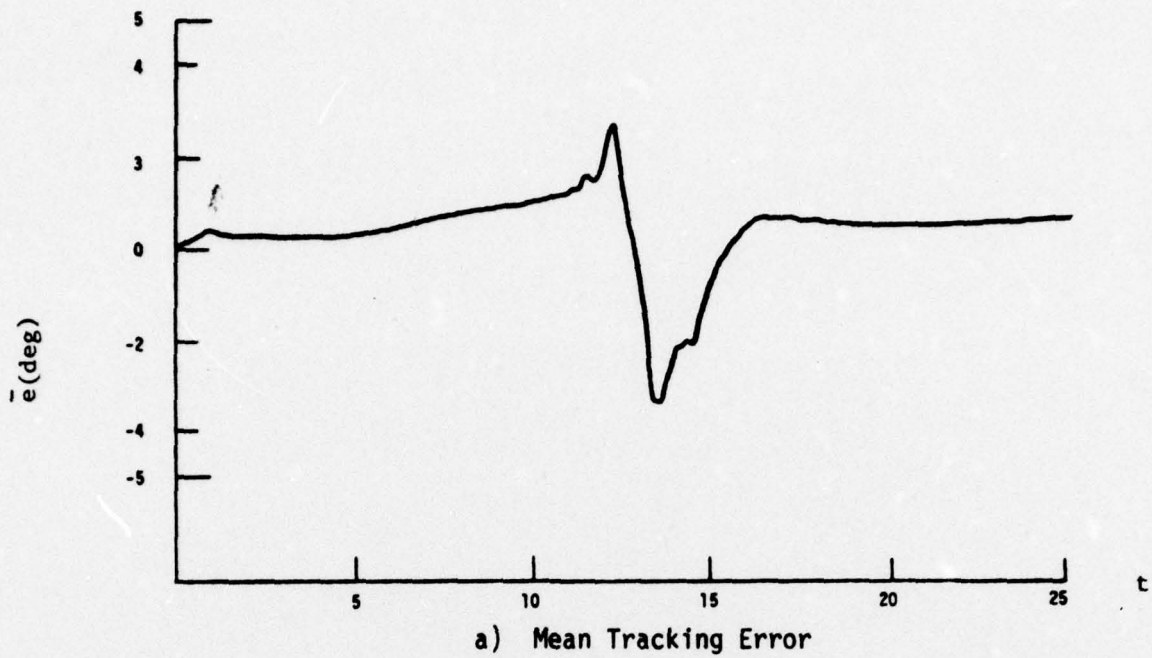


Fig. 28: ELEVATION PREDICTIONS, SHARED ATTENTION $p = \infty$

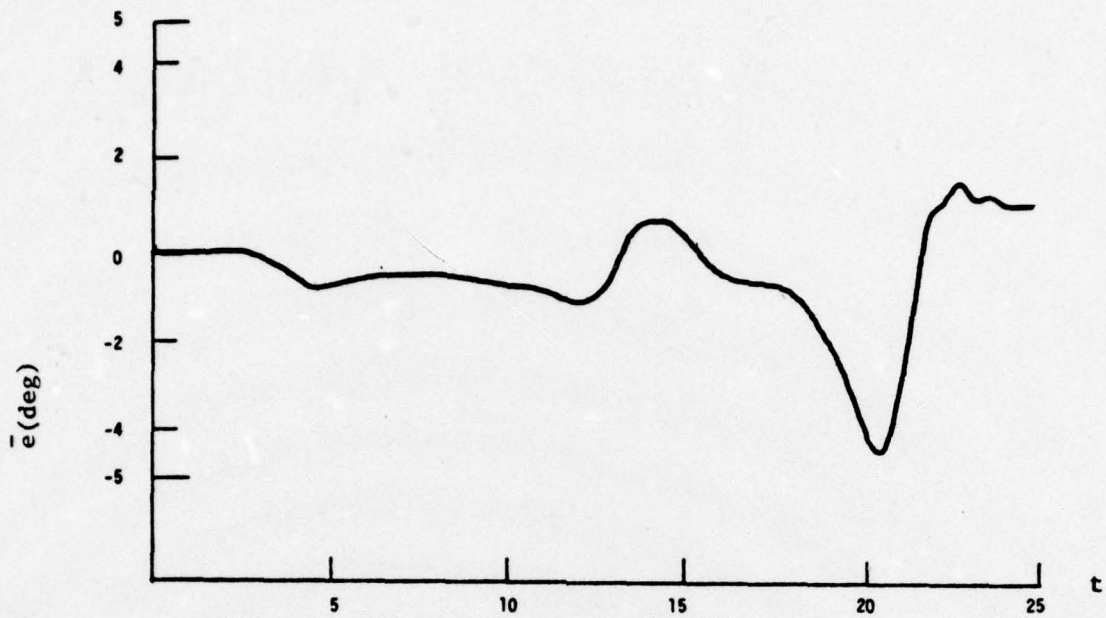
experimental results (attention sharing, no visual cues) are shown in Figs. B3-B4 for the 50 x 50 straight-and-level flyby. The comparisons of model-vs-data results are quite encouraging. The qualitative trends in the data have been very well captured by the model predictions; quantitative % increases in \bar{e} and σ_e also agree closely.

We are somewhat puzzled by the steady-state mean error offset ($.5^\circ$ -. $.6^\circ$) in the model predictions. A brief numerical analysis indicates that it arises in part from the large model thresholds, and is compounded by the increase in V_y due to attention sharing. There have also been numerical approximations made in the time-varying α case that introduce propagation errors. Allowing estimation of $\hat{z}(t)$ on all states should help reduce this offset.

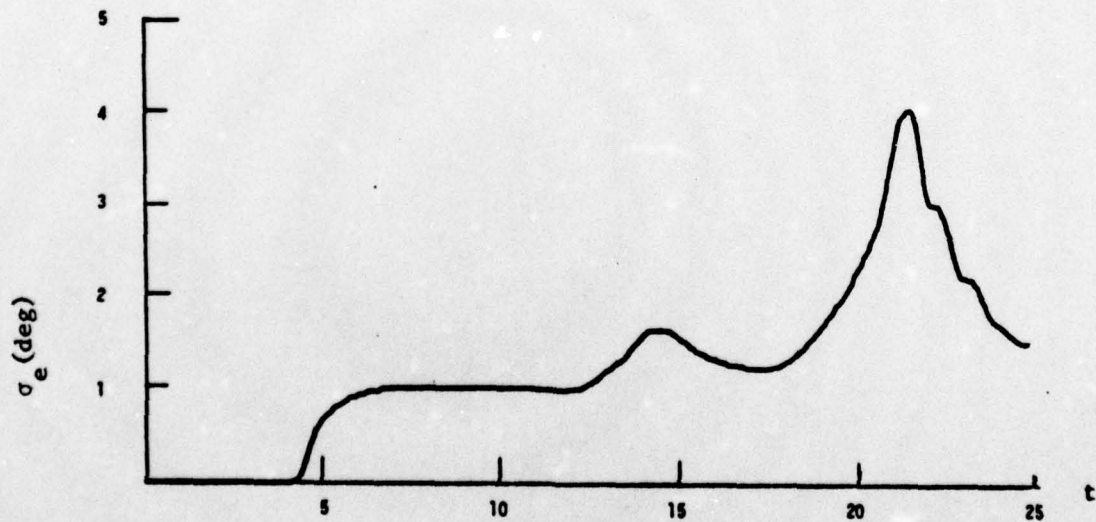
At this point there is no statistically significant differences among the three ($p=1,2,\infty$) attentional allocation schemes when compared with data. This is especially true for $p=1$ or 2 . Our current preference is towards the $p=2$ model, which treats the human operator as a parallel channel information processor. In order to distinguish further between the $p=2$ vs $p=\infty$ cases it will be advisable in future efforts to:

1. examine model vs. data results for control stick input signals, searching for any piecewise-constant control trends,
2. determine whether the pseudo-noise W_d should be modeled as a function of $f_1(t)$,
3. examine interactions between probabilistic editing schemes (Section 3.1.3) and attentional allocation.

Under the selection $p=2$ the model predictions of \bar{e} and σ_e for trajectory C (the random pitching target) are given in Figs. 29 and 30. The corresponding experimental results are shown in Figs. B5-B6, respectively. The comparisons are excellent, lending further credence to the OCM modifications thus far introduced to treat target tracking and human information processing behavior.



a) Mean Tracking Error



b) Standard Deviation

Fig. 29: AZIMUTH PREDICTIONS, PITCHING TARGET, SHARED ATTN., NO VISUAL CUES

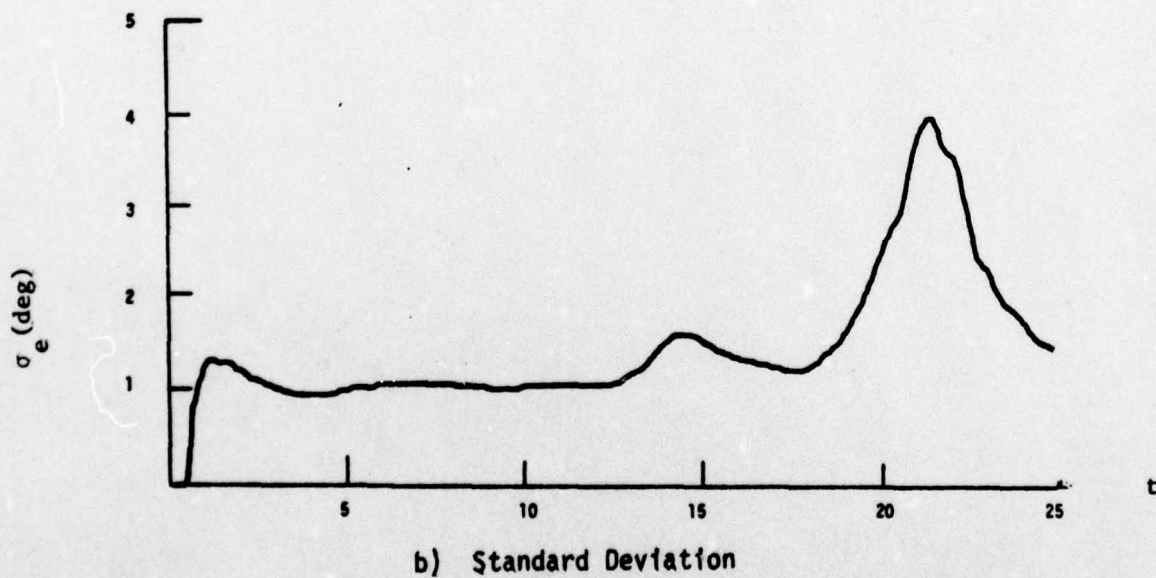
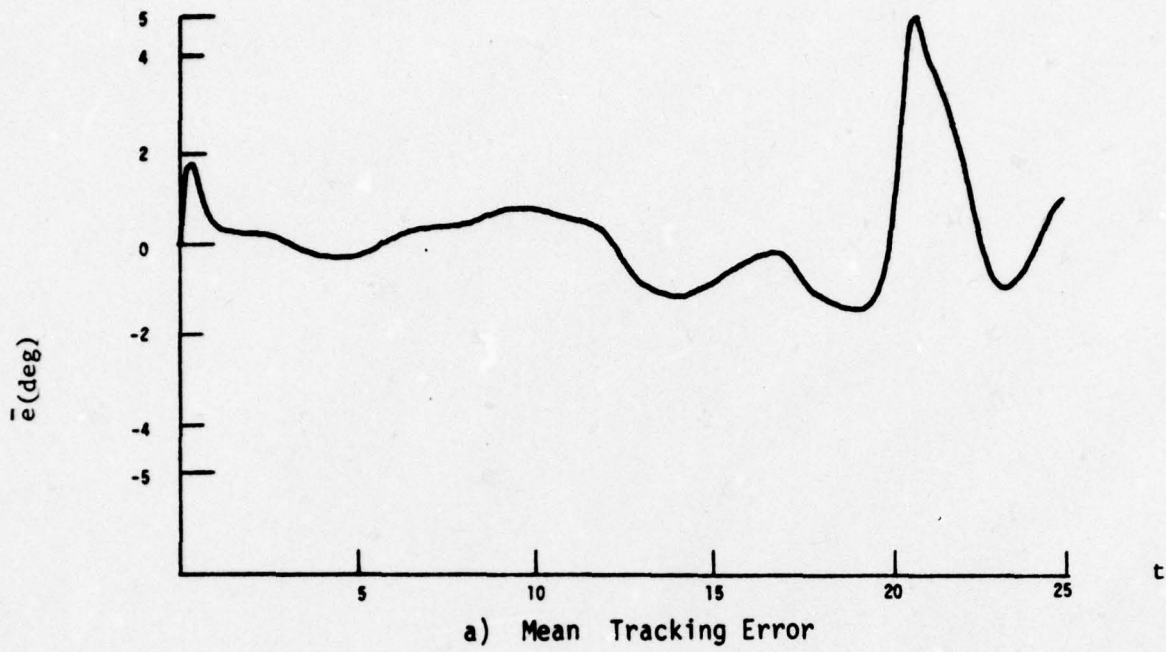


Fig. 30: ELEVATION PREDICTIONS, PITCHING TARGET, SHARED ATTN., NO VISUAL CUES

3.4 Modeling Target Visual Cues

A set of experiments was conducted to explore the effects of visual cues, both with and without the presence of inter-axis attentional allocation requirements. The three experiments of concern are:

1. Straight-and-level pass with full attention to either azimuth or elevation, (see Figs. B7-B8)
2. Straight-and-level pass with attention sharing (see Fig. B9-10)
3. Random pitching trajectory with attention sharing (see Figs. B11-12).

Our model development work focuses on item 1, since this experiment is not complicated doubly by the attentional allocation subprocess. The model can then be used to predict the results of the more complex cases 2 and 3. The initial assumption regarding the visual cues is that the target image provides the human with enhanced information relative to the target motion. In the OCM, the only target-related variables are $\dot{\theta}$ and $\ddot{\theta}$. Thus, we have investigated the hypotheses that the image provides explicit (relative) target velocity and/or velocity plus acceleration cues.

3.4.1 Potential Use of Target Acceleration Cues

It is first assumed that a human can derive both velocity and acceleration cues from the target image. The rationale behind this assumption is that target velocity $\dot{\theta}_T$ in azimuth is related to the target's aspect angle and relative heading angle. In elevation, $\dot{\theta}_T$ is related to observed pitch angle. Thus, assuming implicitly derived rate information by the human, we obtain the two additional "observations"

$$y_3(t) = \dot{\theta}_T$$

$$y_4(t) = \ddot{\theta}_T$$

In order to include this position-velocity pair within the OCM it is necessary to go to an acceleration model, Eq. (1.19), with observations

$$y = Cx + Du$$

$$= \begin{bmatrix} 0 & 0 & 1 \\ 1 & 0 & 0 \\ 1 & 0 & 0 \\ 0 & 1 & 0 \end{bmatrix} \underline{x} + \begin{bmatrix} 0 \\ -1 \\ 0 \\ 0 \end{bmatrix} u \quad (3.39)$$

This is true for both azimuth and elevation axes.

By adding a second set of information to each axis, the problem of intra-axis attention allocation between (e, \dot{e}) and $(\ddot{\theta}, \ddot{\theta})$ must be addressed. While there are potential arguments for assuming no interference between the image being tracked and the crosshairs, our initial work assumes interference to determine the relative importance of image cues. This was done using a steady-state analysis for the system

$$\dot{\underline{x}} = \begin{bmatrix} -1 & 1 & 0 \\ 0 & -1 & 0 \\ 1 & 0 & 0 \end{bmatrix} \underline{x} + \begin{bmatrix} 0 \\ 0 \\ -1 \end{bmatrix} u + \begin{bmatrix} 0 \\ 1 \\ 0 \end{bmatrix} w \quad (3.40)$$

where $w(t)$ is a white $N(0,1)$ noise. This equation corresponds to a filtered $1/(s+1)^2$ random target velocity. The observation set is the same as Eq. (3.39), except that

$$y_4 = \ddot{\theta}_T = [-1 \quad 1 \quad 0] \underline{x} + [0] u$$

Three attentional allocation cases were considered

1. Full attention to (e, \dot{e}) , i.e. $f_1=f_2=1$ and $f_3=f_4=0$.
2. No attentional interference, $f_1=f_2=f_3=f_4=1$.
3. Attention optimization with $f_1 + f_3 = 1$, $f_1=f_2$, $f_3=f_4$.

The results are shown in Table 1, using the nominal OCM parameter values.

Case No.	f_1	f_3	$-\frac{\partial J}{\partial f_1}$	$-\frac{\partial J}{\partial f_2}$	$-\frac{\partial J}{\partial f_3}$	$-\frac{\partial J}{\partial f_4}$	J
1	1.0	0.0	.19	.38	1.1	5.5	.0156
2	1.0	1.0	.05	.07	.03	.08	.0062
3	.54	.46	.24	.26	.14	.35	.0088

Table 1. ATTENTION ALLOCATION RESULTS

As can be seen, the introduction of $(\dot{\theta}, \ddot{\theta})$ information has a great effect on reducing tracking errors. The relatively large gradients $\partial J / \partial f_i$ for $i=3,4$ in case 1 evidences this fact. When we allow optimization there is roughly a 50:50 split between (e, \dot{e}) and $(\dot{\theta}, \ddot{\theta})$, with a large (~40%) decrease in cost $J(u^*, f)$. The differences between cases 2 and 3 show the effects of non-interference. But clearly, the more dramatic effect is between cases 1 and 3.

The OCM was exercised under the hypothesis of the observations Eq. (3.39) with an acceleration model Eq. (1.19). A 50:50 attentional split between information pairs was assumed for azimuth tracking only. The relative results were much the same as for the steady-state case; tracking errors were reduced by almost 50%. Moreover, the structure of the mean error response changed significantly. Now, $\bar{e}(t)$ resembled the target jerk, $\ddot{\theta}$. This result remained true -- in varying degrees -- over numerous modeling modifications involving estimation of \hat{z} , probabilistic editing schemes, etc. The combination of small errors with a form not resembling the data lead us to conclude that acceleration cues $\ddot{\theta}$ are probably not provided from the visual image. Indeed, the experimental results of $\bar{e}(t)$ with and without image cues are structurally similar, with $|\bar{e}(t)|$ being somewhat smaller in the former case.

3.4.2 Potential Use of Target Velocity Cues

The analysis of the potential use of $\dot{\theta}_T$ information followed a process

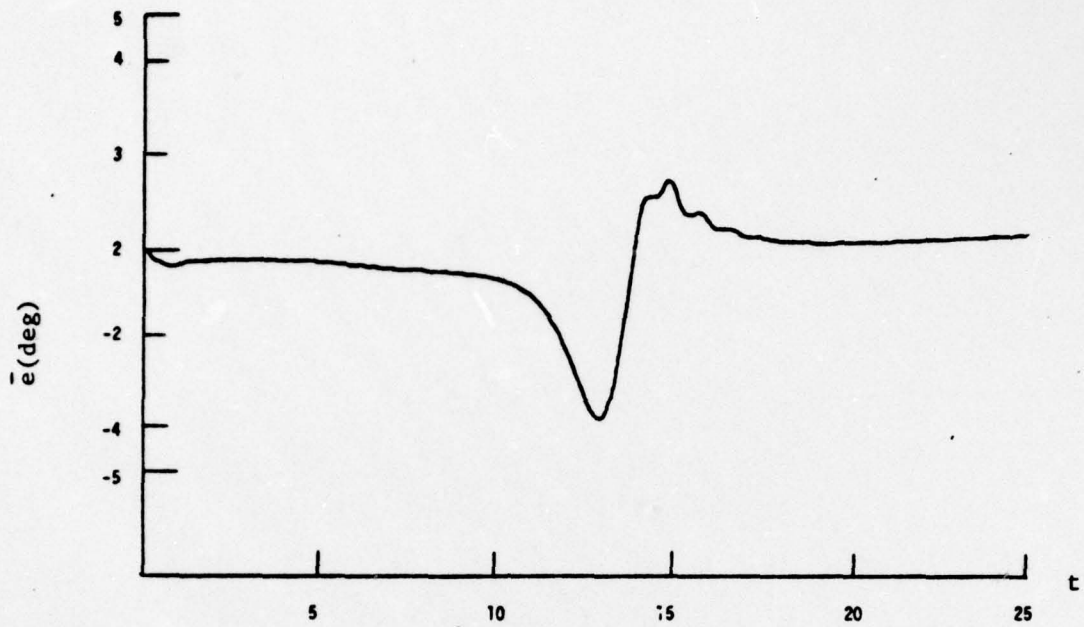
similar to that described above. Preliminary steady-state studies showed that optimizing attention allocation of (e, \dot{e}) vs. $\dot{\theta}_T$ resulted in a 65:35% split. However, unlike the previous case, the decrease in performance cost (J) was less than 5% over the 100:0% case. As a result, use of $\dot{\theta}_T$ information is expected to be minimal for target tracking. Thus, to accentuate any effects introduced by $\dot{\theta}_T$, we will assume that the visual cues from the target image are perceived with no interference.

Using a threshold on $\dot{\theta}_T$ of 3° , the OCM predictions of tracking error have been obtained for:

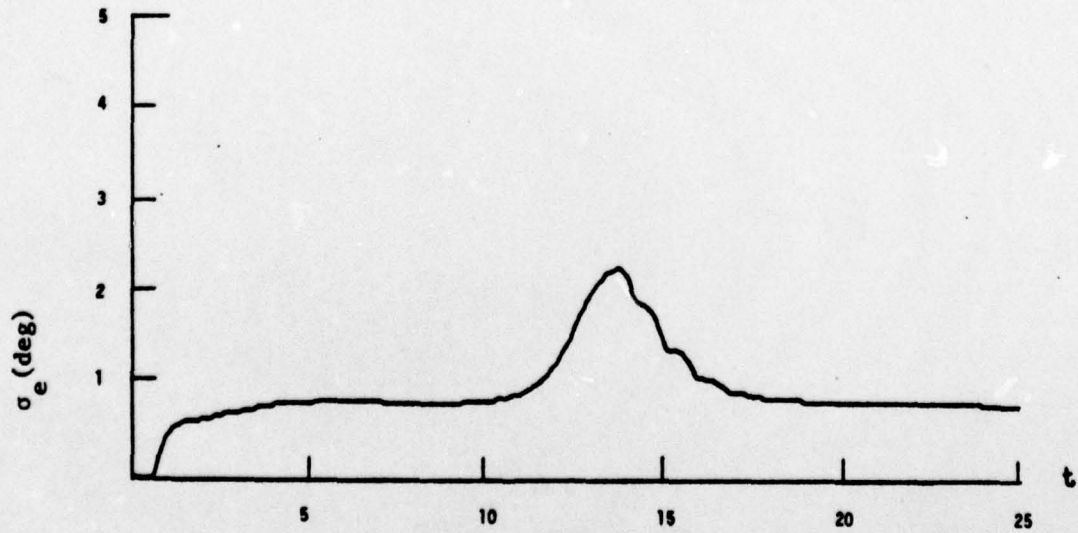
1. Full attention to azimuth and elevation axes (Figs. 31 and 32, respectively). Straight-and-level target.
2. Shared attention, straight-and-level flyby
3. Shared attention, random pitching target.

The inter-axis attention allocation scheme in runs 2 and 3 used $p=2$ as described in Section 3.3. The comparisons between Figs. 31-32 and the no-visual cues case, Figs. 20-21 show that $\dot{\theta}_T$ information has little effect, as anticipated. There are slight decreases in $|\bar{e}(t)|$ and in $\sigma_e(t)$. These results are somewhat disappointing, when contrasted with the corresponding experimental findings (Figs. B7-8) which show more pronounced visual vs. no-visual differences. Similar comparisons have been found for the two dual-axis tracking cases. The model results are in the right direction, but do not go far enough in their magnitude decrease for $\bar{e}(t)$. It appears that either smaller noise ratios are needed on $\dot{\theta}_T$ observations, or that target visual cues may actually affect the error/error rate noise ratios. These would give noticeably smaller model errors for $|\bar{e}(t)|$ and $\sigma_e(t)$.

On the other hand, the data (Figs. B9-12) show an increase in $\sigma_e(t)$ over the no visual cues cases. This is especially true for the random pitching target. It appears that to match the data we need to have a threshold on

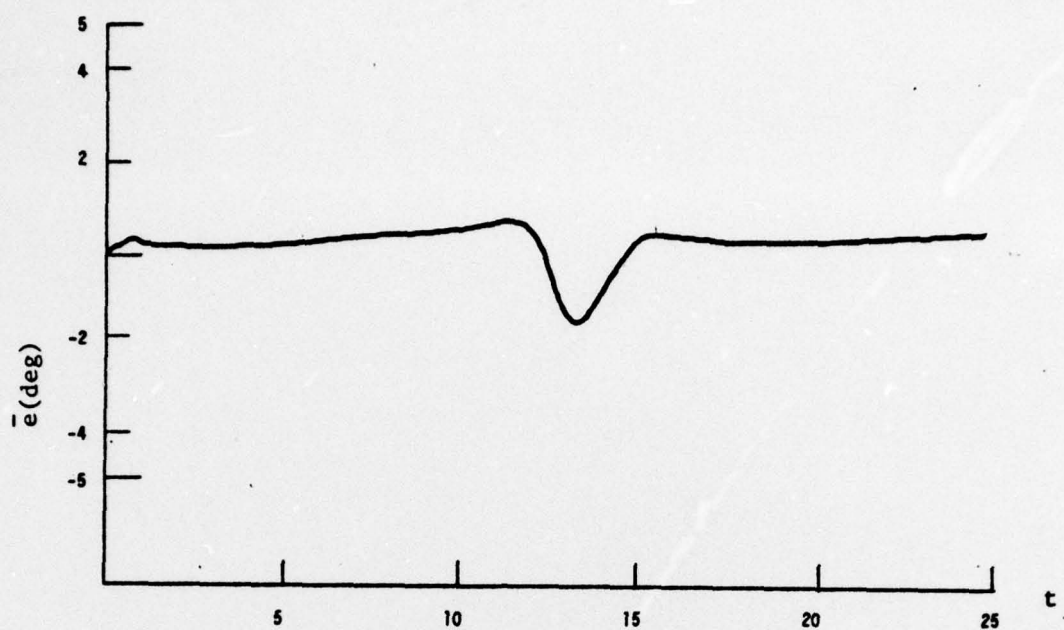


a) Ensemble Mean

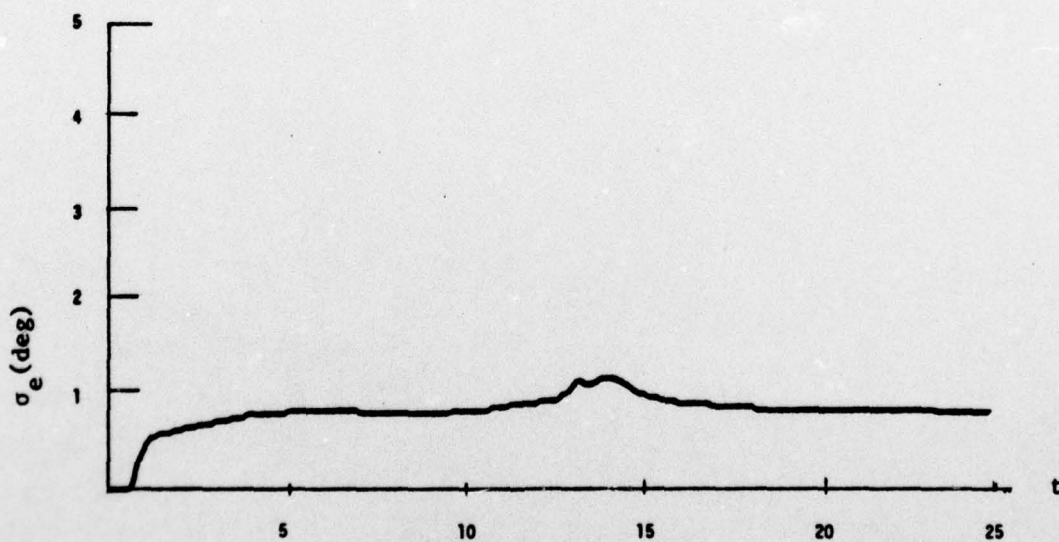


b) Ensemble Standard Deviation

Fig. 31: MODEL AZIMUTH PREDICTIONS, S & L TARGET WITH $\hat{\theta}$ OBSERVATIONS



a) Ensemble Mean



b) Ensemble Standard Deviation

Fig. 32: MODEL ELEVATION PREDICTIONS, S & L TARGET WITH $\dot{\theta}$ OBSERVATIONS

error/error-rate that is monotonic with image size, or to assume that the correlation time τ_c increases. Either of these changes would have a minor effect on $\bar{e}(t)$, but would tend to increase $\sigma_e(t)$. The idea of changing thresholds with image size has been used successfully at AMRL, and appears to be a valid model modification in our effort. One of the reasons we did not see any differences between tracking a fixed size triangle and tracking a dot, was that we placed a zero-error "dot" inside the triangle. Apparently it was the dot that the subjects tracked and not the image. In the visual cues case, the "dot" was still present but was more difficult to discern possibly because of confusion as the subjects saw the target roll, pitch and yaw.

The experimental mean error results show a trade-off between dual-axis attention sharing, and the use of a visual image. Thus, the mean errors $\bar{e}(t)$ in Figs. B1 and B2 compare very closely with their counterparts in Figs. B9-B10.

IV. CONCLUSIONS

A combined analytic-experimental program has been undertaken to examine, in more detail, various issues that have impact on human performance in target tracking tasks. The use of different internal model representations has been clarified, along with a scheme for adaptation of the Kalman filter pseudo-noise. Different assumptions relative to target visual cues and inter-axis attention allocation have been exercised using the Optimal Control Model. Data-model comparisons have been used to isolate correct model assumptions and hypotheses. However, not all of the originally posed questions have been answered fully. These are now under continuing investigation.

V. REFERENCES

1. Tustin, A., "The Nature of the Operator's Response in Manual Control and its Implications for Controller Design", Journal of IEE, Vol. 94, 1947.
2. Kleinman, D.L., and Perkins, T.R., "Modeling Human Performance in a Time-Varying Anti-Aircraft Tracking Loop", IEEE Trans. AC, Vol. AC 19, No. 4, Aug. 1974.
3. Phatak, A.V. and Kessler, K.M., "Formulation and Validation of a PID Structure Modified Optimal Control Model for the Human Gunner in an AAA Tracking Task", Proc. 1976 Decision and Control Conference, Clearwater, Fla.
4. Kleinman, D.L. and Glass B., "Modeling AAA Tracking Data Using the Optimal Control Model", 13th Annual Conference on Manual Control, M.I.T., June 1977.
5. Kleinman, D.L., Baron, S., and Levison, W.H., "A Control Theoretic Approach to Manned-Vehicle Systems Analysis", IEEE Trans. Autom. Control, Vol. AC-16, No. 6, 1971.
6. Kleinman, D.L. and Baron, S., "Analytic Evaluation of Display Requirements for Approach to Landing", NASA CR-1952, Nov. 1971.
7. Kleinman, D.L., "Covariance Propagation Equations for the Optimal Control Model", Univ. of Conn., Dept. of EECS, Tech. Rept. TR-77-6, Sept. 1977.
8. Kleinman, D.L., "Monte-Carlo Simulation of Human Operator Response", Univ. of Conn., Dept. of EECS, Tech. Report TR-77-1, Feb. 1977.
9. Kleinman, D.L., Berliner, J. and Summers, W., "Monte-Carlo Simulation of Human Operator Response", presented at 13th Annual Conference on Manual Control, M.I.T., June 1977.
10. Kleinman, D.L., "Solving the Optimal Attention Allocation Problem in Manual Control", IEEE Trans. AC, Vol. AC-21, No. 6, Dec. 1976.
11. Baron, S. and Levison, W.H., "Analysis and Modeling of Environmental Effects on AAA Tracking", BBN Report No. 2557, prepared for AMRL under contract F33615-72-C-1637, June 1973.
12. Kleinman, D.L. and Curry R.E., "An Equivalence Between Two Representations for Human Attention Sharing", IEEE Trans. SMC, Vol. SMC-6, No. 9, 1976.
13. Rao, P.K., "Methods for Adaptive Filtering and Bias Estimation", in preparation.

APPENDIX A

Mapping a Three-Dimensional World onto a Two-Dimensional Viewing Screen

In mapping a target (a low-flying aircraft, in our case) onto a CRT screen, the basic approach is to view the screen as a semi-transparent "window" between the observer and the target; the target image on the screen is then the observer-centered projection of the real target on this "window" (see Fig. 1).

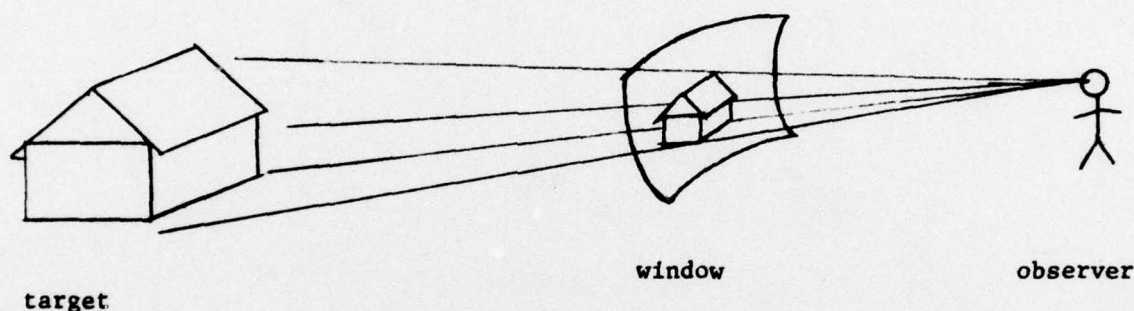


Figure 1

It is not necessary that the "window" be planar; as a matter of fact, in our simulation the "window" was assumed to be hemispherical, to simulate the effects of the observer's head motion while visually following a moving target.

The position of the projected target image on the screen, d_1 , is determined by geometry (see Fig. 2).

$$\alpha = \operatorname{tg}^{-1} \frac{D'}{H'} \quad (\text{A.1})$$

$$D = H \cdot \alpha = H \cdot \operatorname{tg}^{-1} \frac{D'}{H'}$$

$$\gamma = -\operatorname{tg}^{-1} \left(\frac{D' - d_1'}{y_1'} \right)$$

$$\begin{aligned} d_1 &= D - H \cdot (-\gamma) \\ &= D - H \cdot \operatorname{tg}^{-1} \frac{D' - d_1'}{y_1'} \end{aligned}$$

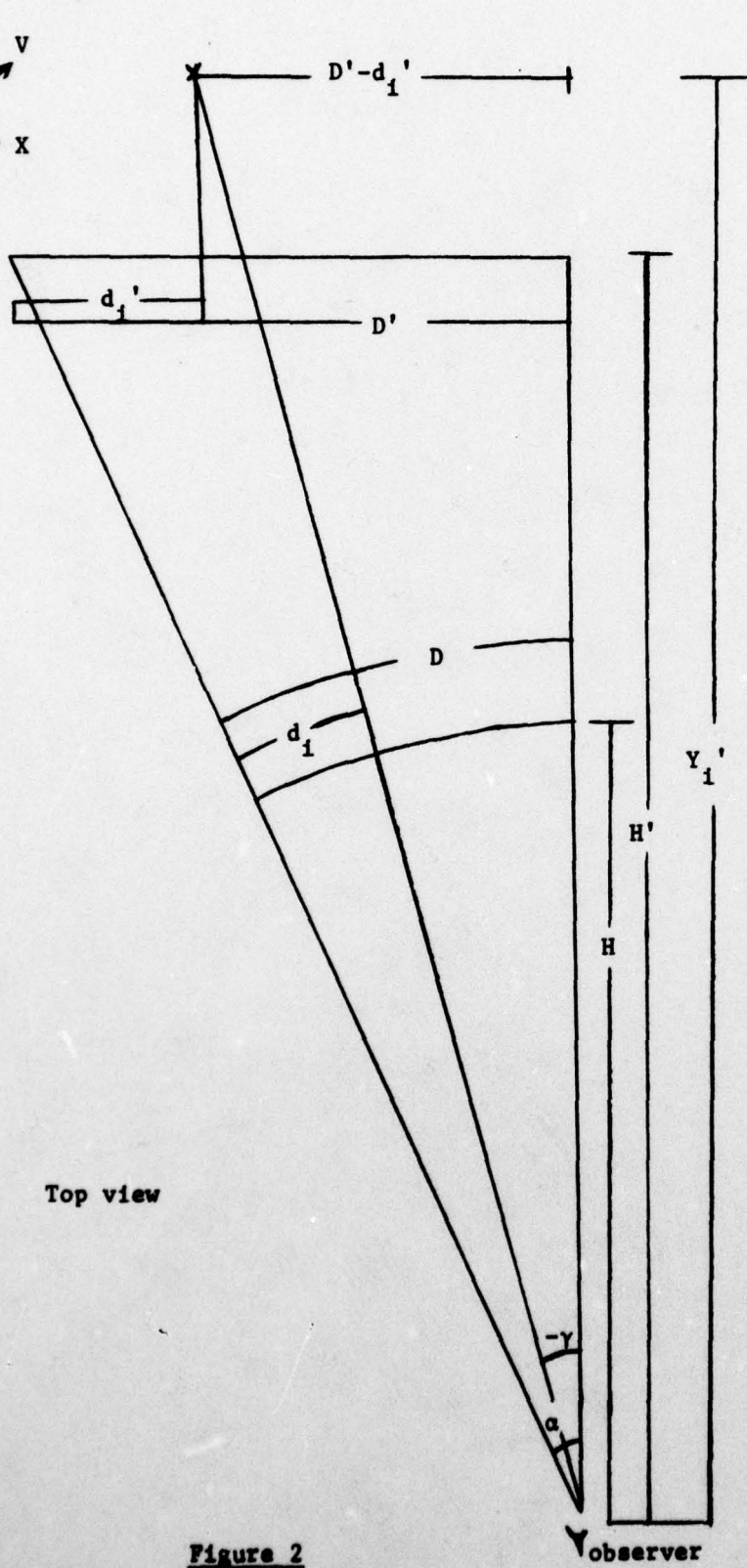


Figure 2

1. Image size (see Fig. 3):

The projected image size, ℓ , is determined from the target's size, L , as follows:

$$\text{dist} = \left[(Y_1')^2 + (D' - d_1')^2 + (\text{Altitude})^2 \right]^{1/2}$$

$$\beta = \text{tg}^{-1} \frac{L/2}{\text{dist}}$$

$$\ell/2 = H \cdot \beta = H \cdot \text{tg}^{-1} \frac{L/2}{\text{dist}}$$

$$\Rightarrow \ell = 2 \cdot H \cdot \text{tg}^{-1} \frac{L/2}{\text{dist}}$$

2. Image Aspect Ratio (see Fig. 4)

The projected image's aspect ratio due to the difference in elevation between the observer and the target is determined by the elevation angle δ :

$$\delta = \text{tg}^{-1} \frac{A}{\left[(Y_1')^2 + (D' - d_1')^2 \right]^{1/2}}$$

3. Rotation

In general, given a point (x_o, y_o, z_o) in the coordinate system (x, y, z) , its coordinates in the system (X, Y, Z) which is rotated with respect to (x, y, z) will be:

$$\begin{bmatrix} X_o \\ Y_o \\ Z_o \end{bmatrix} = \begin{bmatrix} \cos(X, x) & \cos(X, y) & \cos(X, z) \\ \cos(Y, x) & \cos(Y, y) & \cos(Y, z) \\ \cos(Z, x) & \cos(Z, y) & \cos(Z, z) \end{bmatrix} \begin{bmatrix} x_o \\ y_o \\ z_o \end{bmatrix}$$

where (A, b) is the angle between the axes A and b .

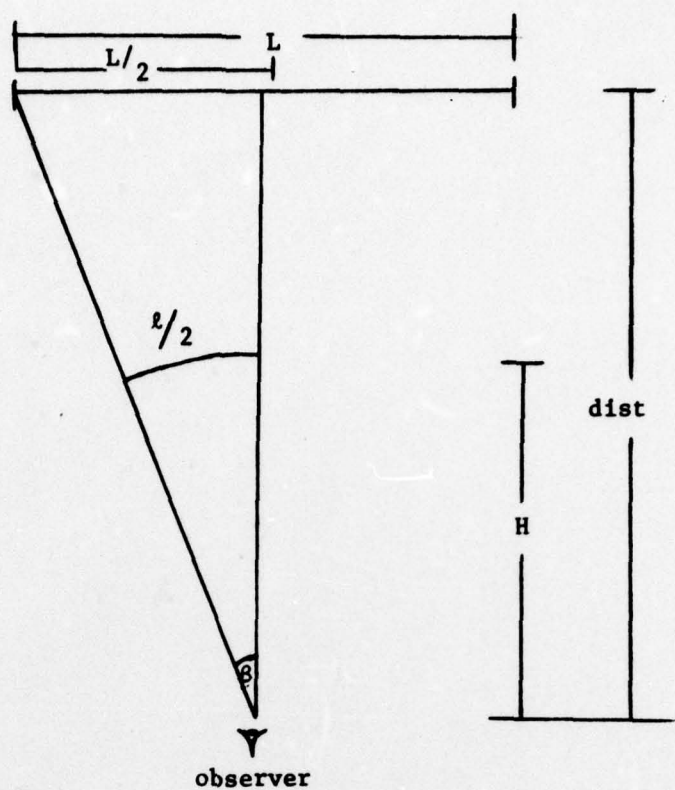


Figure 3

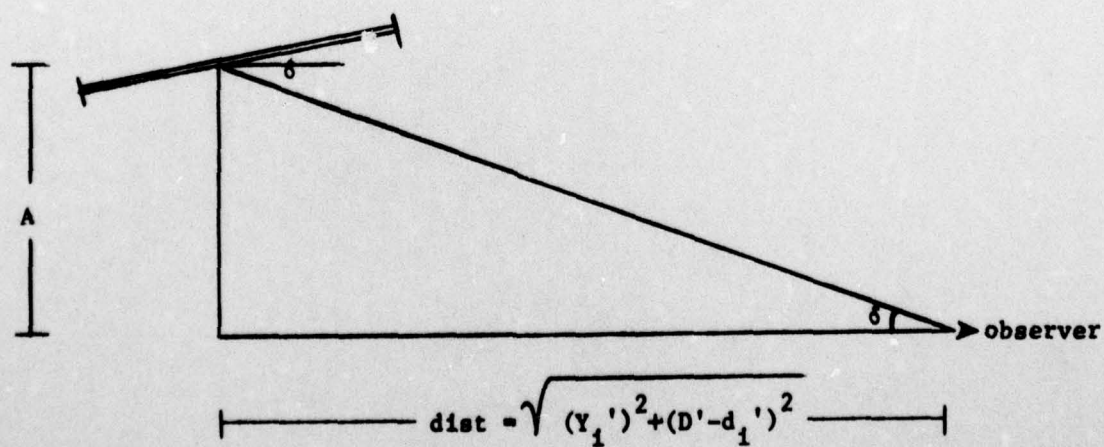


Figure 4

Define a coordinate system (X,Y,Z) with the axes (X,Z) defining a plane tangent to the CRT screen, and a second coordinate system (x,y,z) attached to the target aircraft (see Figure 5). The systems (X,Y,Z) and (x,y,z) are initially parallel.

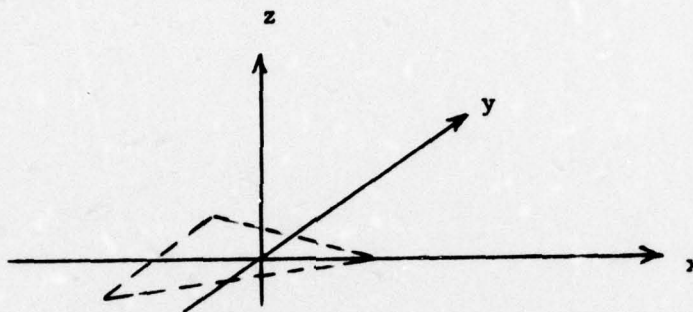


Figure 5

- a. Roll, ϕ : The aircraft [and its coordinates (x,y,z)] roll around the X axis. The rotation matrix \underline{R}_ϕ is then:

$$\underline{R}_\phi = \begin{bmatrix} 1 & 0 & 0 \\ 0 & \cos\phi & \sin\phi \\ 0 & -\sin\phi & \cos\phi \end{bmatrix}$$

- b. Pitch, θ , around the Y axis:

$$\underline{R}_\theta = \begin{bmatrix} \cos\theta & 0 & -\sin\theta \\ 0 & 1 & 0 \\ \sin\theta & 0 & \cos\theta \end{bmatrix}$$

- c. Heading, ψ , around Z axis (define $\psi = 0$ along X).

$$\underline{R}_\psi = \begin{bmatrix} \cos\psi & -\sin\psi & 0 \\ \sin\psi & \cos\psi & 0 \\ 0 & 0 & 1 \end{bmatrix}$$

- d. The tilt δ due to the difference in elevations between the observer and the target may be modeled as another rotation of the aircraft around the X axis, after its ϕ , θ and ψ rotations:

$$\underline{R}_\delta = \begin{bmatrix} 1 & 0 & 0 \\ 0 & \cos\delta & \sin\delta \\ 0 & -\sin\delta & \cos\delta \end{bmatrix}$$

and the coordinates of the aircraft in the CRT coordinate system are:

$$\begin{bmatrix} X_o \\ Y_o \\ Z_o \end{bmatrix} = \underline{R}_\delta \cdot \underline{R}_\psi \cdot \underline{R}_\theta \cdot \underline{R}_\phi \begin{bmatrix} x_o \\ y_o \\ z_o \end{bmatrix}$$

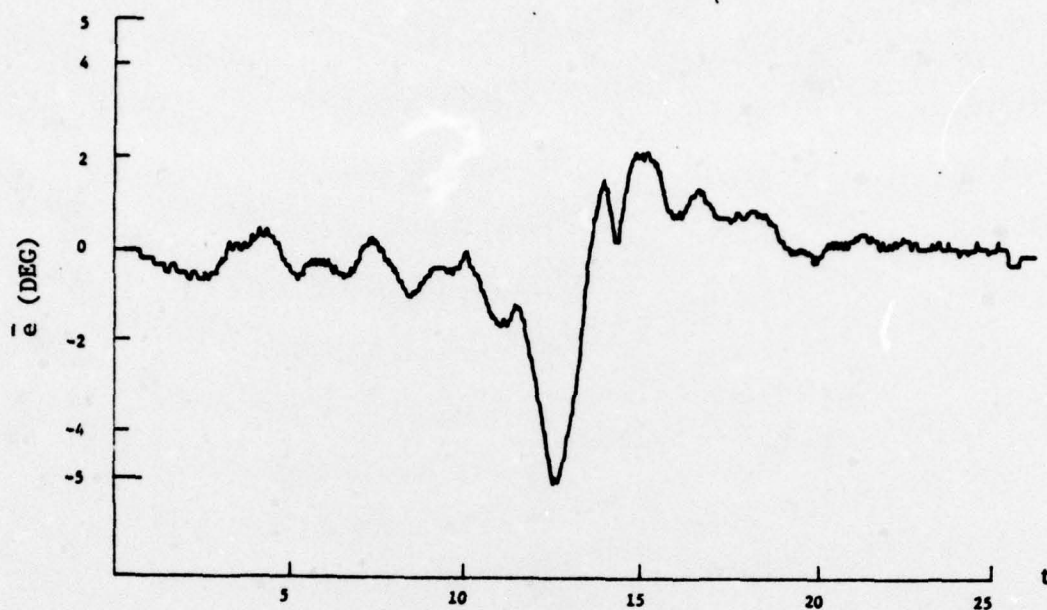
or

$$X_o = \cos\psi \cdot \cos\theta \cdot x_o - (\sin\psi \cdot \cos\phi - \cos\psi \cdot \sin\theta \cdot \sin\phi)y_o - (\cos\psi \cdot \sin\theta \cdot \cos\phi + \sin\psi \sin\phi) z_o$$

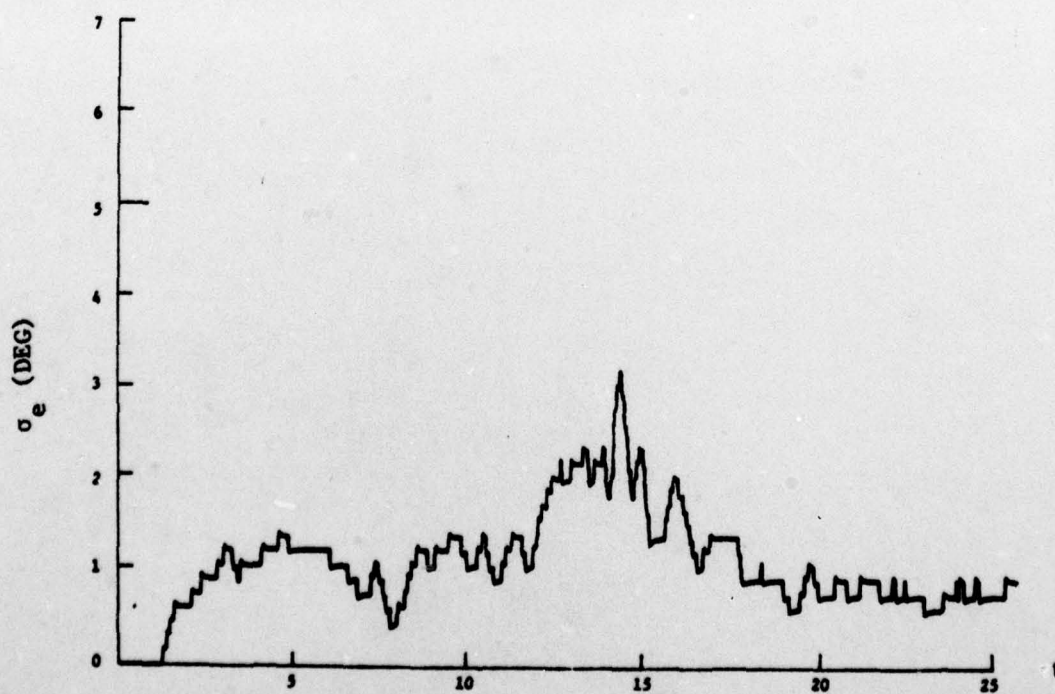
$$Z_o = (\cos\delta \cdot \sin\theta - \sin\delta \cdot \sin\psi \cdot \cos\theta)x_o - (\sin\delta \cdot \sin\psi \cdot \sin\theta \cdot \sin\phi + \sin\delta \cdot \cos\psi \cdot \cos\phi + \cos\delta \cdot \cos\theta \cdot \sin\phi)y_o + (\sin\delta \cdot \sin\psi \cdot \sin\theta \cdot \cos\phi - \sin\delta \cdot \cos\psi \cdot \sin\phi + \cos\delta \cdot \cos\theta \cdot \cos\phi)z_o$$

APPENDIX B

SUMMARY OF EXPERIMENTAL ENSEMBLE STATISTICS

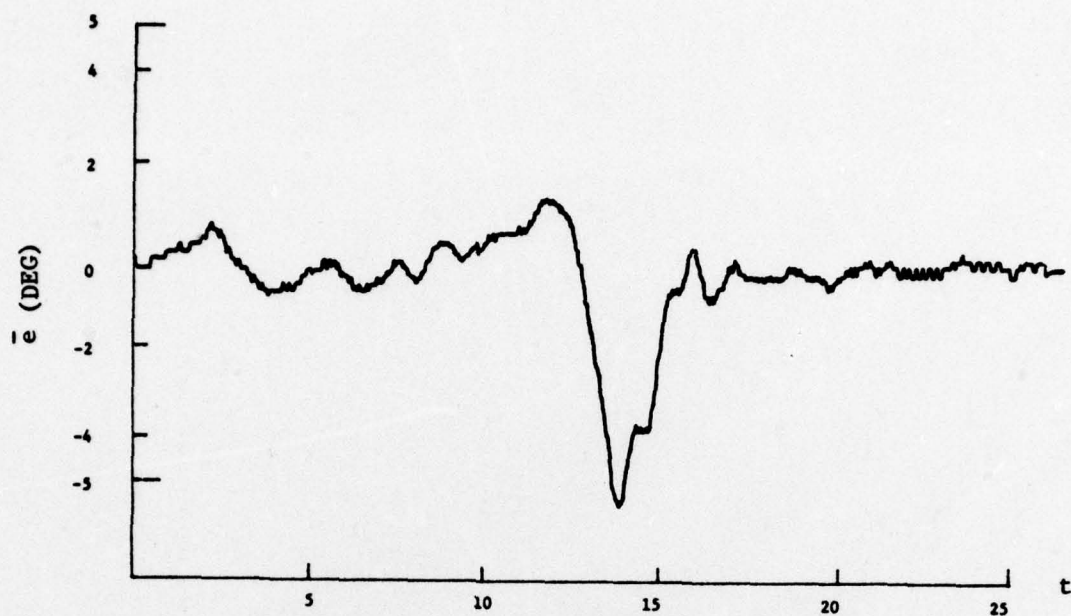


a) Ensemble Mean, N=18

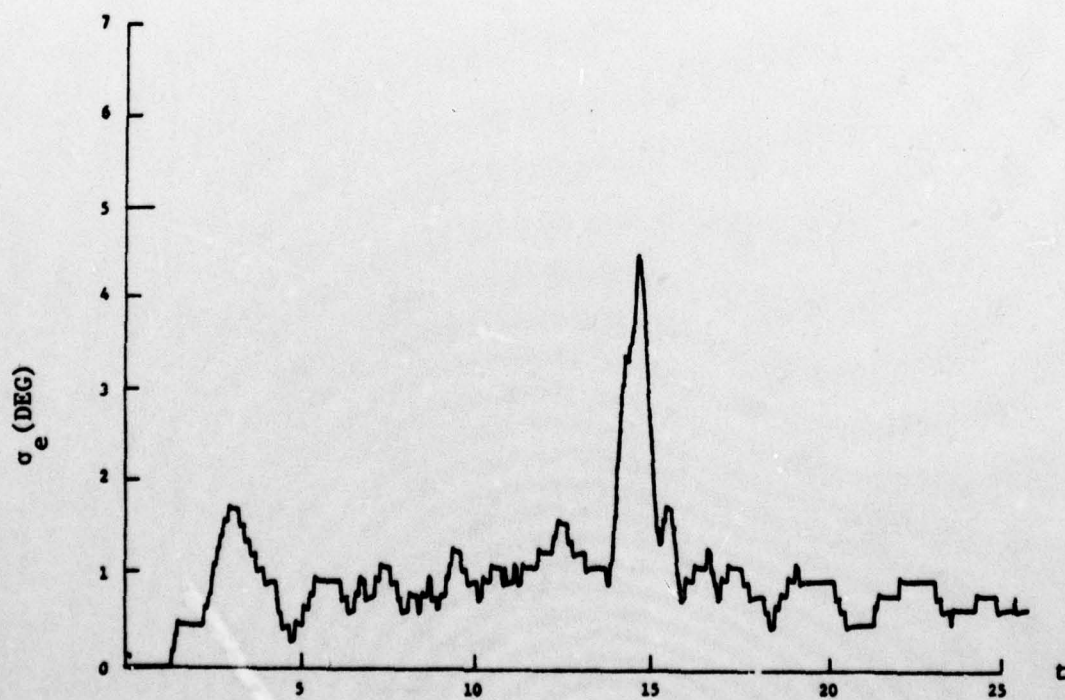


b) Ensemble Standard Deviation, N=18

Fig. B1: AZIMUTH ERRORS, S & L TARGET, FULL ATTENTION, NO VISUAL CUES

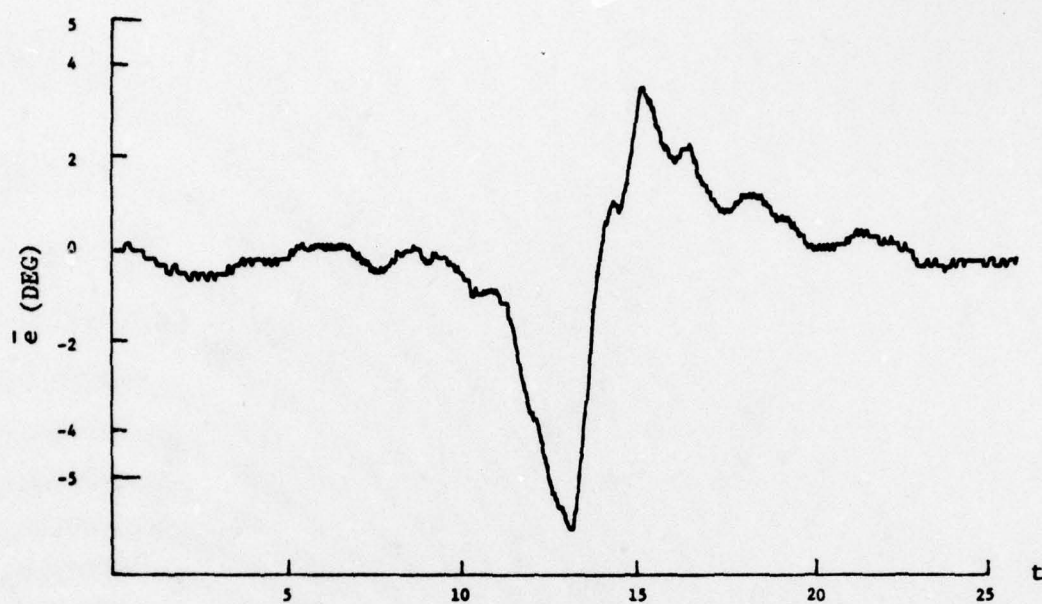


a) Ensemble Mean, N=18

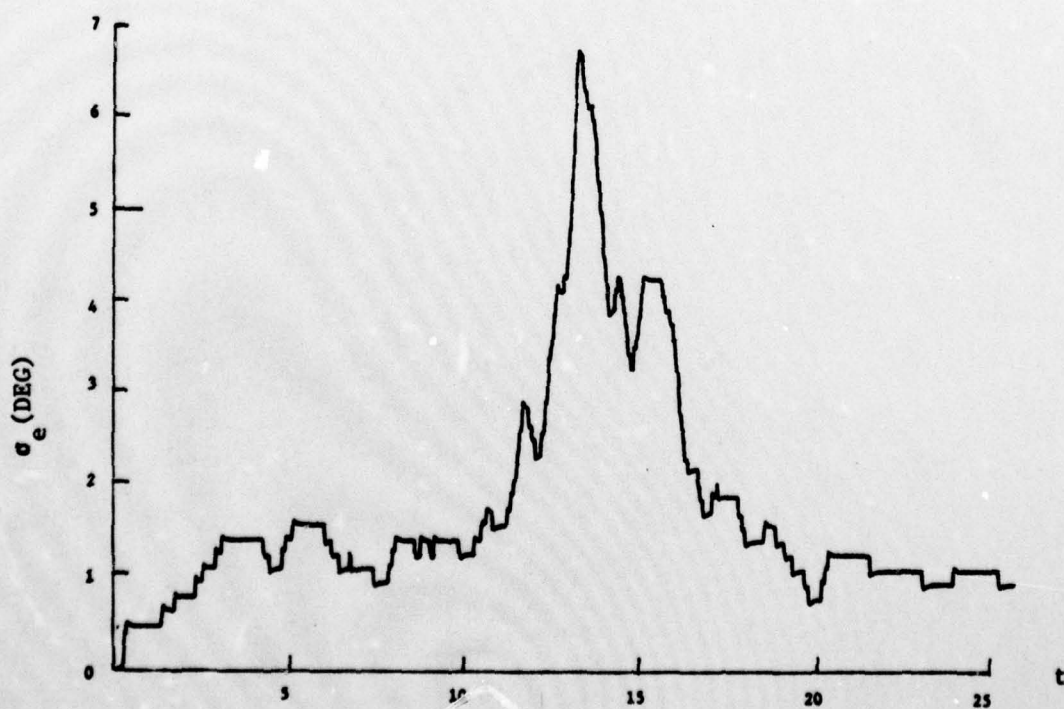


b) Ensemble Standard Deviation, N=18

Fig. B2: ELEVATION ERRORS, S & L TARGET, FULL ATTENTION, NO VISUAL CUES



a) Ensemble Mean, N=42



b) Ensemble Standard Deviation, N=42

Fig. B3: AZIMUTH ERRORS, S & L TARGET, SHARED ATTN., NO VISUAL CUES

AD-A050 290

CONNECTICUT UNIV STORRS DEPT OF ELECTRICAL ENGINEERI--ETC F/G 19/5
EFFECTS OF TARGET MOTION AND IMAGE ON AAA TRACKING.(U)

NOV 77 D L KLEINMAN, A R EPHRATH, P K RAO

AFOSR-77-3126

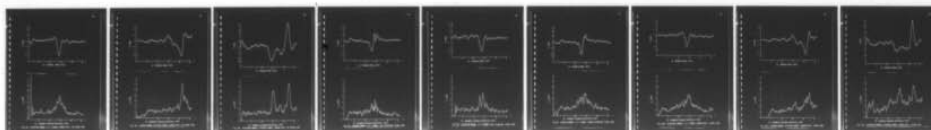
UNCLASSIFIED

TR-77-7

AFOSR-TR-78-0138

NL

2 OF 2
AD
A050290



END
DATE
FILMED

3-78

DDC

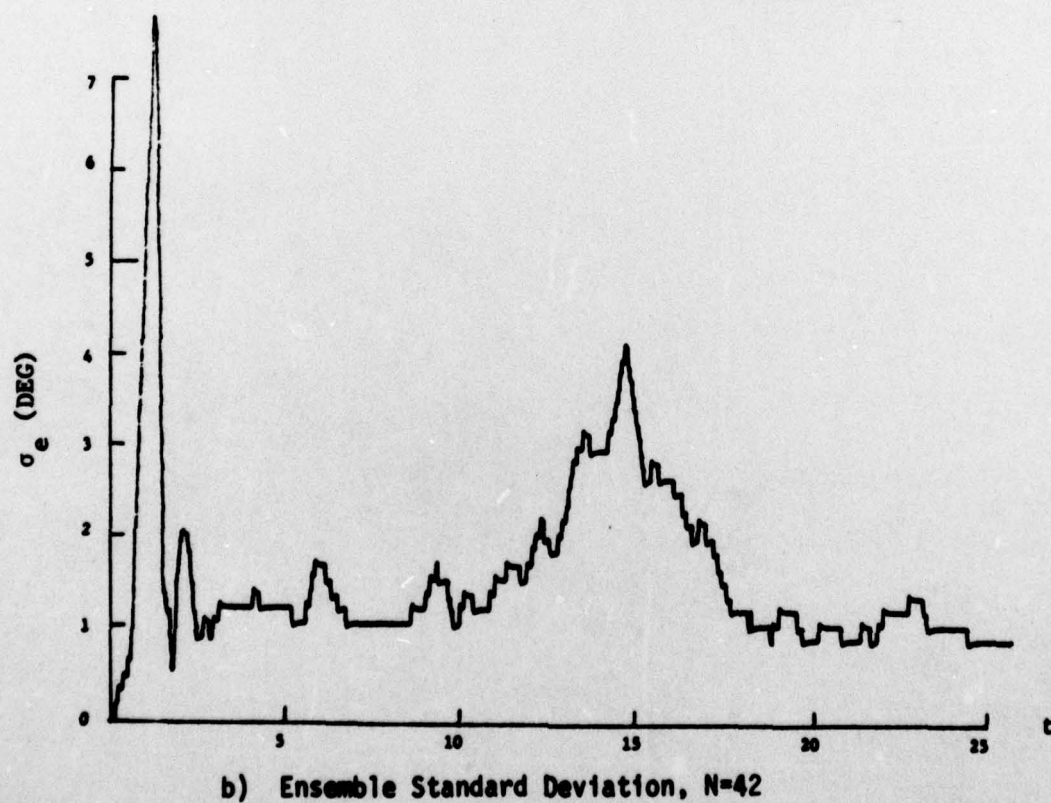
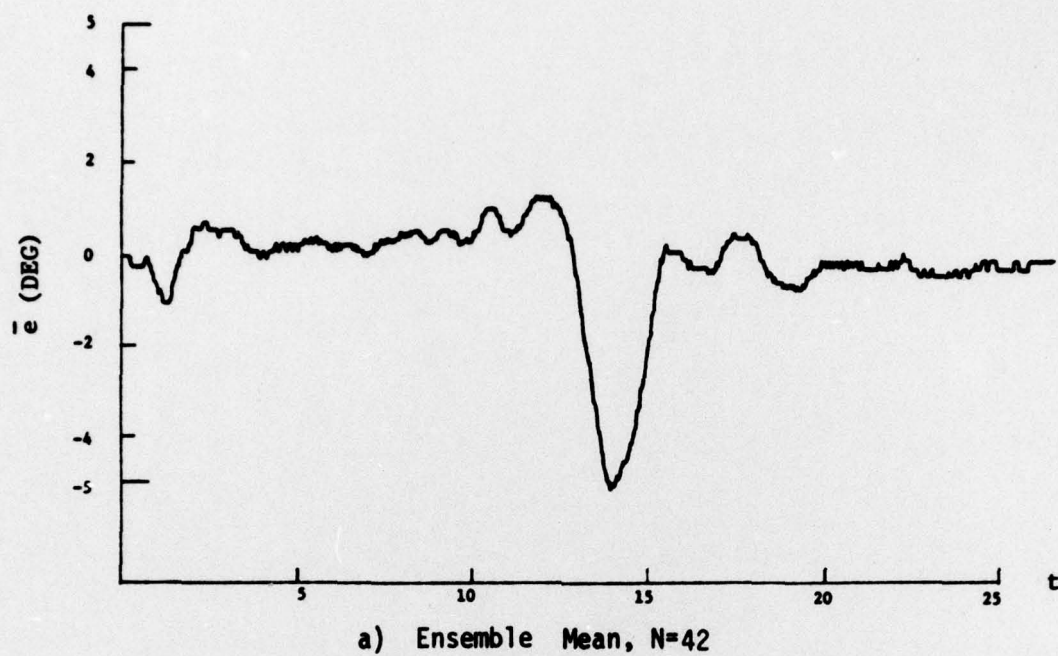
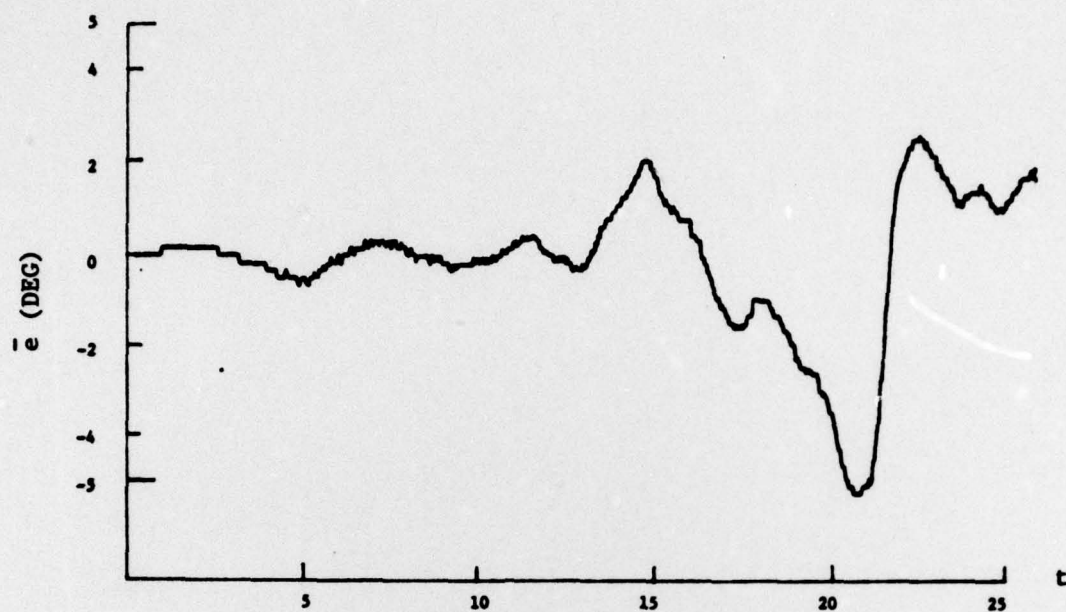
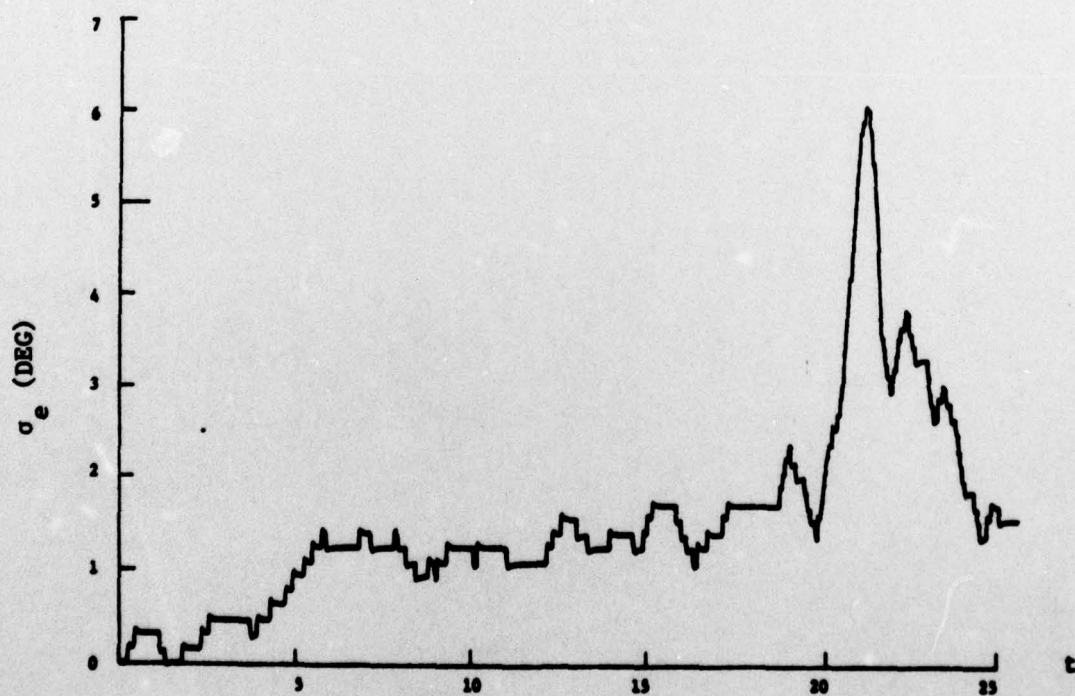


Fig. B4: ELEVATION ERRORS, S & L TARGET, SHARED ATTN., NO VISUAL CUES

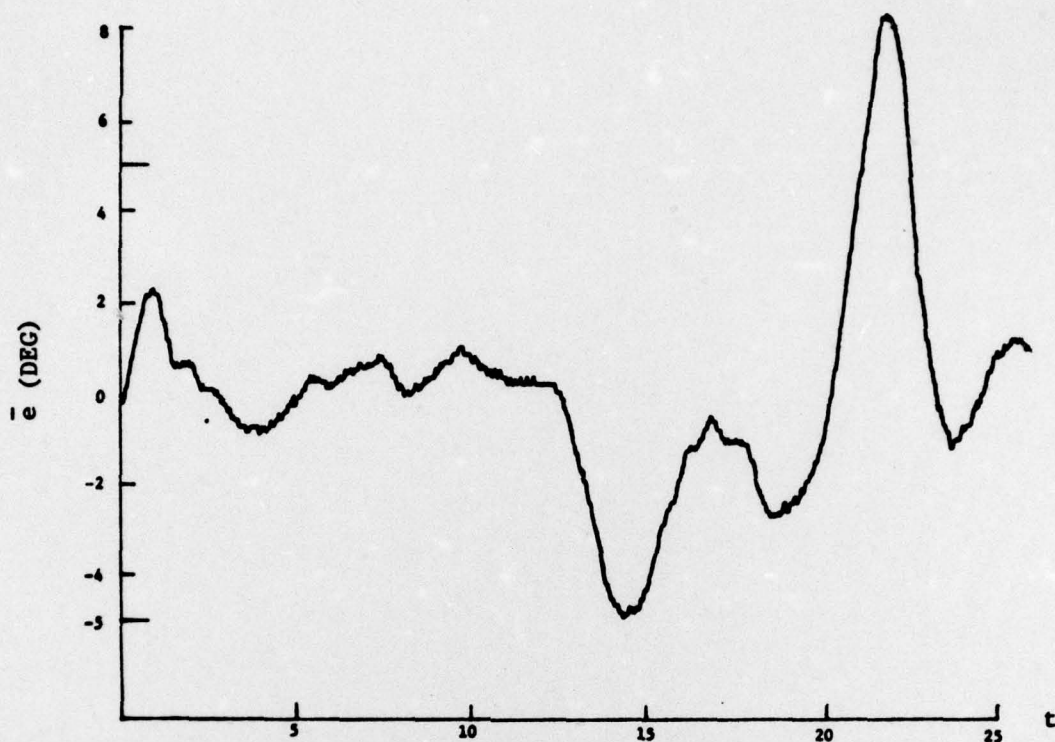


a) Ensemble Mean, N=42

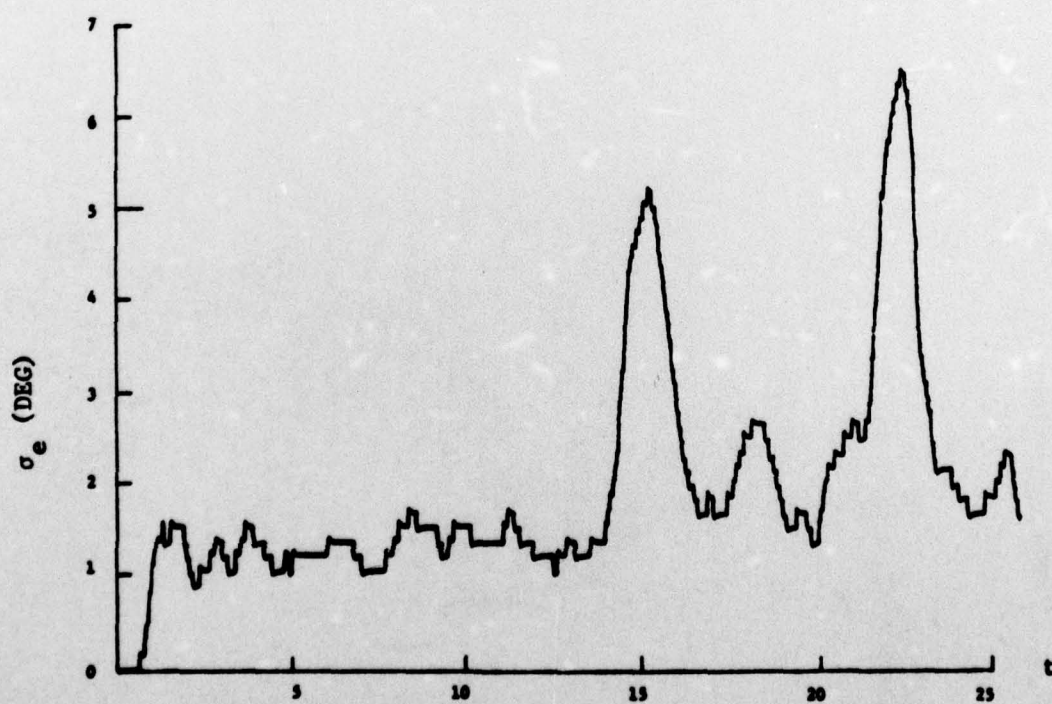


b) Ensemble Standard Deviation, N=42

Fig. B5: AZIMUTH ERRORS, PITCHING TARGET, SHARED ATTN., NO VISUAL CUES

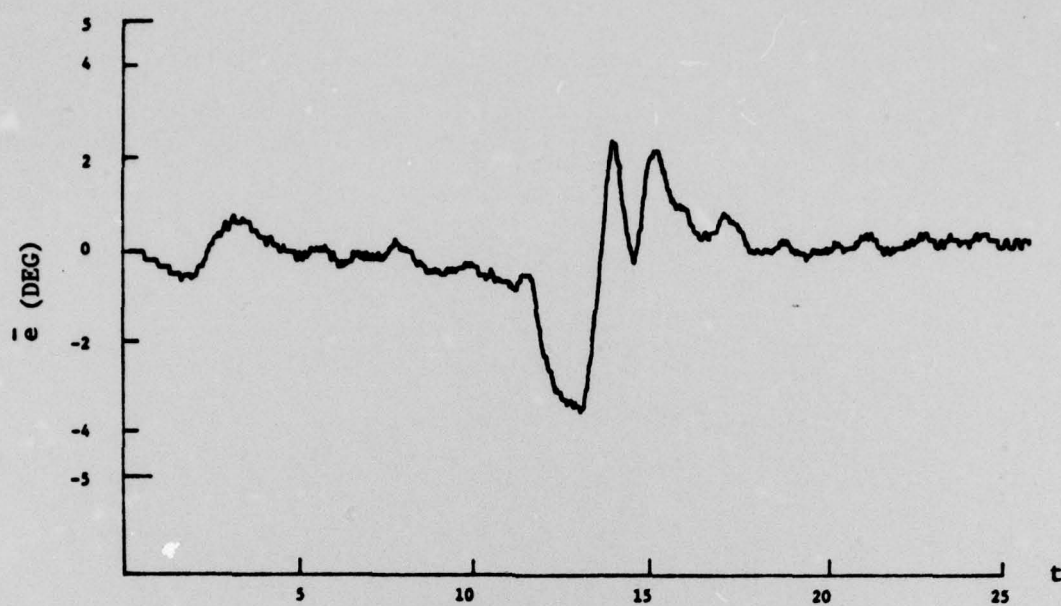


a) Ensemble Mean, N=42

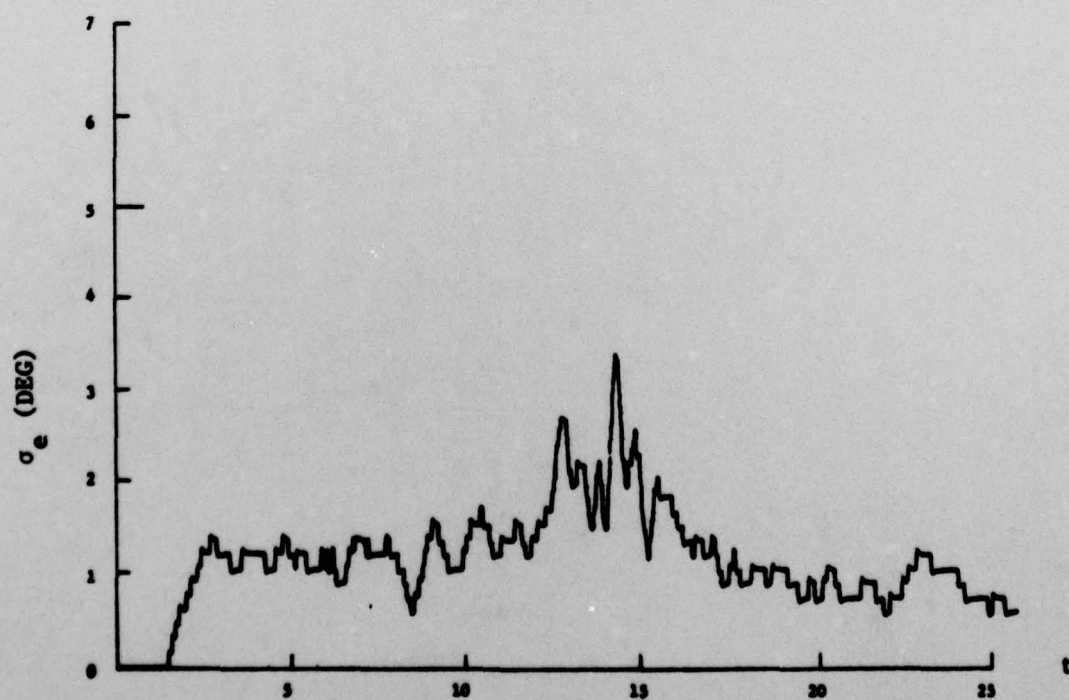


b) Ensemble Standard Deviation, N=42

Fig. B6: ELEVATION ERRORS, PITCHING TARGET, SHARED ATTN., NO VISUAL CUES

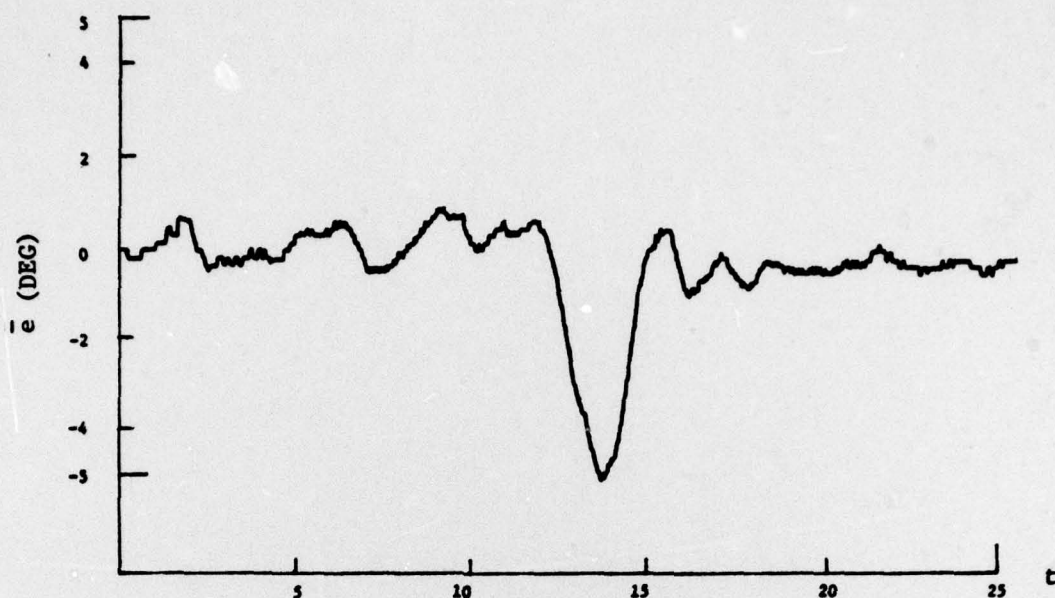


a) Ensemble Mean, N=18

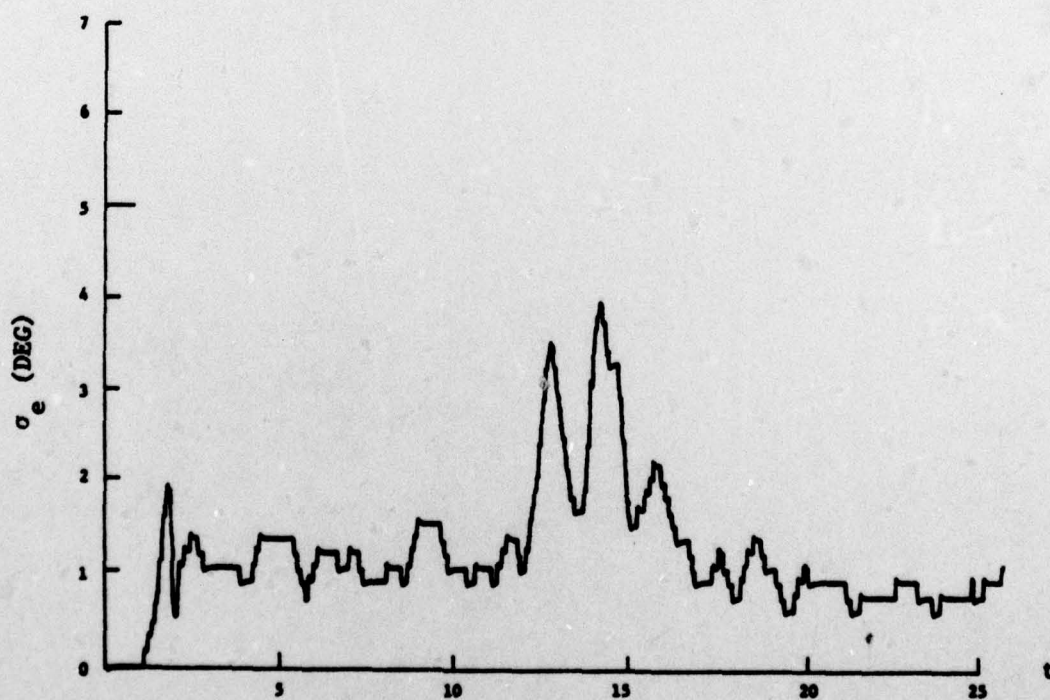


b) Ensemble Standard Deviation, N=18

Fig. B7: AZIMUTH ERRORS, S & L TARGET, FULL ATTENTION, VISUAL CUES

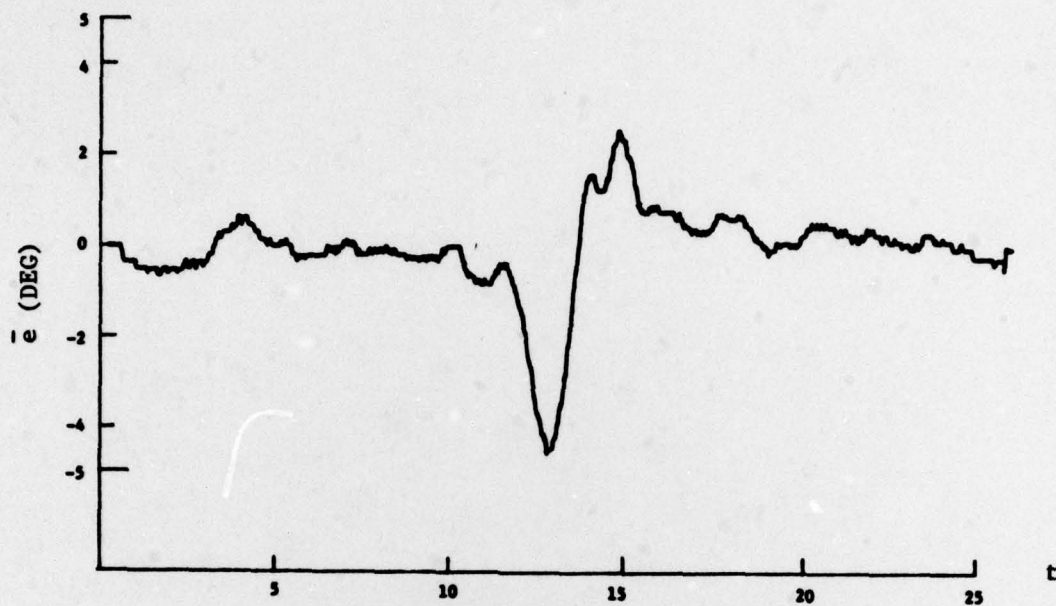


a) Ensemble Mean, N=18

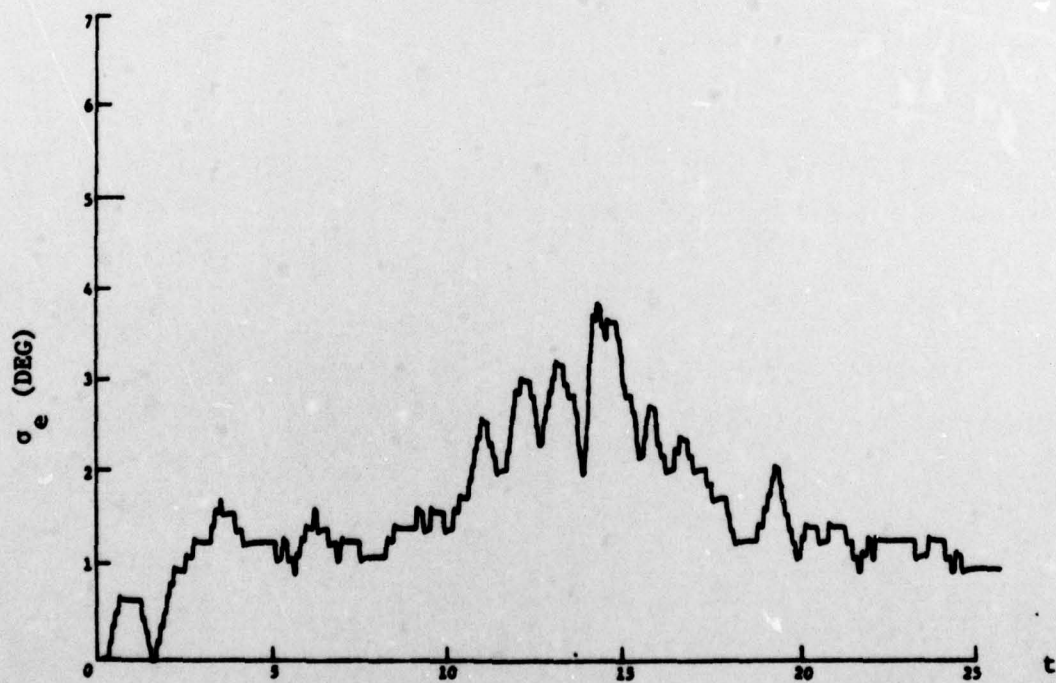


b) Ensemble Standard Deviation, N=18

Fig. B8: ELEVATION ERRORS, S & L TARGET, FULL ATTENTION, VISUAL CUES

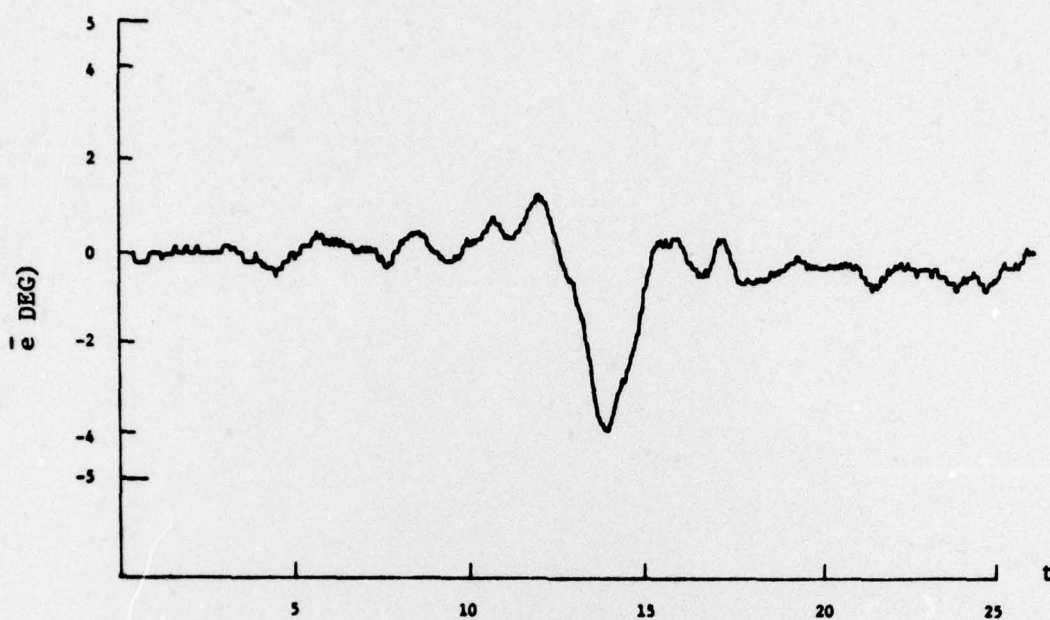


a) Ensemble Mean, N=43

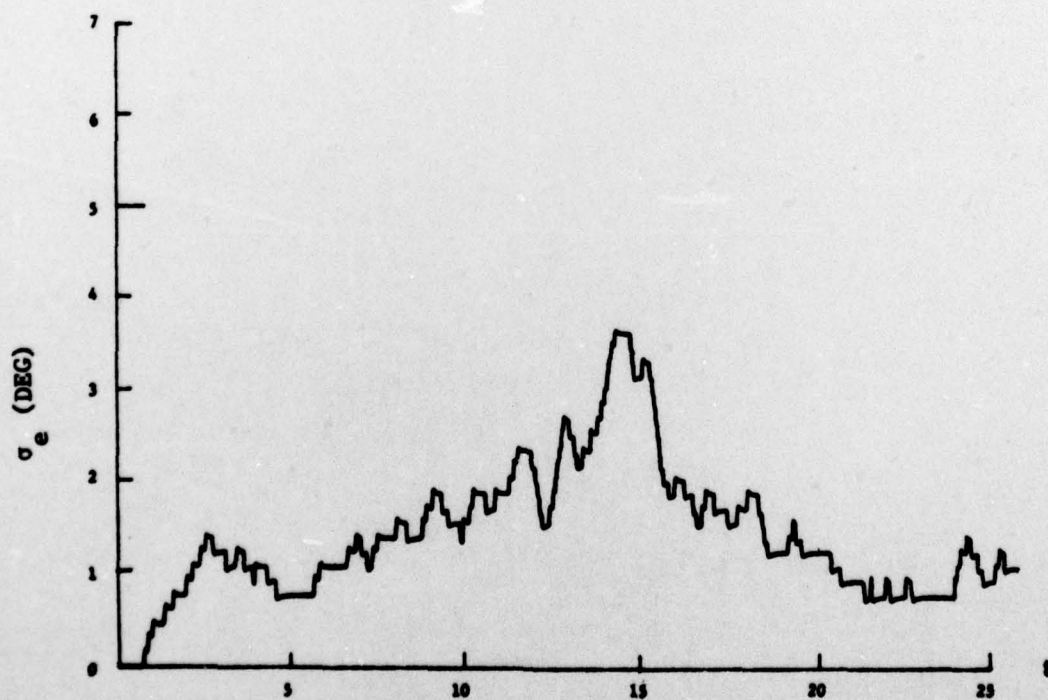


b) Ensemble Standard Deviation, N=43

Fig B9: AZIMUTH ERRORS, S & L TARGET, SHARED ATTENTION, VISUAL CUES

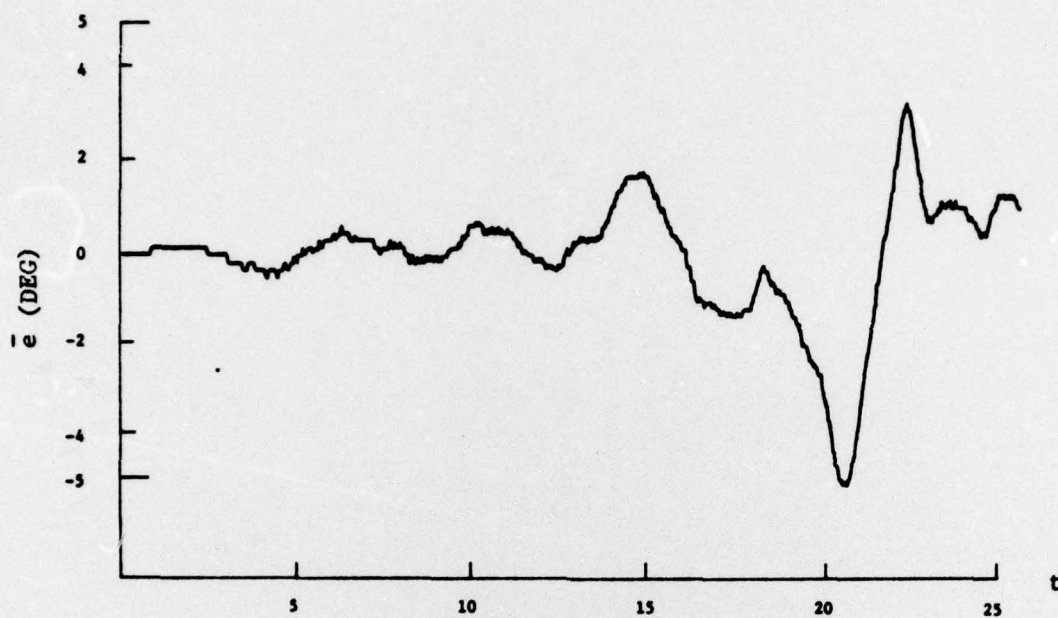


a) Ensemble Mean, N=43

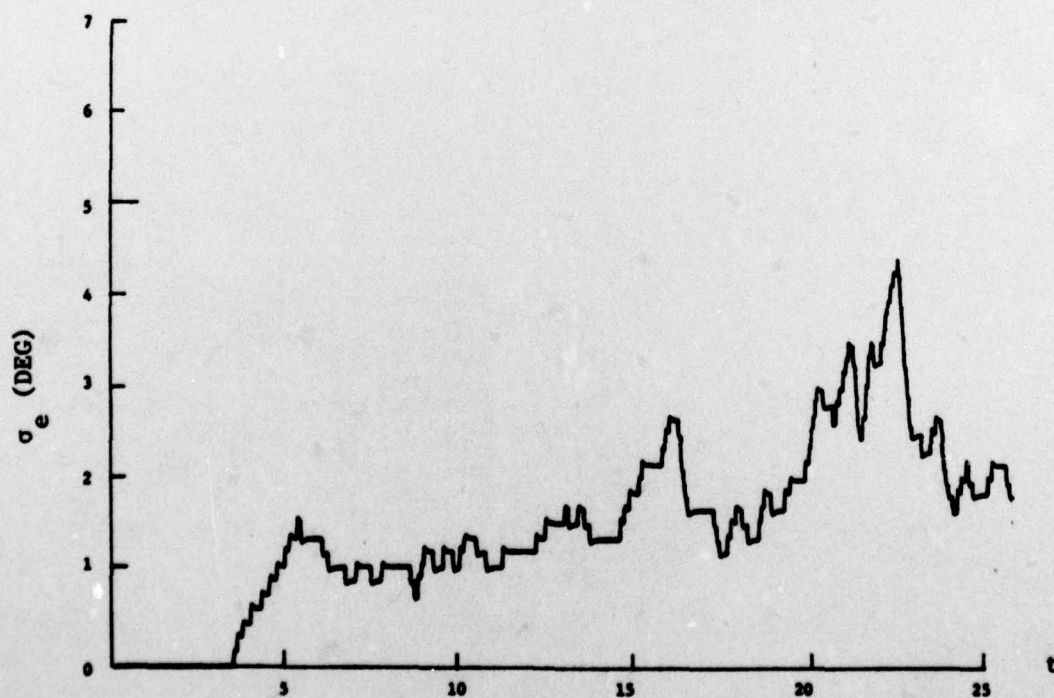


b) Ensemble Standard Deviation, N=43

Fig. B10: ELEVATION ERRORS, S & L TARGET, SHARED ATTN., VISUAL CUES

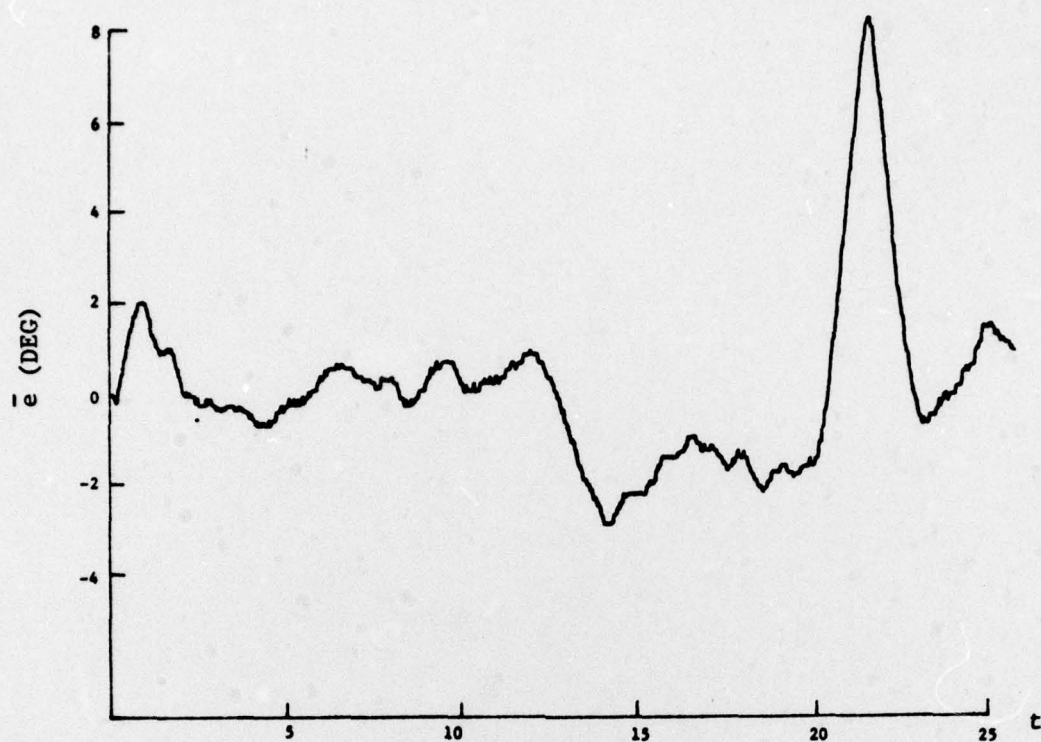


a) Ensemble Mean, N=42

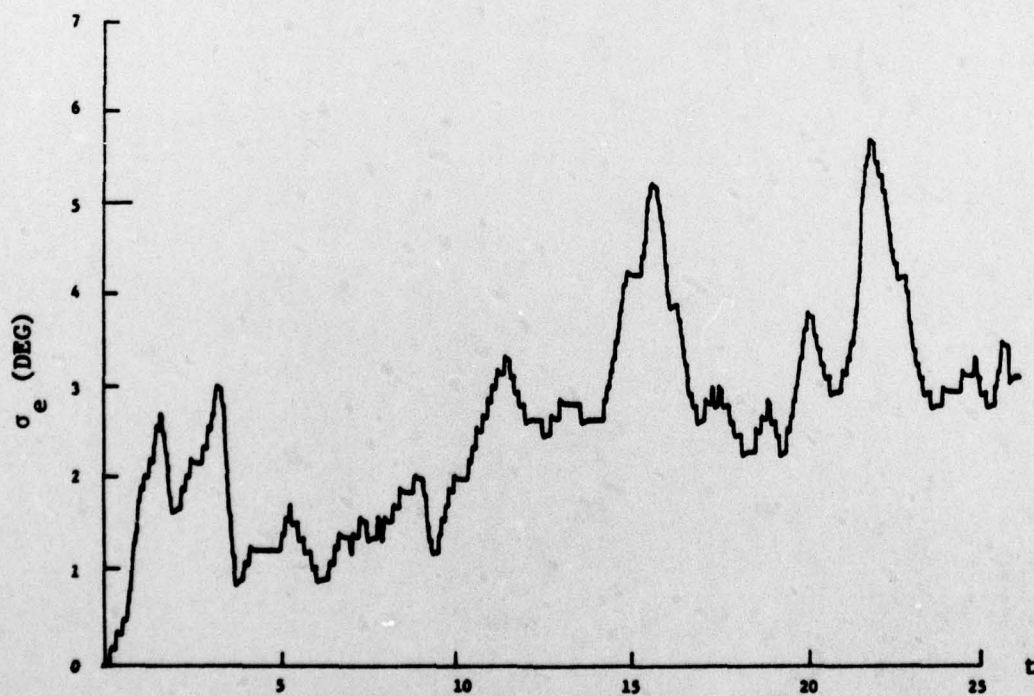


b) Ensemble Standard Deviation, N=42

Fig. B11: AZIMUTH ERRORS, PITCHING TARGET, SHARED ATTN., VISUAL CUES



a) Ensemble Mean, N=42



b) Ensemble Standard Deviation, N=42

Fig. B12: ELEVATION ERRORS, PITCHING TARGET, SHARED ATTN., VISUAL CUES